High performance polyaniline membranes for nanofiltration

Amura, Ida

Award date:
2020

Awarding institution:
University of Bath

UNIVERSITY OF BATH

High Performance Polyaniline Membranes for Nanofiltration

Volume 1 of 1

Ida Francesca Amura

A thesis submitted for the degree of Doctor of Philosophy

University of Bath

Department of Chemical Engineering

August 2020

Acknowledgments

First, I would like to thank my supervisor Dr Emma Emanuelsson for the constant support, invaluable advice and critical review. I am very grateful for her hard work in supervising me throughout this period.

I would like to thank my co-supervisor Dr. Salman Shahid and all the researchers of the Emanuelsson's research group for the great support and encouragement in the lab and during the writing process.

I deeply appreciate the support and the excellent advice of the technical and research staff of the Department of Chemical Engineering at the University of Bath. A special thanks to Dr. Junjie Shen, Dr Abouther Al-Shimmerry, Dr Parimala Shivaprasad and Dr Serena Casanova for their amazing friendship. They supported me greatly and they were always willing to help.

I also express my gratitude to my dear friends with whom I have shared the lab and the office for three years. They have been all part of this journey and I am grateful for that.

Finally, I wish to acknowledge the support and great love of my family. My parents and my sister Elisabetta spent endless hours on skype speaking with me, encouraging me trying and to cheer me up, even in the gloomiest moments of this bumpy PhD journey. They kept me going on. I also wish to thank my fiancée Gavino, a special and kind soul. Thank you for being an exceptional partner in life and in the lab.

This work would not have been possible without the input of all these amazing people.

Abstract

Sulfonated polyaniline (S-PANI) is a self-doped conducting polymer of the polyaniline family with improved chemical stability over a wide range of pH, easy of synthesis and better processability. The sulfonic groups are covalently bond to the PANI backbone, resulting in a permanent chemical modification and doping. Despite the interesting chemical properties, its widespread use in membrane fabrication is still limited and the few available studies have only investigated the addition of S-PANI to hydrophobic membranes to modify the surface properties and obtain low fouling systems to be used for ultrafiltration. There is also a lack of studies on the development of self-doped S-PANI membrane systems and the effect of the bulky sulfonic groups on the rejection of small molecules, performance in organic solvents, electrical conductivity and fouling behaviour of the membrane. Therefore, the aim of this research was to investigate the development of a new family of self-doped sulfonated polyaniline (S-PANI) membranes addressing i) the current limitations of PANI membranes namely acid leaching, fouling and limited solvent stability and ii) the need for robust nanofiltration membranes that could be used in complex chemical environments for the recovery of small molecules. The thesis has two components and has focused on trialling commercial membranes in complex reaction environments and on the synthesis, fabrication and testing of novel self-doped S-PANI membranes.

The work initially focused on the benchmarking of relevant industrial reaction systems such as the Suzuki coupling of aryl pyridines catalysed by palladium (II) catalyst and the lipase mediated kinetic resolution in organic solvents using commercial DURAMEM 500 and PURAMEM S600 nanofiltration membranes. The object was to evaluate product yield, catalyst activity, fouling and operating pressure and flux. Both catalytic systems were successfully retained by the membranes; furthermore, the monitoring of the reactions in batch offered a better understanding of the species contributing to membrane fouling and catalyst deactivation.

The work then focused on using S-PANI to prepare membranes that could be applied in these chemical challenging environments. Ultrafiltration and tight ultrafiltration membranes were prepared using well-established methodologies such as phase inversion in water and cross-linking using both chemical and thermal method as well as testing a novel fabrication method which make use of hexane in the coagulation bath to densify the porous polymer structure and obtained a nanofiltration S-PANI membrane. Pure S-PANI and cross-linked S-PANI membranes showed excellent antifouling behaviour when tested in BSA filtration, with the latter being resistant and reusable in DMF filtration. Furthermore, the membrane prepared via

phase inversion in hexane was reusable in toluene, acetone and 2-propanol at least three times with no loss in mechanical stability at a maximum pressure of 30 bar and showed 100% rejection of low molecular weight polypropylene glycols in water.

Overall, this work has reported for the first time the development of a new family of low fouling, solvent resistant self-doped sulfonated polyaniline membranes that could be applied in various chemical environments

Table of contents

Abstract ii

Table of contents iv

List of figures xi

List of tables xvii

List of publications xviii

Chapter 1 Introduction 1

1.1 Overall project and aims 2

1.2 Structure of the thesis 2

Chapter 2 Background 4

2.1 Overview 4

2.2 Membrane filtration 4

2.2.1 Introduction 4

2.2.2 Membrane performance 5

2.2.3 Classification of membrane filtration processes 7

2.2.4 Filtration modes 8

2.2.5 Theoretical models 9

2.2.5.1. The pore flow model 9

2.2.5.2. The Solution diffusion model 10

2.2.5.3. Donnan exclusion 10

2.3 Membrane materials and preparation methods 11

2.3.1 Introduction 11

2.3.2 Type of membranes 11

2.3.2.1. Integrally skinned asymmetric membranes ISA 12

2.3.2.2. Thin film composite membranes TFC 13

2.3.3 Fabrication methods 13

2.3.3.1. Solvent casting 14

2.3.3.2. Phase inversion 14
2.3.3.3. Membrane surface modification 15
2.3.4 Applications of polymer membranes 17
2.3.4.1. Resource recovery 17
2.3.4.2. Recycling of homogeneous transition metal catalysts and biocatalysts. 18
2.3.5 The fouling issue 20
2.3.5.1. Fouling mitigation 21
2.3.6 Advance polymer membranes /stimuli responsive membranes 22
2.3.6.1. Overview 22
2.3.6.2. Electrical responsive membranes 23
2.3.6.3. Mechanism 24
2.4 Conducting polymers: self-doped sulfonated polyaniline membrane 26
2.4.1 Introduction 26
2.4.2 Properties of PANI: chemical structure and doping mechanism 26
2.4.3 Polyaniline derivatives: self-doped systems 29
2.4.4 Synthetic routes for self-doped sulfonated polyaniline 30
2.4.4.1. Sulfonation of PANI precursors 30
2.4.4.2. Copolymerisation of monomers 31
2.5 Conclusion and gaps in the literature 31
2.6 Aims and objectives 33
Chapter 3 Materials and method 35
3.1 Introduction 35
3.2 Materials 35
3.2.1 Chemicals 35
3.2.2 Membranes 36
3.3 Polymer synthesis 37
3.3.1 Synthesis of self-doped sulfonated polyaniline 37

3.3.2 Synthesis of polyaniline 38
3.4 Membrane fabrication 39
3.4.1 Preparation of polymer dope solution 39
3.4.1.1. S-PANI for preparation via non-solvent phase inversion in water 39
3.4.1.2. PANI for preparation via non-solvent phase inversion in water 40
3.4.1.3. S-PANI for preparation via non-solvent phase inversion in hexane 40
3.4.1.4. Incorporation of graphene oxide 41
3.4.2 Membrane preparation 41
3.4.2.1. Phase inversion in water 42
3.4.2.2. Phase Inversion in hexane 42
3.5 Characterization techniques 42
3.5.1 Powder analysis 42
3.5.1.1. Fourier transform infrared spectroscopy 42
3.5.1.2. UV-VIS spectroscopy 42
3.5.1.3. Scanning electron microscope- energy dispersive X-ray (SEM-EDX) 43
3.5.2 Membrane analysis 43
3.5.2.1. Field emission scanning slectron microscopy (FESEM): membrane morphology 43
3.5.2.2. Dynamic contact angle: membrane hydrophilicity 43
3.5.2.3. Swelling degree 44
3.5.2.4. Differential scanning calorimetry (DSC): thermal properties 44
3.5.2.5. Four point probe conductivity meter: conductivity 45
3.5.2.6. Dynamic mechanical analysis (DMA) mechanical properties 45
3.5.2.7. XRD 45
3.5.2.8. Cyclic voltammetry 45
3.6 Cross-linking of S-PANI membranes 45
3.6.1 Thermal cross-linking 45
3.6.2 Chemical Cross-linking 46

3.7 Membrane permeance and rejection 47
3.7.1 Dead-end filtration 47
3.7.1.1. Membrane solute rejection and determination of MWCO 48
3.7.2 Fouling experiments 51
3.7.2.1. Cross-flow filtration: permeance and rejection 51
3.7.2.2. Study of membrane low fouling ability: flux recovery 51
3.8 Catalyst recovery: benchmarking of commercial membranes in organic solvent systems 52
3.8.1 Palladium catalysed Suzuki coupling 52
3.8.1.1. NMR analysis of permeate 54
3.8.1.2. Uv-Vis analysis of $Pd(OAc)_2$ in the permeate 54
3.8.2 Kinetic resolution of 1-phenylethanol catalysed by free lipase 55
3.8.2.1. UV VIS analysis of permeate Bradford Essay 55
Chapter 4 Benchmarking of industrial relevant reactions with commercial OSN membranes 57
4.1 Introduction 57
4.2 Suzuki coupling in a biphasic mixture 59
4.2.1 Reaction benchmarking in batch 59
4.2.2 Membrane compatibility with reaction conditions 60
4.2.2.1. MWCO suitability 60
4.2.3 Membrane performance and catalyst reuse 61
4.2.4 Fouling Characteristics 63
4.2.4.1. Investigation of catalyst de-activation in batch mode 64
4.3 Kinetic resolution in organic solvents 66
4.3.1 Conversion and kinetics of reaction in toluene and ethyl acetate 66
4.3.2 Filtration in dead-end cell and lipase reuse 67
4.4 Conclusion 70
Chapter 5 Self-doped sulfonated polyaniline membrane: fabrication, fouling resistance and properties 72

5.1 Introduction....72
5.2 Synthesis of self-doped sulfonated polyaniline S-PANI....75
5.2.1 FTIR characterisation....75
5.2.2 UV-VIS analysis....76
5.2.3 SEM EDX....77
5.3 Preparation of S-PANI membranes....78
5.3.1 Optimisation of membrane fabrication conditions....78
5.3.2 Characterisation of (UF) S-PANI membranes....79
5.3.2.1. Membrane morphology....79
5.3.2.2. Contact angle....80
5.4 Cross-linking of S-PANI membranes....81
5.4.1 Thermal cross-linking....81
5.4.1.1. Mechanical properties and solvent stability of thermally cross-linked membranes....82
5.4.2 chemical cross-Linking: synthesis of S-PANI GA, S-PANI DCX and S-PANI TCL membrane....83
5.4.2.1. FTIR of chemical cross-linked membranes....84
5.4.2.2. XRD analysis....84
5.4.2.3. Morphology of chemically cross-linked membranes....85
5.4.2.4. Stability in organic solvents: visual stability study....89
5.4.2.5. Membrane surface hydrophilicity; effect of chemical cross-linking....91
5.5 Investigation of membrane performance....92
5.5.1 Water flux and PEGs rejection of S-PANI membrane, thermally cross-linked S-PANI membrane and chemically cross-linked S-PANI membrane in dead-end cell....92
5.5.2 Solvent stability study: investigating DMF resistance of chemically cross-linked S-PANI membrane in the dead-end cell....96
5.5.3 Fouling study: comparing the fouling resistance of S-PANI, PANI and S-PANI GA membrane in cross-flow....97

5.6 The conductivity of S-PANI membranes and synthesis of composite S-PANI/graphene oxide membranes 100
5.6.1 Electrochemical properties 101
5.6.2 Characterisation of S-PANI-GO membrane 103
5.6.3 Conclusions 106
Chapter 6 Preparation of nanofiltration S-PANI membranes 109
6.1 Introduction 109
6.2 Membrane preparation: synthesis of SPWT and SPHX membrane 112
6.3 Effect of coagulation bath on membrane morphology 113
6.3.1 Membrane hydrophilicity 115
6.4 Solvent stability of SPHX and SPWT membrane and study of the swelling behaviour 116
6.5 Investigating nanofiltration performance in dead-end cell 118
6.5.1 Water flux and PEGs/PPG rejection 118
6.5.2 Rejection of PPGs in solvents and the effect of the swelling degree on membrane performance 120
6.6 Conclusion 124
Chapter 7 Conclusion and recommendations for future work 126
7.1 Benchmarking of industrial relevant organic reactions with commercial OSN membranes 126
7.1.1 Conclusions 126
7.1.2 Future work 126
7.2 Self-doped sulfonated polyaniline membrane: fabrication, fouling resistance and properties 127
7.2.1 Conclusion 127
7.2.2 Future work 128
7.3 Fabrication of nanofiltration self-doped S-PANI membranes 130
7.3.1 Conclusion 130
7.3.2 Future work 130

Chapter 8 References 132

Appendix A Analysis of the reaction components and membrane characterisation 154

A.1. Nuclear magnetic resonance 154

A.2. Chemical characterisation of Pd-XPhos complex 157

A.3. Polymers and membranes properties 158

A.3.1. Matrix-assisted laser desorption/ionization MALDI 158

A.3.2. Additional SEM images of the S-PANI polymer and membranes 159

A.3.3. FTIR of thermally cross-linked S-PANI membranes 160

A.3.4. Mechanical properties of chemically cross-linked membranes 161

A.4. Membrane performance 162

Appendix B Calibration curves 165

Appendix C Preparation of solvent stable PANI-PAMPSA membrane: Characterisation, Chemical cross-linking and phase inversion in hexane 166

C.1. Introduction 166

C.2. Materials and methods 167

C.2.1. Materials 167

C.2.2. Synthesis of PANI-PAMPSA 167

C.2.3. Membrane preparation 168

C.2.4. Physical and chemical characterisation 168

C.2.5. Evaluation of membrane performance in dead-end cell 169

C.3. Results and discussion 169

C.3.1. Membrane fabrication and characterization 169

C.4. Membrane performance 174

C.5. Conclusion 176

List of figures

Figure 1: MWCO curves: ideal *versus* typical curve [2] 7
Figure 2: Different pressure-driven membrane processes [31] 8
Figure 3: Membrane filtration modes: (a) Dead-end and (b) cross-flow filtration 9
Figure 4 Schematic representation of an (a) integrally skinned asymmetric membrane and (b) thin film composite membrane. Adapted from ref.[27] 12
Figure 5: Fluxes of the non-solvent (Jns, Jns') and the solvents (Js, Js') at the interface between coagulation medium and the casting film (Adapted from [52]) 15
Figure 6: Example of positively (A) and negatively (B) responsive mechanism 23
Figure 7: Schematic diagram showing the electrosensitive permeability in PAMPS gel-g-PETE nanocomposite membranes. Reproduced with permission from [103] Copyright (2007) American Chemical Society. 25
Figure 8: Scheme representing polyaniline main chain structure 27
Figure 9: Schematic representing the doping of PANI [106] 29
Figure 10: Schematic representing the synthesis of S-PANI through post treatment of PANI emeraldine base. 31
Figure 11: Schematic representing the co-polymerisation of aniline and metanilic acid 31
Figure 12: Apparatus showing (left) the synthesis of S-PANI by the dropwise addition of aniline to APS and metanilic acid in HCl 1M and (right) washing under vacuum of the powder. 38
Figure 13: Radical polymerization of aniline and metanilic acid mediated by APS in HCl ... 38
Figure 14: preparation of a dope solution 41
Figure 15: Equipment showing the OCA 15 PRO system used to perform contact angle of the produced membranes 44
Figure 16: Example of reaction scheme for the chemical cross-linking of S-PANI with TCL. Chemical cross-linking with DCX and GA is reported for PANI here [13]. 47
Figure 17: Schematic of the dead-end cell used to study membrane performance 48
Figure 18: Molecular structure of (A) Polypropylene glycol (PPG) and (B) Polyethylene glycol (PEG) 49
Figure 19: Representation of the cross-flow membrane cell apparatus used during fouling experiments 52
Figure 20: Reaction carousels used to carry out optimization and screening of the reaction conditions 53

Figure 21: Reaction scheme of the Suzuki coupling of 3-chloropyridine and phenyl boronic acid 54
Figure 22: Reaction scheme of the kinetic resolution of 1-phenylethanol catalysed by free lipase. 55
Figure 23: (A) Conversion % of 3-chloropyridine over time for reaction IASC65. Standard Reaction conditions: 1 eq. 3-choloropyridine, 1 eq. phenylboronic acid, 2% mol of $Pd(OAc)_2$. Offline NMR acquisition: data are average of 2 experiments. (B) Evolution of the 3-chloropyridine and 3-phenylpyridine concentration over time. Reaction conditions: 1 eq. 3-choloropyridine, 1 eq. phenylboronic acid, 2% mol of $Pd(OAc)_2$. Online NMR monitoring was performed at the Dynamic Reaction Monitoring facility (DReaM) at the University of Bath. 60
Figure 24: (A) Illustration of the conversion of 3-chloropyridine over time before the dead-end filtration (Reaction I), re-initiation after the first filtration (Reaction II) and re-initiation after the second filtration (Reaction III), Standard reaction conditions: 1 eq. 3-choloropyridine, 1 eq. phenylboronic acid, 2% mol of $Pd(OAc)_2$, Offline NMR acquisition: data are an average of 2 experiments. (B) Evolution of 3-chloropyridine and 3-phenylpyridine concentration over time in standard conditions and re-initiation without dead-end filtration of the post- reaction mixture. Online NMR acquisition was performed at the Dynamic Reaction Monitoring facility (DReaM) at the University of Bath. 62
Figure 25: EDS spectrum and mapping of fouled D500 membrane after 3 cycles of filtrations of PdXPhos catalysed Suzuki coupling 64
Figure 26: % loss of 3-chloropyridine for 2%mol of Pd catalyst and 5% mol of Pd catalyst. Reaction is re-initiated by adding fresh substrates after reaching complete conversion, the crude mixture is not filtrated with membranes. 65
Figure 27: Concentration (mM) of 3-chloropyridine and 3-phenylpyridine over time. Reaction conditions: 2 eq. 3-Chloropyridine, 1 eq. phenylboronic acid. The reaction is initiated by $Pd(OAc)_2$. The catalyst is reused 3 times by re-initiating the reaction at 60 min, 180 min and 240 min with 1.7 eq. of CsOH, 1 eq. phenylboronic acid and 2 eq. of 3-chloropyridine. Offline acquisition. 66
Figure 28: Conversion % of (R)-1-phenylethyl acetate over time for reaction IAKR01 in toluene and IAKR02 in ethyl acetate catalysed by lipase. Offline NMR acquisition: data are an average of 2 experiments. 67
Figure 29: Visual stability of commercial PS600 and D500 after dead-end filtration in toluene and ethyl acetate respectively 69

Figure 30: Illustration of the conversion of 1-phenylethanol over time before the dead-end filtration (Reaction I), re-initiation after the first filtration (Reaction II) and re-initiation after the second filtration (Reaction III), Standard reaction conditions: 25 eq. 1-phenylethanol, 5 eq. vinyl acetate, 1.0 g lipase, Offline NMR acquisition: data are an average of 2 experiments. .70
Figure 31: Vibrational spectra of S-PANI and PANI 76
Figure 32: UV-VIS spectra of PANI powder and S-PANI powder in NMP (0.01 g/L).....77
Figure 33: SEM images of S-PANI powder at 2 different magnifications.....78
Figure 34 : SEM surfaces and cross-sections of (a,A) PANI and (B,b) S-PANI membrane...80
Figure 35: Contact angles as a function of time for PANI and S-PANI membranes 81
Figure 36: DSC thermogram register from 20 to 100 °C of S-PANI membrane. 82
Figure 37: Variations with temperature of storage (E') and loss (E") modulus of S-PANI membranes. 83
Figure 38: Comparison of S-PANI, S-PANI GA, S-PANI DCX and S-PANI TCL to characterise membranes after cross-linking.....84
Figure 39: XRD patterns of S-PANI membrane and S-PANI membranes cross-linked with GA, TCL and DCX. 85
Figure 40: Cross-section SEM images of (A) S-PANI GA (B) S-PANI DCX and (C) S-PANI TCL and (D) SPT170.Top Surface SEM images of (a) S-PANI GA, (b) S-PANI DCX and (c) S-PANI TCL and (d) SPT170.....87
Figure 41: Cross-section SEM images of the top surface layer of (A) S-PANI (B) S-PANI GA (C) S-PANI DCX and (D) S-PANI TCL. 89
Figure 42: Effect of DMF and DMAc on membrane stability. Picture is taken after half an hour from immersion in solvents. 90
Figure 43: Contact angles as a function of time for S-PANI DCX, S-PANI TCL and S-PANI GA membranes 92
Figure 44: Pure water fluxes for S-PANI (average of two membrane samples of batch MSP2300 and MSP2302),PANI (average of two membrane samples of the same batch MP20) S-PANI TCL and S-PANI DCX (average of two membrane samples from batch MSP2302), S-PANI GA (average of two membrane samples from batch MSP2303 and thermally cross-linked S-PANI membranes (data are average of two membrane samples of batch MSP2301) conditions: dead-end cell 2 bar and 20 °C. 94

Figure 45: Rejection curve of (A) S-PANI and chemically cross-linked S-PANI membranes: (B) S-PANI DCX, (C) S-PANI TCL and (D) S-PANI GA. Operation conditions are 1 bar, 25 °C, dead-end filtration. The red line at 90% marks the MWCO. 96
Figure 46: DMF permeance over time of (A) S-PANI TCL, (B) S-PANI DCX, (C) S-PANI GA. Operation conditions are 5 bar, 25 °C, dead-end filtrations. The same membrane sample was used twice. 97
Figure 47: Time dependent flux of S-PANI, PANI and S-PANI GA membranes tested in cross-flow with BSA 99
Figure 48: Cyclic voltammetry of (A) S-PANI and S-PANI/GO membranes from -0.2 V to X0.8V. and (B) additional voltammograms of S-PANI GO membranes taken at wider potential windows. 103
Figure 49: Picture of the top surface and bottom surface of S-PANI and S-PANI GO membranes. 104
Figure 50: SEM Surfaces and cross-sections of S-PANI/GO membranes 106
Figure 51: Composition paths of a casted film immediately after immersion (t < 1 s) showing (a) instantaneous demixing and (b) delayed demixing; T and B represent top and bottom of the film, respectively [191] 111
Figure 52: Top surfaces of (A) SPWT and (B) SPHX membrane 113
Figure 53 SEM surfaces and cross-sections at different magnification of (A-C) SPWT and (D-F) SPHX. 115
Figure 54: Contact angle over time of SPWT and SPHX membranes. Data are average of 3 samples. 116
Figure 55: Mass swelling degree of SPHX and SPWT membranes plot against Hansen solubility parameters[54, 198] 118
Figure 56: MWCO curves for SPHX and SPWT membrane in water using PEGs. Filtration conditions: 25 °C and 20 bar for SPHX membrane and 25° and 1 bar for SPWT membrane. Data are averages of 2 membrane samples. 119
Figure 57: MWCO curves for SPHX membrane in water using PPGs. Filtration conditions: 25 °C and 20 bar Data are average of 2 membrane samples. 120
Figure 58: Rejection curves for SPHX membranes in toluene, acetone and 2-propanol. Operating conditions are 30 bar and 25°. 122
Figure 59: Correlation between i) PPGs rejection of SPHX membrane in toluene, acetone, 2-propanol and water and ii) the mass swelling degree of the membrane in the same solvents plot against the Hansen solubility parameters. 123

Figure 60: Permeance of (A) SPWT and (B) SPHX membranes in different solvents. Filtration conditions were i) 2 bar for SPWT and ii) 20 bar for SPHX. Data in water are average of 2 membrane samples belonging to two different batches. 124
Figure 61: 1H NMR spectra showing the evolution of the Suzuki coupling reaction when the conversion of 3-chloropyridine is not complete. Offline acquisition. Reaction IASC57, conditions: 1 eq. 3-choloropyridine, 1 eq. phenylboronic acid, 2% mol of $Pd(OAc)_2$. 154
Figure 62: ^{1}H NMR spectra showing the evolution of the conversion of 3-chloropyridine over time for reaction IASC65. Standard Reaction conditions: 1 eq. 3-choloropyridine, 1 eq. phenylboronic acid, 2% mol of $Pd(OAc)_2$. 155
Figure 63:1H NMR spectrum of the reaction IAKR01in toluene - kinetic resolution of 1-phenylethanol mediated by lipase. Reaction conditions: Pseudomonas lipase (1g), 1-phenylethanol (5 mmol), vinyl acetate (25 mmol) and 1,3,5-TMB (1 mmol) as internal NMR standard. 156
Figure 64: ^{31}P NMR spectra showing the shift of the peak of the XPhos ligand in different stage of the catalytic cycle. The samples were prepared by dissolving XPhos (0.16 mmol) and $Pd(OAc)_2$ (0.08 mmol) in 5 ml of butanol. 0.5 ml of the solution was then collected in an NMR tube and analysed by ^{31}P NMR on 500 MHz Bruker instrument using the solvent suppression technique. 157
Figure 65:FTIR spectra showing XPhos (red), $Pd(OAc)_2$ (black) and the $Pd(OAc)_2$ -XPhos mixture (blue)..... 158
Figure 66: Example of MALDI spectrum of the S-PANI powder showing its chemical composition based on the elemental analysis. The data were obtained using a Bruker AutoFlex MALDI coupled with Time of Flight (TOF) mass spectrometer. The sample was prepared via solventless technique [201]. S-PANI and a matrix (DHB) were used in molar ratio 1:30 and mixed and ground for 15 minutes. The prepared ground sample was then spread out on the plate and then any excess was removed in order to obtain a thin film ready to be analysed. Spectra were generated with an acceleration voltage of 19 kV and were the average of 200 laser shots. 158
Figure 67:SEM surface and cross-section of SPHX membrane prepared via phase inversion in hexane. Fabrication conditions: S-PANI 21% wt 4.5 g NMP, 1.0 g 4-MP and 300 µm thickness. 159
Figure 68:Picture displaying the bottom surface of SPHX membranes prepared via phase inversion in hexane using different concentration of 4-MP and NMP in the dope solution and different thickness. Fabrication conditions are reported in Table 8..... 160

Figure 69: FTIR spectra of thermally cross-linked S-PANI membranes. 160
Figure 70: Change in Young Modulus E' with temperature for chemically cross-linked S-PANI membranes 161
Figure 71: Additional PPG rejection curves for S-PANI TCL membrane in 2-propanol. Filtration condition: 5 bar. Permeance is 1.3 L m^{-2} h^{-1} bar^{-1}.....162
Figure 72: Typical flux profile of initial period for filtration in dead-end cell of S-PANI, PANI and chemically cross-linked S-PANI membranes. Operation conditions: 1 bar and 25 °C. .163
Figure 73: Additional PPG rejection curves for S-PANI TCL membrane in acetone. Filtration conditions: 6 bar. Permeance is 3.7 L m^{-2} h^{-1} bar^{-1}. 164
Figure 74: Fouling experiment using HA and SPHX membrane. Filtration conditions: 30 bar. 164
Figure 75: Calibration curve of the UV-Vis Bradford Essay of the lipase in the permeate samples from the semi-continuous kinetic resolution of 1-phenylethanol in solvents. 165
Figure 76: Calibration curve of the UV-Vis analysis of $Pd(OAc)_2$ in the permeate samples from the semi-continuous Suzuki coupling nanofiltration in dead-end cell. 165
Figure 77: FTIR spectra of PANI PAMPSA membrane, PPDCX membrane and PPHX membrane.....170
Figure 78: DMF stability - 24h immersion test. From left to right: PANI PAMPSA membrane (20% wt NMP/4-MP, PANI PAMPSA membrane (20%wt NMP/4-MP/THF), PANI PAMPSA membrane (20% wt NMP), PPDCX01 (20%wt NMP/4-MP), PPDCX02 (20% wt NMP/4-MP/THF). 171
Figure 79: SEM surface and cross-section of (A) PANI PAMPSA membrane prepared from a solution of 20 %wt PANI PAMPSA in NMP, 4-MP and THF, (B) PPDCX prepared from a 20% wt solution of PANI PAMPSA in NMP, 4-MP and THF and later cross-linked for 3 days in 0.2M DCX, (C) PPHX prepared from a 20% wt solution of PANI PAMPSA in NMP, 4-MP and THF. 173
Figure 80: Evolution of contact angle with time of PANI PAMPSA, PPHX, and PPDCX membrane. 174
Figure 81: PPG rejection of the PPHX and PPDCX in acetone. Filtration condition is 20 bar, 20 °C in dead-end cell. 175
Figure 82: PPG rejection of the PPHX and PPDCX in 2-propanol. Filtration condition is 35 bar, 20 °C in dead-end cell for PPHX membrane and 20 bar, 20 °C in dead-end cell for PPDCX membrane. 176

List of tables

Table 1: Main features of conventional separations and membrane processes. Adapted from [2] ---------- 5

Table 2: Polymers used to prepare ISA membranes and their application as NF or UF membrane Adapted from ref.[27] ----------13

Table 3: Application of nanofiltration membranes in organic solvents and conventional used techniques ----------18

Table 4: List of transition metal complexes separated with membranes and type of reaction 19

Table 5: MW of commercial grade oligomers used ----------36

Table 6: Technical specifications of flat sheet nanofiltration membranes ----------37

Table 7: Screening of thickness, concentration, and composition for preparation of S-PANI membranes ----------39

Table 8: Optimisation of membrane fabrication conditions----------40

Table 9: Optimization conditions for thermal cross-linking of S-PANI membranes----------46

Table 10: Solvent gradient used during the HPLC elution of PPG mixture ----------50

Table 11: Standard concentration of the calibration curves for BSA and HA----------50

Table 12: Performance of D500 membrane in n0butanol/H_2O 5:1 and during filtration of the post-reaction mixture.----------63

Table 13: Performance of D500 membrane in Ethyl acetate and PS600 membrane in toluene during filtration of the post- reaction mixture. ----------68

Table 14: Atomic % and weight% of S-PANI powder ----------78

Table 15: % Weight loss data for S-PANI membranes and S-PANI GA, S-PANI TCL and S-PANI DCX membranes in different organic solvents. Data were collected after 1 month of soaking in the chosen solvent. ----------91

Table 16: Fouling indexes for S-PANI and PANI membranes related to the first cleaning-fouling cycle.---------- 100

Table 17: The conductivity of the prepared S-PANI-GO and S-PANI membranes was tested using a 4-probe conductivity meter by applying a current of 10 mA. The data are an average of 2 membrane samples. Data from PANI EB and PANI doped with PAMPSA are also reported. ---------- 101

Table 18: Properties of S-PANI/GO and S-PANI membranes ---------- 105

Table 19: Swelling degree in different solvents of SPHX and SPWT membranes. Results are the average of two experiments.---------- 117

List of publications

Amura, I., Shahid, S. & Emanuelsson, E. A. C., 17 Oct 2018, Advanced Materials for Membrane Fabrication and Modification. Gary, S., Tsuru, T., Cohen, Y. & Lau, W-J. (eds.). 1 ed. Taylor and Francis, p. 51-70 20 p.

Amura, I., Shahid, S. Sarihan, A., Shen J., Patterson D. A., Emanuelsson, E. A. C., Fabrication of self-doped sulfonated polyaniline membranes with enhanced antifouling ability and improved solvent resistance, Journal of Membrane Science, 2019, 117712, ISSN 0376-7388, https://doi.org/10.1016/j.memsci.2019.117712.

Chapter 1

Introduction

The increasing world population and the way manufactured goods are produced and consumed have had a significant effect on the environment [1]. Membrane separation processes have the potential to replace conventional energy-intensive techniques to improve the performances and the efficiency of reactive processes. Hence, they have found applications in many industrial sectors such as food, chemical manufactures, pharmaceuticals, wastewater treatment and biomedical applications [2]. In a chemical and pharmaceutical industry, common synthetic routes occur in chemically challenging environment in which the size of the involved molecules, such as catalysts and products and impurities is often very small (with molecular masses of 200-1000 g/mol). Extensive work-up is required during the downstream process to achieve high product purity [3]. Organic solvent nanofiltration (OSN) membranes allow the separation of small molecules from organic reaction streams, and could increase catalyst productivity [4], reducing product contamination. Hence, nanofiltration membrane are considered a greener alternative for their low energy demand, and limited generation of waste [5, 6].

In membrane processes, the key challenge is the high tendency to fouling and concentration polarisation, which negatively affect membrane performance over time and limit their applications [7, 8]. Because of the deposition of macromolecules or suspended particles, the yield of permeate decrease, higher pressures are required to achieve the same flow rate and additional chemical procedures are necessary to restore membrane flux, increasing the overall costs. [9, 10]. In the last two decades, research has focused on overcome the compatibility in harsh reaction conditions and fouling.

Polyaniline (PANI) is a conducting polymer that has been widely used in membrane technology because of its environmental stability, low cost and its

interesting redox chemistry [11-13]. The porosity in PANI can be induced through doping with small or large acid dopants. However, the most common used acid dopants were found to leach out of the membrane during filtration leading to worse membrane performance [11, 14]. Besides, the stiffness of the PANI backbone represents an obstacle for its solubility and further processing, and the current de-doping/re-doping approach only partially improve the polymer solubility [15]. A common route to improve PANI solubility is the addition of sulfonic groups to PANI to form S-PANI, resulting in a permanent modification and doping of the system [16, 17]. Chemical binding keeps the sulfonic groups in proximity with the nitrogen of the main chains, enhancing the stability of the polymer over a wide range of pH. However, this self-doped PANI readily forms a gel like structure, making it hard to form a membrane; hence, studies so far have reported blends with other hydrophobic polymers before casting to prepare low fouling ultrafiltration membranes [16, 18-21]

1.1 Overall project and aims

This project will investigate self-doped S-PANI as material to prepare novel nanofiltration membranes. The focus will be to understand the role of sulfonic groups on membrane morphology, performance in water and solvents, fouling behaviour, and electrical responsiveness. The produced membranes could be applied to different applications and chemical environments to develop more efficient chemical processes.

1.2 Structure of the thesis

The thesis is divided in seven chapters:

- Chapter 1 is the Introduction of this work and outlines the motivations of this research.
- Chapter 2 reports the background of this work, starting with an overview of membrane basic principles. Thereafter, the focus is on polymer membranes, and their fabrication methods and applications. The chapter

concludes with a gap in the literature analysis and the overall and the specific objectives to achieve the aim.

- Chapter 3 Outlines methods and materials for the preparation, characterisation and testing of the membranes.

Chapter 4 to Chapter 6 are the Results and Discussion sections and comprise of the following:

- Chapter 4 describes the benchmarking of commercial nanofiltration membranes with metal and enzyme catalysed reactions focussing on membrane performance and catalyst lifetime.
- Chapter 5 focuses on the fabrication of self-doped S-PANI membranes, the effect of thermal and chemical cross-linking on membrane properties and performance as well as the conductivity.
- Chapter 6 focuses on the fabrication of S-PANI membranes by changing the composition of the coagulation bath during the preparation process.
- Chapter 7 outlines the overall conclusions and the future work.

Chapter 2
Background

2.1 Overview

This chapter summarises pressure driven membrane processes, preparation techniques of polymeric membranes and advanced polymer membrane systems with a focus on S-PANI as versatile and functional membrane material.

2.2 Membrane filtration

2.2.1 Introduction

Membranes are selective barriers that regulate the transport of species between two compartments and allow the separation of components with different physical/chemical properties. The driving force that permit permeation of a liquid or gas phase through a membrane can be pressure, concentration or potential [2]. A membrane divides a mixed fluid stream, feed, in two streams with different features: one is the fraction that contains all the solutes unable to be transported through the membrane and it is called retentate (r) or concentrate. The permeate or filtrate, is instead the fraction able to pass through the barrier, with the right characteristics to be permeated [22]. Membranes are used for both gas and liquid separation, but the scope of this thesis will limit to the preparation of membranes for separation of solutes from liquid streams.

Table 1: Main features of conventional separations and membrane processes. Adapted from [2]

Other separations	Membrane processes
– Complex separation mechanism	– Process based on molecular size/weight
– May require additional solvents	– No additives are necessary
– May involve waste production	– No additional waste is involved
– Expensive for low concentrations/azeotropic conditions	– Require modest energy and have relatively low running cost
	– Flexible process with tailor-made membranes

2.2.2 Membrane performance

Typically, the performance of a membrane is determined by permeance (characterized by trans-membrane flux) and selectivity[23]. The first one describes the rate at which the permeate flows through the membrane whereas the selectivity is defined by the ability of the membrane to allow certain species to pass while rejecting others. Membrane flux is defined as follow:

$$J = \frac{V}{A \times \Delta t} \quad (1)$$

Where J is flux, A is the effective surface area of membrane, V is the volume through membrane and Δt is the time. The flux can be affected by the nature of the membrane used (material and structure) and external factors (pressure, temperature and concentration). Filtrations at different applied pressures can be compared by using the membrane flux normalised for the pressure:

$$Permeance = \frac{J}{\Delta P} = \frac{V}{\Delta P \times A \times \Delta t} \quad (2)$$

The ability of the membrane to discriminate between different molecules is expressed as rejection of these solutes:

$$Rj = \left(1 - \frac{Cp}{Cf}\right) \times 100 \quad (3)$$

Where *R*j is the rejection of membrane, *C*f is the solute concentration in the feed and *C*p is the solute concentration in the permeate. The value of the rejection varies between 0% (non-selective membranes) and 100% (complete retention of the solute). Often, membranes are described by their molecular weight cut-off MWCO that is defined as the molecular weight of the reference solute that is rejected by 90% [24, 25]. A solute with a higher MW than the MWCO will get a higher rejection [26].Figure 1 shows the MWCO curves obtained by plotting the rejection of reference solutes t against their molecular weights. An ideal MWCO curve should have a sharp cut-off, representing a high separation selectivity, whilst a shallower slope means the membrane does not separate molecules distinctively. The MWCO values are obtained from rejection experiments and therefore they depend on the solutes and solvents characteristics and the experimental operating conditions [27].

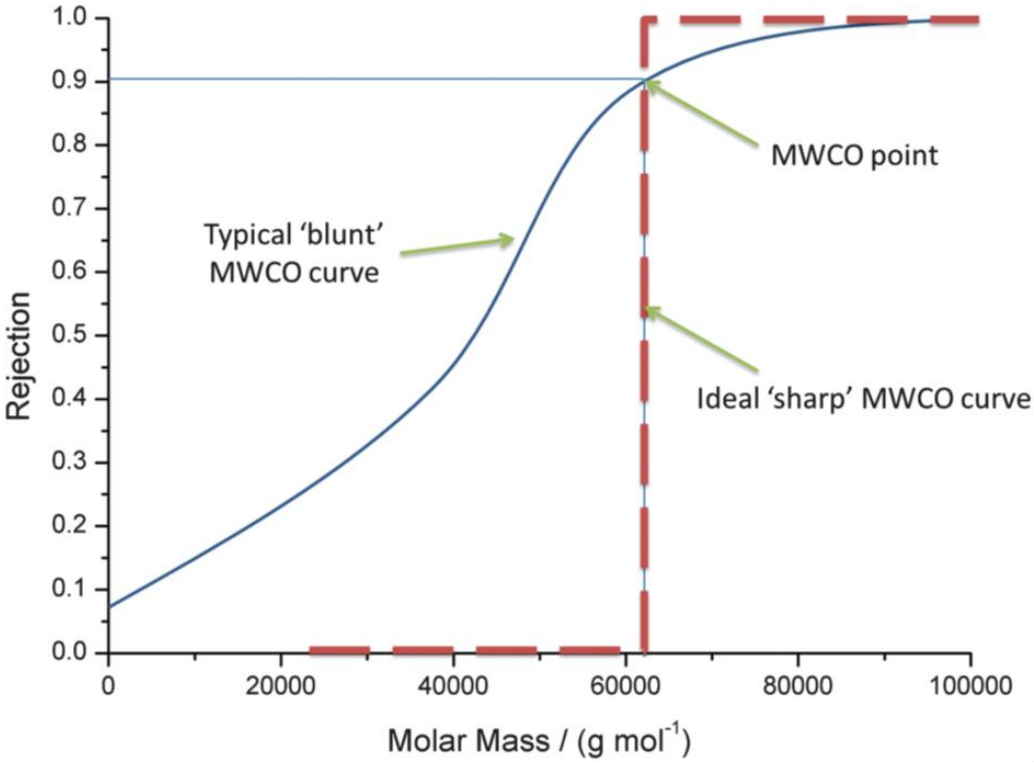

Figure 1: MWCO curves: ideal *versus* typical curve [2]

2.2.3 Classification of membrane filtration processes

Membrane processes for separation of liquids typically are microfiltration MF, ultrafiltration UF, nanofiltration NF, reverse osmosis RO (Figure 2). MF membranes have the largest pore size with diameters between 0.1 and 2 μm, operating pressures below 2 bars and can be used as pre-filtration of UF process in the wastewater treatment or for the retention of proteins from the biochemical solutions. UF membranes can retain molecules with diameter ranging from 2 to 100 nm and the membranes have operating pressures between 1 and 10 bar. UF membranes are used in the removal of solids, bacteria, microorganisms and natural organic material [28]. NF membranes have pore sizes up to 2 nm and a MWCO of 200 to 1000 g mol^{-1}. The operating pressures can vary from 5 bar to 40 bar. Nanofiltration has been proposed as an alternative technology to perform concentration, salt/solvent exchange, catalyst recovery and solvent recycling [29]. RO membranes have dense separation layers without distinct pores and

only solvents permeate. The RO process is effective in removing dissolved matters and monovalent ions, and found application in desalination of seawater and brackish water [30].

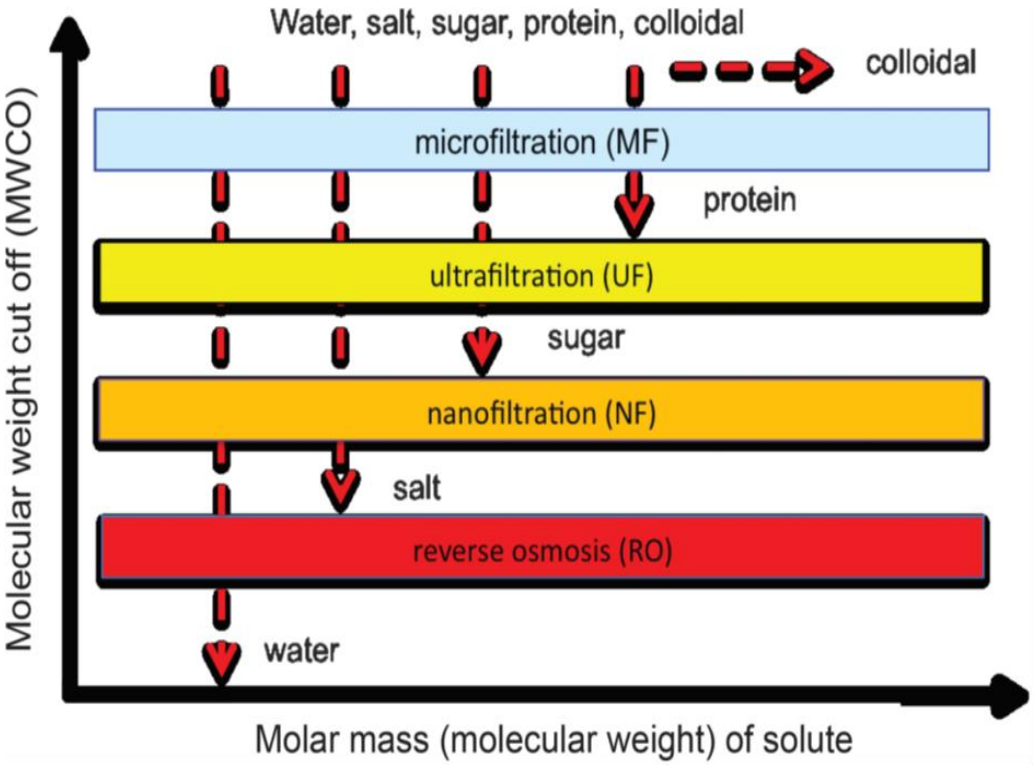

Figure 2: Different pressure-driven membrane processes [31]

2.2.4 Filtration modes

In membrane processes there are two main modes of filtration: i) dead-end and ii) cross-flow (Figure 3). The dead-end filtration unit is usually employed in laboratory settings and not scaled up to an industrial scale. The pressure is applied to force the reactants and products through the membrane and because no retentate stream is involved, the operation is termed “dead-end”. Cross flow membrane filtration is often used to pilot scale and, as for the dead-end unit, the pressure is applied to allow the separation of the solutes. The feed flows across the membrane and only a fraction is collected as permeate whilst what is left in the system is the concentrate.

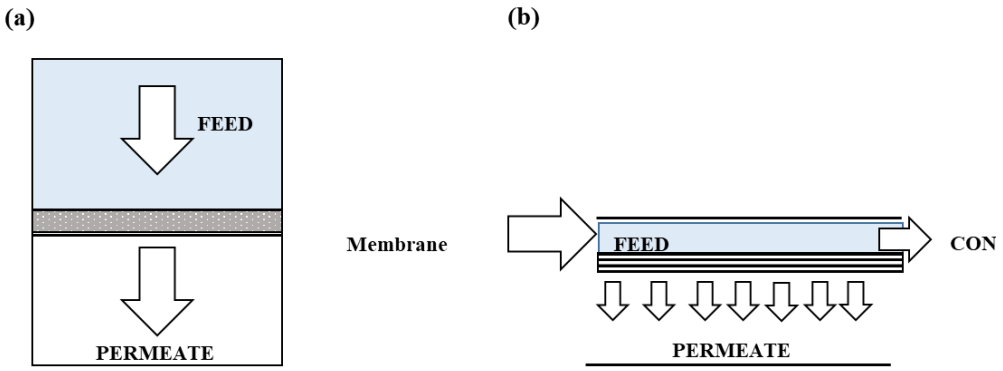

Figure 3: Membrane filtration modes: (a) Dead-end and (b) cross-flow filtration

2.2.5 Theoretical models

Conventionally, solute and solvent transport through membranes is explained with three mechanisms: i) the pore flow model, ii) the solution diffusion model and iii) the Donnan exclusion model. Each of them is briefly described.

2.2.5.1. The pore flow model

This model is used to describe transport of solutes through porous membranes such as UF and MF. The separation is based on pressure-driven convective flow through tiny pores and the selectivity of the membrane depends from the exclusion (because of size, shape and charge) of the solutes from the pores. The equation that describe this model is the Darcy's Law [32] (Equation 4):

$$J_i = K' c_i \frac{dp}{dx} \qquad (4)$$

where J_i is the flux of a component *i*, *dp/dx* is the pressure gradient in the porous membrane, and c_i is the concentration *i* in the membrane and K^i is the coefficient associated with the nature of the membrane.

2.2.5.2. The Solution diffusion model

This model describes the chemical potential across the membrane as a concentration gradient and it is used to defined transport through pore-less membranes such as RO membranes [32]. The separation of different solutes is possible because they dissolve in the membranes differently and diffuse at different rates. The equation that quantitatively describes this model is the Fick's first law (Equation 5).

$$J_i = -D_i \frac{dc_i}{dx} \tag{5}$$

Where *Ji* is the flux of a component *I*, D_i represents the diffusion coefficient and dc_i/dx is the concentration gradient across the membrane.

2.2.5.3. Donnan exclusion

The Donnan exclusion mechanism is applied to the permeation of charged molecules through a charged or neutral membrane. Charged membranes are made of functional polymers such as conducting polymers or by the co-addition of acidic groups. According to this model, charged groups exclude ions of the same charge and in particular, multivalent ions, but they are freely permeable to ions of opposite charge. The parameters that affect the magnitude of Donnan exclusion and the selectivity of the membrane are i) the concentration of fixed charged or capacity, ii) the degree of swelling, iii) the cross-linking density, iv) and the ion charge density. Furthermore, the density of the polymer network, the hydrophilicity and hydrophobicity and the morphology of the membrane itself need to be taken into account when describing the overall membrane performance [33]. Transport through NF membranes are often described using the Donnan exclusion model.

2.3 Membrane materials and preparation methods

2.3.1 Introduction

Membranes can be prepared from polymers, inorganic or ceramic materials and a mixture of the two called mixed matrix membranes MMMs. Polymer membranes can be conveniently tailormade for a wide range of applications because of their easy-tuneable properties through synthesis, the ready availability of many naturals and synthetic polymers and a cheaper cost compared to ceramic materials [23]. Ceramic materials for the preparation of OSN membranes have shown great potential due to their advantages over polymeric materials, such as a superior solvent stability, and their resistance to compaction and swelling. However, the high costs and their low organic solvent rejection limit their application [34]. Furthermore, ceramic and MMMs membranes usually require multi steps synthesis and have the significant disadvantage of membrane aging and sensitivity to chemical cleaning. In general, the selection of the material for the fabrication of new membranes depends on the separation task and the consequent operating conditions and chemical/mechanical stability. The motivation of this project is preparing membranes based on a polymer for NF applications; therefore, the following sections will cover fabrication methods and challenges of polymer membranes and will not focus on other membrane material.

2.3.2 Type of membranes

The two main types of polymer membranes that can be prepared are integrally skinned asymmetric membrane (ISA) and thin film composite (TFC) membrane), which are displayed in Figure 4.

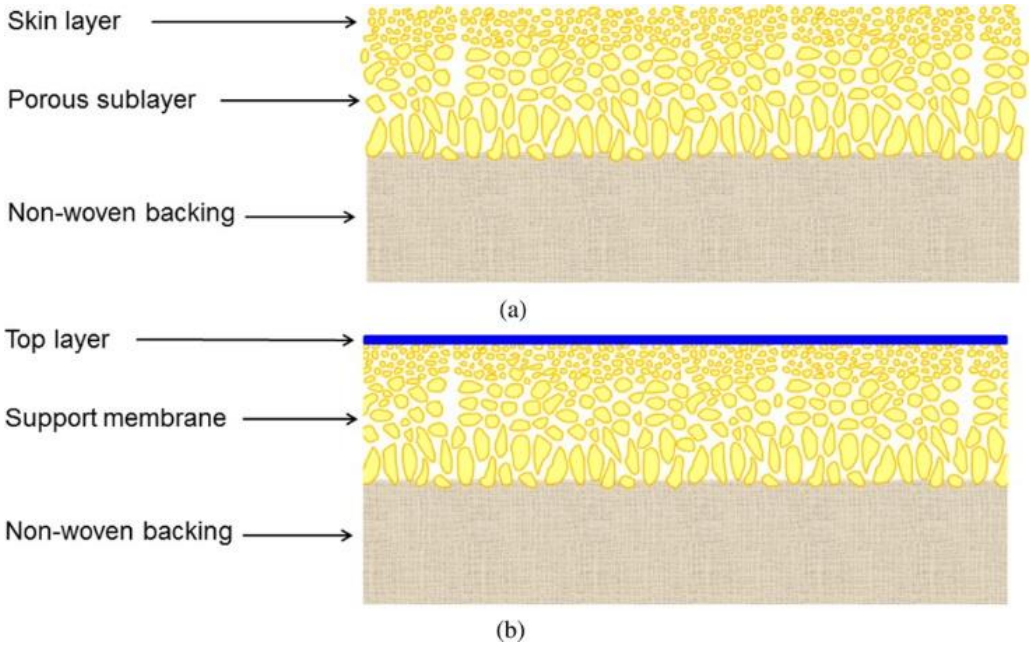

Figure 4 Schematic representation of an (a) integrally skinned asymmetric membrane and (b) thin film composite membrane. Adapted from ref.[27]

2.3.2.1. Integrally skinned asymmetric membranes ISA

The structure of an ISA membrane comprehends a top skin layer and a more porous sublayer of the same composition (Figure 4a). The top skin layer is formed at the same time as the supporting layer and it affects the selectivity and permeance of the prepared membrane. ISA membranes have been used for both NF and UF membranes and various polymeric materials have been employed (Table 2). The main route to prepare asymmetric membranes is via non-solvent phase inversion that is described in 2.3.3.2.

Table 2: Polymers used to prepare ISA membranes and their application as NF or UF membrane Adapted from ref.[27]

Polymer	Membrane application
Polyacrylonitrile (PAN)	UF[35], NF[36]
Polyimide PI	UF[37, 38],NF[39, 40]
Polyaniline PANI	UF[25, 41],NF[12, 13, 42]
Polybenzimidazole PBI	NF[43, 44]
Poly (ether ether ketone) PEEK	UF, NF[45]

2.3.2.2. Thin film composite membranes TFC

TFC membranes have an ultrathin active layer (typically 0.2 mm) on a top of a chemically different porous support (Figure 4b). The top barrier layer properties can be independently optimised from that of the support layer to maximise the overall membrane performance. A considerable research work has been done so far to develop NF and RO membranes as TFC membranes, particularly after the introduction of interfacial polymerisation approach to produce a thin polymeric layer onto a substrate [46, 47]. The method is based on the reaction between an aliphatic/aromatic diamine and an acid chloride monomer. The advantage of this fabrication method is that the properties of the bottom substrate and the barrier film can be individually optimised to obtain the desired water permeation and solute rejection. However, one limitation is the low membrane resistance to high chlorine concentration, one of the main disinfectants used in water and wastewater treatment. The preparation of TFC membranes is beyond the scope of this project that will focus on preparing asymmetric membranes based on polyaniline derivatives.

2.3.3 Fabrication methods

Polymers can be used either as pure single-phase systems or as components of blends or as additives during membrane formation. Classic techniques such as solvent casting and phase inversion are generally employed [48] whilst surface modification can be performed to functionalise membranes for applications.

2.3.3.1. Solvent casting

The solvent casting process involves dissolving the polymers/copolymers in a preferred solvent and casting the obtained solution on a flat surface. The solvent is allowed to evaporate, and the resulting membrane is dried and cross-linked [49, 50]. Solvent casting is normally used with robust polymers and generate relatively thicker membranes. It is a successful technique to produce asymmetric membranes for RO, MF and UF applications; it requires that the chosen polymer is soluble in the preferred solvents and it is widely used to prepare composite materials.

2.3.3.2. Phase inversion

Most of the commercially available and lab researched polymeric membranes are prepared via non-solvent phase inversion technique (NIPS). It is widely accepted that the polymer is transformed in a controlled manner from a liquid dispersion to a solid film through a liquid-liquid de-mixing phenomenon. Typically, a solution containing the polymer, a solvent and additives is prepared until homogeneity is achieved. Then the solution is casted into a thin film and immersed for the desired time in a non-solvent bath. Upon immersion, solvent and non-solvent mix spontaneously according to their mutual affinity and the polymer solidifies [51, 52] as shown in Figure 5. Different de-mixing rate of the polymer – instantaneous or delayed - lead to different type of membrane structure and therefore it is possible to have a tailored morphology for a specific separation [53]. Instantaneous de-mixing is enhanced by higher mutual affinity of the solvent/non-solvent system and most likely membrane that is more porous will occur. In case of low affinity and delayed de-mixing, an asymmetric membrane is obtained. Membrane structure and performance are strongly influenced by the NIPS. The technique allows to obtain membrane with different morphologies and applications by changing the composition of the non-solvents or the temperature during fabrication. Different parameters are investigated such as composition of the casting solution (polymer concentration, solvent type, co-solvent/solvent weight ratio, non-solvent content), post-casting (evaporation

time) and immersion conditions (coagulation bath composition) [54-56]. For instance, it has been reported that the use of different coagulation bath systems such as water and ethanol caused significant differences in morphologies and characteristics of PVDF membranes [57]. For this reason, it can be considered a versatile fabrication method that generally produce much thinner membranes with less diffusive resistance compared to solvent casting. It is cheap and therefore widely applied to prepare asymmetric polymeric membranes, which can be further cross-linking in situ or through post-modification.

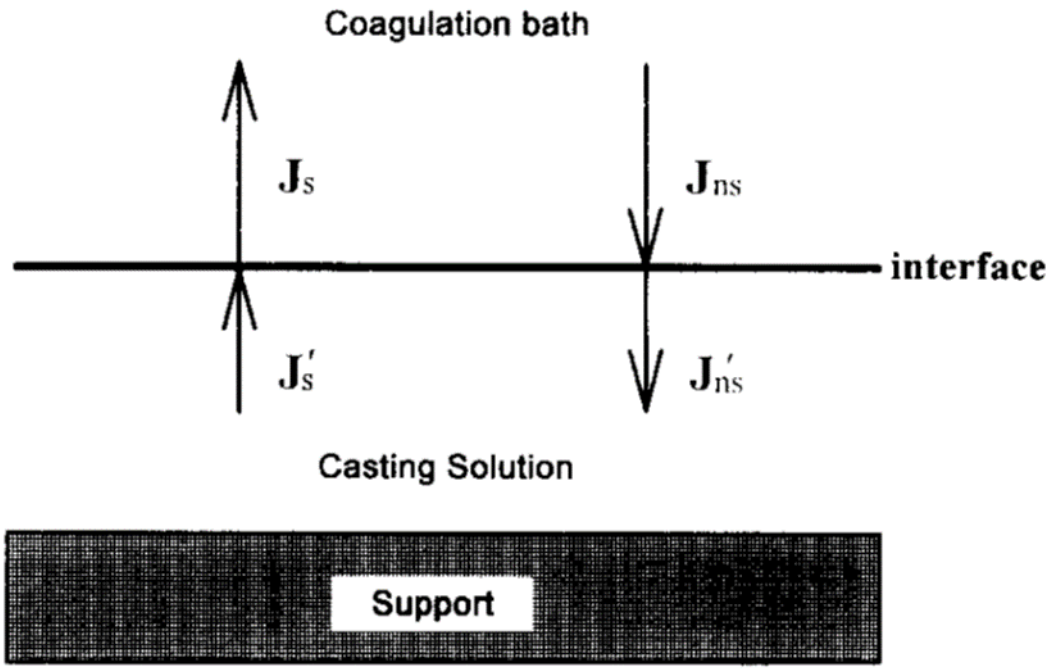

Figure 5: Fluxes of the non-solvent (Jns, Jns') and the solvents (Js, Js') at the interface between coagulation medium and the casting film (Adapted from [52])

2.3.3.3. Membrane surface modification

The properties of membrane surface (top layer) such as surface charge, hydrophilicity/hydrophobicity and surface roughness are the most important factors affecting permeation and separation performances of the membranes and determine the affinity of the membrane selective layer towards the solvent/solute [58]. Membrane surfaces are modified following two distinctive surface-selective approaches: surface grafting and surface segregation.

Surface grafting

Surface grafting can be achieved through the “grafting to” approach and the “grafting from” approach [49, 59]. The first one introduces end-functionalized polymer chains on the membrane surface, whereas in the “grafting from” approach the grafting reaction proceed by polymerization from the surface and polymer chains grow from initiator sites by monomer addition from solution. The result is the formation of a polymer brush layer on the membrane surface that introduce sensitive functionalities.

The “grafting from” modification is done using different methods that differs by the mechanism used for radical generation. The initiator can be a photo-initiator, or a redox species like in the photo-initiated polymerization and redox-initiated polymerization case, or the reaction can be induced by a radiation. Plasma-graft-filling and atom transfer radical polymerization represent two additional approaches.

The surface modification of a membrane by “grafting to” method is carried out by physical adsorption or chemical grafting. Physical adsorption involves coating of the membranes with a stimuli-responsive polymer, alternatively stimuli-responsive additives can be incorporated into thin film polymer composite coating that will be placed on the membranes. The modification of the membranes by chemical grafting results in immobilization of macromolecules onto the membrane surface by reaction of functional group of the membrane material, or photo-generated on it, and a reactive group of the additive polymer.

Surface segregation

Surface segregation has the inherent advantage of being an in-situ modification of the membrane during the phase inversion process, leading to the simultaneous modification of membrane internal pores and outer surface [60]. This method can be described as follow: an amphiphilic modifier is blended to the membrane-forming polymer in the casting solution and then, during phase inversion, the

hydrophilic unit is segregated to the membrane surface whereas the hydrophobic segments are entangled within the membrane matrix [61].

2.3.4 Applications of polymer membranes

Membranes have been applied in a wide range of chemical processes and some of the major uses are in i) the food industry, ii) the chemical manufacture, iii) wastewater treatment and iv) the pharmaceutical sector. The focus of this thesis is developing polyaniline-based membranes for use in organic solvents with potential for their use in resource recovery. Hence, the next section will cover high value products and catalysts recovery -both metal and biological- with membranes. Nanofiltration membranes are used to retain the small transition metal catalysts with MW<1000 Da, whereas biocatalysts are usually separated with UF membranes as these are large and most of the application is limited to enzymatic reactions in water where solvent resistant membranes are not necessary.

2.3.4.1. Resource recovery

Separation processes are of importance for the chemical and pharmaceutical industry as 50 to 90% of the capital invested involves separations [62]. Conventional processes for obtaining products or recovery of solvents/solutes are distillation, chromatography and recrystallisation. However, they are often part of intensive downstream processes that require elevated temperatures, solvent exchange, use of vacuum and phase change. Therefore, potential products degradation, solvent wastes and energy waste occur. NF membranes have been extensively studied and used for i) concentration processes, ii) solvent exchange, iii) purification, iv) catalytic processes (Table 3).

Table 3: Application of nanofiltration membranes in organic solvents and conventional used techniques

Application of nanofiltration membranes in organic solvents		
Type of process	***Application***	***Conventional used technique***
Concentration	Solute enrichment	Distillation
	Solvent enrichment	
Solvent Exchange	Pharmaceuticals	Chromatography
Purification	Removal of Impurity	Crystallisation
		Vacuum
		Chromatography
Catalytic process	Pharmaceutical	Chromatography
	Fine chemicals	Distillation

2.3.4.2. Recycling of homogeneous transition metal catalysts and biocatalysts.

Many organic syntheses of industrial relevance require homogeneous catalysts based on expensive transition metals to complete the reactions [63, 64]. The main difficulty is the separation of these catalysts from the reaction products, which required the use of waste-generating downstream processing. During these energy intensive work-up steps, high solvent volumes are used and often the ligands stabilizing the metal centre are lost. In this context, the use of nanofiltration membranes for catalyst recycling has demonstrated potential in process intensification in both homogeneous catalysis and enzyme catalysis [6, 65, 66]. In some cases, the catalyst requires chemical modification to be able to be retained by the membrane [67, 68]. This process aims at enlarging the catalyst by co-addition of long polymeric chains or organic functional groups to improve their rejections. One of the successful applications reports the coupling of Heck palladium catalysed reaction with a nanofiltration process which lead to substantial increase of the catalyst productivity, catalyst recycling and avoiding metal contamination of the products [66]. Table 4 reports the transition metal

complex retained using membranes and the relevant reaction in which they have been applied.

Table 4: List of transition metal complexes separated with membranes and type of reaction

Reaction	**Catalytic system**	**Membrane**
Heck coupling [4, 66]	Pd-phosphine	STARMEM™
	Pd-imidazolyne	MPF60
	Pd-quat	
	Pd-quat-MECN	GRACE SRNF
	$Pd(OAc)_2(PPh_3)_2$	
Enantioselective	Ru BINap	KOCH, MPF60
Hydrogenation[69]	Rh-EtDUPHOS	
Suzuki Coupling[70]	$Pd_2(dba)_3$-CH_3	STARMEM™ 122

As for transition metal catalysts, in many enzymatic reactions, batch or continuous, separation of the enzyme for reuse is challenging because the enzyme tends to interact with the membrane surface and be adsorbed in it leading to loss in performance. Membranes have been utilised to separate the reaction products from the enzyme and the substrate, allowing it to be retained and re-used [71, 72]. Due to the high MW of the enzymes used in these processes, the UF membranes are preferred and have served as efficient mean to retain the enzyme. In a work from Butterworth *et al.* [73] α-amylase from Bacillus subtilis is retained with no loss in enzyme activity over 30 hr in a UF enzymatic membrane reactor. However, many enzymes - such as proteases, lipases, and esterases -have found application in organic solvents showing excellent performance and retaining their catalytic activity [74]. Therefore, biocatalytic processes would benefit from the use of solvent stable and reliable membranes.

Despite the efforts in increasing the catalyst and biocatalysts productivity by developing semi-continuous or continuous membrane systems, some key issues, such as catalysts deactivation, solvent stability, low permeance and low

selectivity in organic solvents and type of fouling have not been fully addressed yet. Furthermore, the reaction conditions are not fully compatible with the membrane in use such as the temperature, the solvent in which the reaction takes place, or the presence of strong acid/basic group in the reaction mixture, limits the large-scale applications. Hence, a screening of the membrane and the reaction conditions is required to achieve a feasible process.

2.3.5 The fouling issue

Membrane fouling is responsible for the limited performance of membrane processes in both biocatalysis [72, 75, 76] and organocatalys [77]. Different type of fouling may occur depending on the nature of the particles: i) organic/biofouling ii) inorganic fouling and iii) multi fouling.

Organic and Biofouling

In natural organic matter fractions, the substances responsible for fouling are usually polysaccharides, amino sugars, polyhydroxy-aromatics and proteins. These usually accumulates in the internal and external membrane surface and the two main mechanisms that describes the phenomenon are membrane surface pore blocking and cake layer formation. The key factor is the membrane pore size and the size distribution of the foulants in the feed. If the foulants are smaller than the membrane pores, they are usually adsorbed onto the pore walls leading to pore constriction whereas the larger foulants block the pore entrance and the fouling shifts to cake formation [78]. For instance, Sueb *et all*. shows that during the xylan depolymerisation, the main factor affecting the performance of the enzyme reactor is internal pore blocking generated by the oligomers formed during the reactions [72]. Nevertheless, there is still a lack of understanding of fouling phenomena that limit the application of integrated membrane processes.

Inorganic Fouling

Inorganic fouling is caused by different inorganic salts and the most common are $CaSO_4$, $CaCO_3$, SiO_2 and $BaSO_4$. The inorganic fouling mostly happened when, because of the high concentration, they exceed the solubility limit at the

membrane surface [9]. During the inorganic fouling, also referred as scale formation, the two main mechanism of formation are crystallisation and particulate fouling. The former involves the precipitation of ions and their deposition onto the membrane surface whereas the latter occurs because of the convective transportation of the colloids to the membrane surface [79]. In particular, for non-porous membrane the particulate fouling results in the formation of the cake layer because the particles accumulate on the membrane surface. For porous membranes, the formation of the cake layer due to particulate fouling is a consequence of the pore blocking.

During membrane separation, the phenomenon of fouling is often due to the deposition of various foulants (proteins, salt, natural organic matter, microorganism) therefore depending on the membrane system, the nature of the feed and the filtration mode it is usually referred as multi-fouling.

2.3.5.1. Fouling mitigation

Numerous studies have focused on improving membranes long-term performance through chemical and physical cleaning with only partially restore of membrane original properties [19-21]. The importance of hydrophilicity for the prevention of the adhesion of organic matter has also been shown [80, 81], hence existing polymer membranes have been modified to achieve lower fouling by co-addition of hydrophilic polymers and zwitterionic materials that prevent the adhesion of organic matter [82]. These can be co-added by chemical or physical methods. Chemical modification mostly involves chemically induced grafting technique, plasma and UV treatment [83, 84] whereas physical methods involve coating and blending with hydrophilic polymers [19, 85]. Chemical modification has the advantage of being more stable, but it often involves the use of harsh chemicals and energy intensive methods that are not always compatible with large-scale applications. Physical modification is simpler, and the overall costs is generally less but the uniformity and reproducibility of the modification might be less effective [80]. An efficient membrane fabrication method that made use of the additive S-PANI for low fouling membranes was

reported in 2013 [19]. The study described the preparation of blended polysulfone PSf/S-PANI showing enhanced fouling resistance with respect to pure PSf membranes. Recent works introduce S-PANI as zwitterionic polymer because of its positive and negative charges distributed along the polymer chains. A PVDF/PANI membrane was successfully sulfonated to generate a novel zwitterionic surface for ultrafiltration used in sewage treatment [18]. The membrane showed excellent antifouling properties and it was confirmed that S-PANI has great potential as zwitterionic material for preparation of low fouling membranes. Other examples of membranes with incorporation of S-PANI [18, 86] were reported since then with a major focus on S-PANI as additive in ultrafiltration membranes for water separation. These studies have shown the feasibility of S-PANI as membrane material and its potential as readily available low fouling polymer.

2.3.6 Advance polymer membranes /stimuli responsive membranes

2.3.6.1. Overview

As reported in 2.3.5, polymer membranes have a propensity to fouling that irreversibly affect their performance and therefore their applicability. As this is the current main challenge, it has also been the starting point for the developing of smart membrane systems with externally tuneable properties. Due to the potential application of functional materials with reversibly switchable physiochemical properties stimuli responsive membranes based on "intelligent" polymers have rapidly gained attention [49]. These materials are considered superior compared to traditional systems because of the possibility of i) self-regulate the pore size and ii) surface properties in response to a specific environmental change. Tailored polymer systems are used in the fabrication of these membranes, for which properties can be reversibly tune upon the application of an external stimulus such as pH [87, 88], temperature [89], ionic strength [90] light [91, 92] electric [93, 94] and magnetic field [95] and chemical cues [96].

The polymer undergoes a reversible change, either physical or chemical in its properties, based on external stimuli and induce a macroscopic response in the membrane. Using stimuli allow specific conformational transition on a microscopic level and then the responsiveness occurs amplifying these transitions into macroscopically measurable changes in membrane properties (Figure 6). The mutual interactions among pore structure and change in conformation, polarity and reactivity of functional groups of the responsive polymers in the membrane bulk or its surface are the key factors that allow the responsiveness of the membrane [97]. In this work, PANI based membranes will be investigated and because its redox properties can be changed according to the electrochemical environment, the following section will cover electrically responsive polymers and membrane systems.

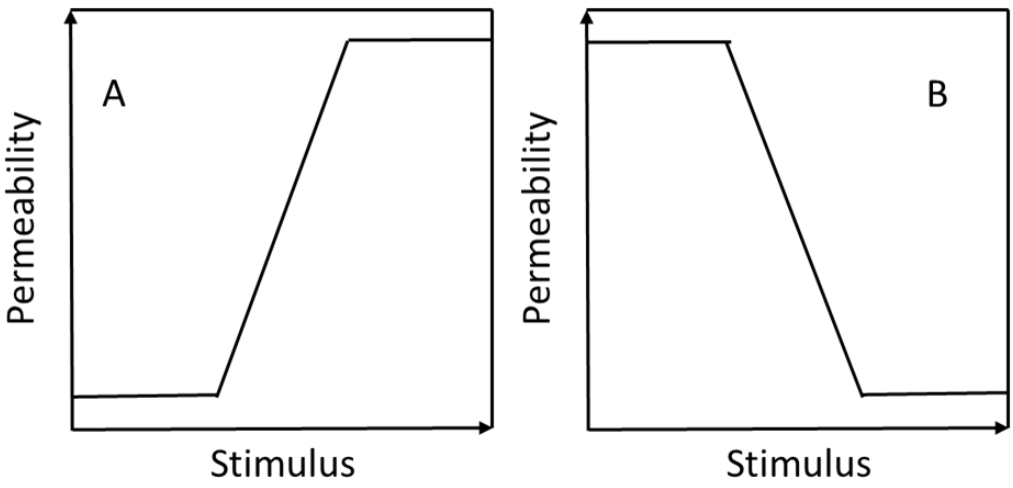

Figure 6: Example of positively (A) and negatively (B) responsive mechanism

2.3.6.2. Electrical responsive membranes

Responsive systems have been researched to overcome traditional membranes (fixed pore size and permeability) that failed to address technically challenging

and commercially attractive separations. In this context, electrical responsive membranes are particularly interesting because the electrical response is generally fast and do not influence the process environment as a change in pH or temperature. Membranes based on electrical polymeric systems have shown potential in water treatment, fuel cells, catalysts and sensors due to the possibility of combining the electrical conductivity of metals with the strength and processability of synthetic polymers [98, 99]. These electrical tuneable responsive membranes can be potentially used to obtain systems with controllable transport properties and in situ self-cleaning mechanism as demonstrated in recent studies [100, 101].

2.3.6.3. Mechanism

Generally, the responsiveness is associated with polymer chain conformation, that upon the application of an external stimulus change from a stretched conformation to a collapsed one and vice versa. These are structural rearrangements due to protonation and deprotonation of ionisable side groups [97] [102] or by the application of an external electrical stimulus [103] as shown in Figure 7. Electro responsive membranes can be also prepared from conducting polymers. Some representative conducting structures include PANI, polypyrrole PPy, polyacetylene and polythiophene. Among these, PANI and PPy are widely investigated in membrane fabrication for their interesting properties such as chemical stability and good processability [104]. These are membrane systems made responsive by changing the electrochemical state of the conducting polymer through doping (oxidation) and de-doping (reduction) [93]. Doping of the conductive backbone with negative charges/anions enhance the conductivity as dopants introduce a charge carrier into the polymer conjugated system by removing or adding electrons and re-localize them as polarons or bi-polarons (part of a macromolecular chain containing two positive charges in a conjugated system. The polaron structure is responsible for the transfer of the electric charge; when an electrical potential is applied, the polarons and bi-polarons start to move along the backbone, passing through the charge [94, 105].

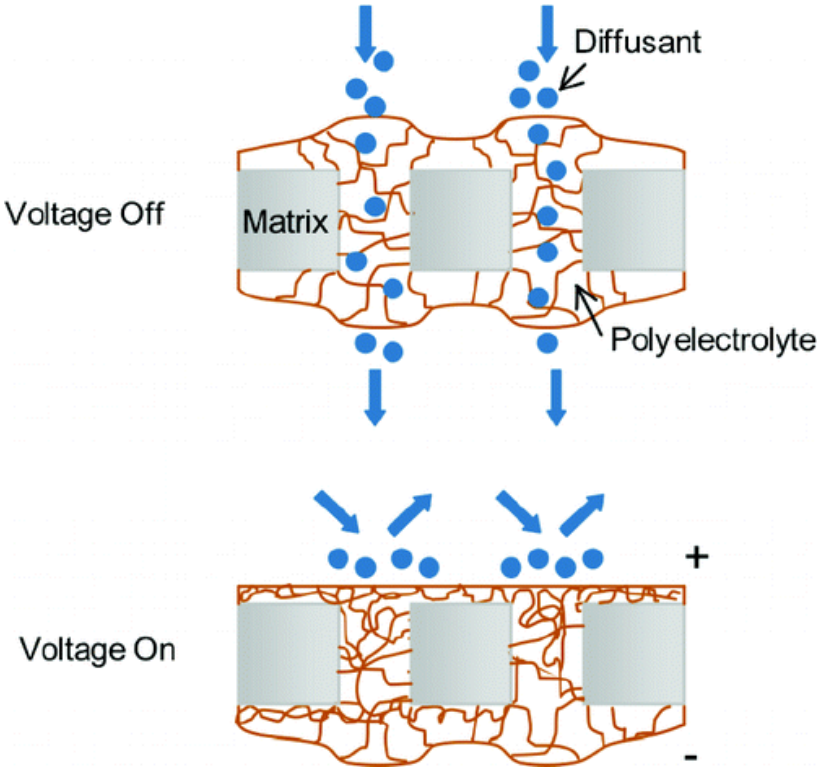

Figure 7: Schematic diagram showing the electrosensitive permeability in PAMPS gel-g-PETE nanocomposite membranes. Reproduced with permission from [103] Copyright (2007) American Chemical Society.

To enhance the conductivity and prepare high performance materials, composite systems with conducting materials such as metals, metalloids, non-metals, inorganic and organic/bioorganic compound have been reported [106, 107]. Among these, carbon materials have been intensively studied for the fabrication of membrane based on conducting polymer [97]. Typical carbon materials are carbon nanotube, graphene and graphite. All of them have been incorporated into PANI as conducting fillers [108]. Carbon nanotubes are allotropes of carbon with cylindrical structure and walls formed by graphene sheets with nanoscale diameters. CNTs membranes can be prepared as composites or self-supported systems, however the latter tend to have irregular pores and limited control over the pore size moreover potential leakage since CNTs are not chemically bonded. Large scale applications are limited by the high cost of the material itself. It has also been reported that PANI/ graphene composites may show better

conductivity of PANI/CNTs prepared with the same fabrication method [106, 109]. Furthermore, the PANI/graphite composite exhibits an electrical conductivity greater than either of the two compounds resulting from the increased carrier mobility [110]. However due to the small interspacing of graphite layers, it is often difficult to prepare this composite by simple intercalation, and graphite is usually chemically modified to expand the layers or graphene oxide is used instead because of its better processability [111, 112], [113].

2.4 Conducting polymers: self-doped sulfonated polyaniline membrane

2.4.1 Introduction

In the last twenty years, many studies have present polyaniline PANI as a desirable polymer for membrane fabrication because of its stability, simple chemical doping and the rather cheap cost with respect to other materials [11, 12, 114]. Since its first appearance in 1991 as film to separate mixture of gases [115], many examples of both UF and NF membranes have been reported in the literature [13, 116-118]. In this section the doping chemistry is covered, and then self-doping is presented. Synthetic methods of self-doped polyaniline and the application as membrane material will be finally covered.

2.4.2 Properties of PANI: chemical structure and doping mechanism

Polyaniline is a conducting polymer which possesses a conjugated system consisting of alternating single and double bonds (Figure 8).

Conductivity in polyaniline arises from this conjugated backbone where due to the strong delocalization, electrons are freely to move between atoms [104, 119].

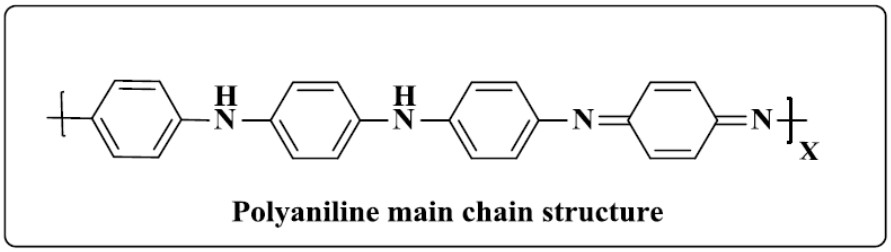

Figure 8: Scheme representing polyaniline main chain structure

Polyaniline possesses three different common structures, corresponding to three different oxidation states. The fully reduced leucoemeraldine PANI (x=1), the half oxidised emeraldine base EB (x=0.5) and finally the fully oxidise pernigraniline PANI (x=0). The conductivity can be enhanced by doping of the conductive backbone with negative charges/anions. Dopants introduce a charge carrier into the polymer conjugated system by removing or adding electrons and re-localise them as polarons or bi-polarons, and as an electrical potential is applied, the polarons and bi-polarons start to move along the backbone, passing through the charge [120].

Figure 9 reports the doping mechanism of PANI. The emeraldine base is the only form susceptible of chemical doping by a protonic acid, in fact the imide site can be protonated to form the bi-polaron. The bi-polaron then dissociates in two stable polarons giving the conductive emeraldine salt form of PANI. The acid dopants protonate the emeraldine base form without changing its oxidation state. Through base de-doping, the EB can be reformed [121, 122]. As mentioned above, dopants have a crucial role, since they introduce charge carriers into the polymer backbone making it conductive, but also it is studied to improve the processing of PANI. In fact, lack of solubility is associated with chain stiffness and the existence of a strong conjugated electron π system [123]. Classical dopants in the fabrication of polyaniline ranges from small mineral acids such as HCl, HBr, HNO_3, H_2SO_4 and H_3PO_4 to organic acids containing long alkyl side chains such as camphorsulphonic acid (CSA), dodecylbenzenesulfonic acid

(DBSA), sodium polystyrenesulfonate or p-toluenesulfonic acid (*p*-TSA) [124-126]. The key advantage with large dopants is that they ensure a good electrical stability because they do not leach out of the material if an electrical stimulus is applied [41]. Smaller dopants such as chloride ions, are less integrated in the polymer that sometimes become brittle and are not efficient as the large one, since they tend to volatise leading to de-doping of PANI [127]. Shen *et al*. recently reported the use of polyacids poly(4-styrenesulfonic acid) (PSSA) and poly(2-acrylamido-2-methyl-1-propanesulfonic acid) (PAMPSA) as dopants to prepare nanofiltration PANI membranes [42]. PSSA and PAMPSA possess flexible polymer backbone and sulfonic groups located at short distances along the chains. It is believed that PANI macromolecules form a double strand structure as resulting interpolymer complex [128]. In previous works from our research group, the performance of PANI membranes were compared with commercial membranes. It was observed that the small acid (e.g., HCl) doped PANI membranes showed much higher anti-fouling properties compared to solvent resistant commercial membranes but they lack the solvent stability and could not be used in harsh solvents [42, 129]. Additionally, doped PANI membranes tend to lose their antifouling properties as the small acid leached out during the filtration process.

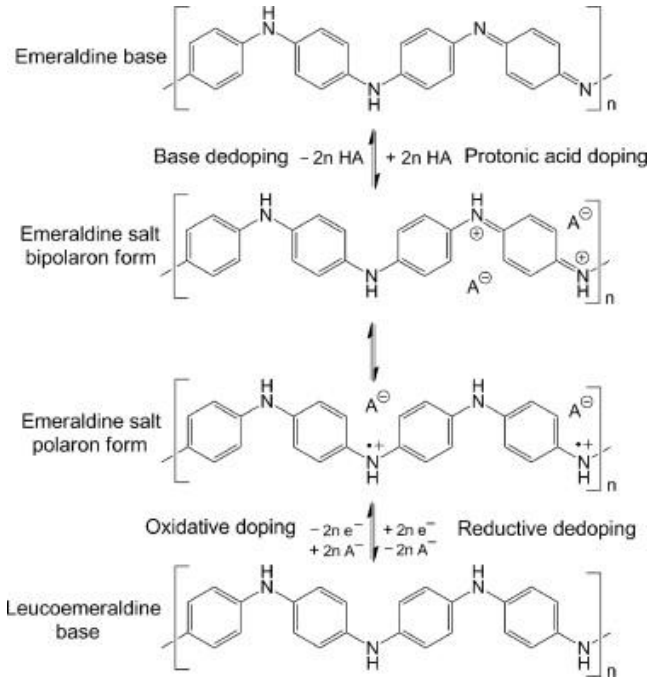

Figure 9: Schematic representing the doping of PANI [106]

2.4.3 Polyaniline derivatives: self-doped systems

The main disadvantage associated with PANI is inherent to its solubility and thus processability in solvents. The insolubility of PANI in common solvents is caused by chain stiffness and interchain interactions [130, 131]. For this reason, much research has focused on enhancing the polymer solubility through doping or modification of the monomer [16]. However, the addition of dopants affects the electrochemical properties of PANI, but the effect on the solubility is not always equally efficient [15]. The modification of PANI through synthesis has been reported to prepare PANI with enhanced solubility by incorporation of phenolic, carboxylic and sulfonic acid substituents. The incorporation of sulfonic acid groups in the polymer represents the simplest and cost-effective synthetic route as it does not require any catalyst and it can be performed in one synthetic step [132]. Furthermore, the sulfonic acid group is also a doping agent that is covalently bound to the benzene rings resulting in a six-member self-

doped ring. Sulfonated polyaniline was firstly reported and characterized by Yue and Epstein [16] in 1990 in their studies about self-protonic acid polyaniline and since then it has been used for various application such as batteries, H_2O_2 sensors, synthesis of nanofibers, additive in low fouling membranes and hydrogels [133, 134] [135, 136]. Current research has found that S-PANI has better performance, better processability in aqueous systems, improved thermal stability and good electrical properties. As the sulfonic group is covalently bound to the PANI backbone, so it is self-doped, there is no need for additional acid dopants.

2.4.4 Synthetic routes for self-doped sulfonated polyaniline

Through synthesis it is possible to achieve various degree of sulfonation or S:N ratio. Currently, S-PANI is prepared via electrochemical or chemical synthesis and the sulfonic groups are added mainly following two synthetic routes: *i*) sulfonation of PANI precursors and *ii*) preparation from mixture of comonomers.

2.4.4.1. Sulfonation of PANI precursors

Fuming sulphuric acid is the most common sulfonation agent in the post polymerisation sulfonation of emeraldine base and pernigraniline base forms of PANI [16] as shown in Figure 10. The reaction is an electrophilic aromatic substitution that involves the benzenic rings of PANI. Also fuming sulfuric acid, chlorosulfonic acid, and sulfur trioxide/triethyl phosphate complex have been used to prepare S-PANI with degree of sulfonation 50 % [16, 137, 138] and 75% [139, 140]. A S:N ratio of 0.5 is enough to compensate for the positive charges of the protonated nitrogen atoms and correspond to a fully doped S-PANI. The properties of this S-PANI are lower conductivity than parent PANI (0.1 S cm-1 lower) but independent of up to pH 7. The highly sulfonated S-PANI has improved solubility in aqueous alkali solution (1.6 times more) than the 50% sulfonated S-PANI and an improved conductivity of about 1 S/cm^{-1} independent over the entire pH range.

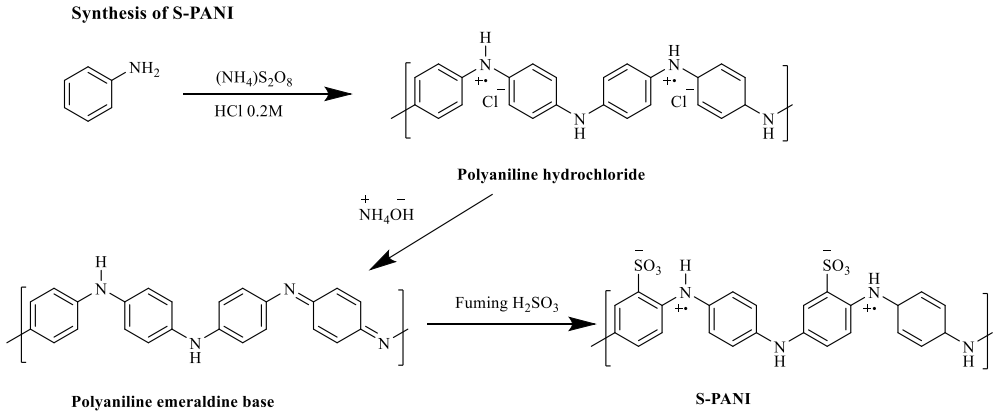

Figure 10: Schematic representing the synthesis of S-PANI through post treatment of PANI emeraldine base.

2.4.4.2. Copolymerisation of monomers

The copolymerisation of aniline with monomers containing a sulfonic group can be performed in acidic conditions using both chemical and electrochemical techniques. The S-PANI prepared by the copolymerisation method is reported to be more thermally stable because of the diminish distortion of the chains[130, 141]. Furthermore the copolymerisation of sulfonated aniline with aniline proceeds under mild conditions[142] such as room or lower temperature and atmospheric pressure and does not require metal catalysts. A schematic for the co-polymerisation of Aniline and metanilic acid is reported in Figure 11.

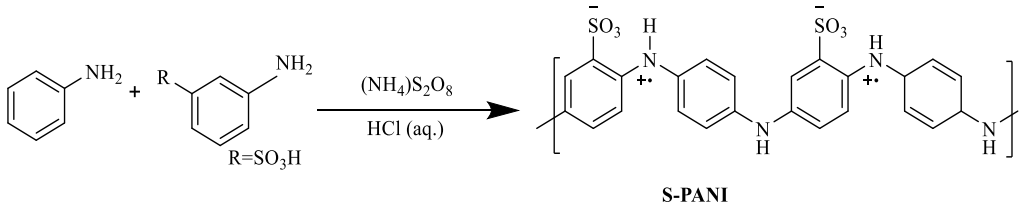

Figure 11: Schematic representing the co-polymerisation of aniline and metanilic acid

2.5 Conclusion and gaps in the literature

The previous paragraphs have outlined the current state of the art of materials, fabrication, and applications of polymer membranes. It has highlighted that

purification processes benefit from the use of NF membrane, but often these procedures require membranes that are stable in solvents, resistant to harsh chemical environments or cleaning, and have a low tendency to fouling to avoid deterioration of membrane performance and frequent replacement. The progress done so far to develop more selective membranes with controllable fouling properties, using PANI as conducting polymer have been summarised. The easy of synthesis, the environmental stability and the polymer availability and cheap cost have made PANI a widely researched material or various applications. Yet, membranes based on PANI requires external doping, have limited solvent solubility and loose the filtration stability and conductivity because the small acid leaches out at high operating pressure.

Self-doped S-PANI has potential as responsive membrane system for fouling mitigation and selective separations. Low fouling S-PANI membranes can overcome the issues related to the recovery of catalyst and products from organic reaction systems such as adsorption on membrane surface and pore blocking. The zwitterionic behaviour of the polymer and its chemical stability can be exploited to prepare robust membranes to be used in harsh chemical environments with the additional advantage of being self-doped, overcoming the current need for time consuming and waste generating doping/de-doping.

The available research works have only partially addressed sulfonated polyaniline membranes limiting its use as a hydrophilic additive for hydrophobic membranes. There is lack of studies on the synthesis of self-doped S-PANI membranes, the performance and the chemical properties as well as modification to achieve tight UF/ nanofiltration range. The bulky SO3H groups, while limiting the adsorption of substrates/catalysts onto the membrane surface could limit the shrinking of the membrane structure, but currently no studies have focused on the role of the anionic sulfonic groups on membrane properties. Furthermore, only a few studies have addressed the use of NF membranes for the separation of catalysts or products of complex reaction system reporting that

the used membranes are not often compatible with reaction conditions such as the temperature, the solvent in which the reaction takes place, or the presence of strong acid/basic group in the reaction mixture. Hence, benchmarking of model reactions with commercial membranes could be used to evaluate the key parameters such as fouling in organic solvents, catalysts deactivation, product yield to gain of better understanding of how the reaction characteristics will influence the prepared S-PANI membranes. The outcome of the benchmarking could be used as a reference in the development of self-doped S-PANI membranes.

2.6 Aims and objectives

The aim of this research is to develop robust, solvent stable and fouling resistant membranes based on self-doped sulfonated polyaniline and investigate their use in ultrafiltration and nanofiltration processes.

The specific objectives to achieve this aim are:

- To benchmark relevant industrial reaction systems such as the Suzuki coupling of aryl pyridines catalysed by palladium (II) catalyst and the lipase mediated kinetic resolution in organic solvents.

- To synthesise S-PANI via co-polymerisation of aniline and a sulfonated monomer and fabricate a membrane via non-solvent phase inversion

- To investigate the effect of thermal and chemical cross-linking on membrane MWCO, solvent stability and surface properties.

- To understand the mechanism of membrane fouling in zwitterionic surfaces for improving the membrane long-term performance.

- To fabricate conducting composite membranes with conducting fillers and initial assess the conductivity of the prepared membranes.

Chapter 3

Materials and method

3.1 Introduction

This Chapter presents the experimental part for the fabrication of sulfonated polyaniline membranes, its characterisation and the benchmarking of commercial NF membranes with organometallic and bio catalysed reactions. It contains the details of all the experimental equipment: dead-end cell, cross-flow and reaction carousels. The analytical techniques used in this work are listed and explained.

3.2 Materials

3.2.1 Chemicals

Aniline, ammonium persulfate (APS), hydrochloric acid (HCl), HPLC grade acetone, DMF, DMAc, Toluene, N-methyl-2-pyrrolidone (NMP) and 4-methyl piperidine (4-MP), Poly (2-acrylamido-2-methyl-1-propanesulfonic acid) (MW=800,000 g mol-1, 10 wt% in water) were purchased from Sigma-Aldrich (UK) along with the chemical crosslinkers α,α′-Dichloro-p-xylene (DCX), glutaraldehyde (GA) and terephtaloyl chloride (TCL). Metanilic acid, ethanol, methanol and isopropanol were obtained from Fisher (UK).

All reagents and solvents used in the optimisation of the model reactions were purchased from Sigma Aldrich and used as bought unless stated otherwise. Dried n-butanol was purchased from Acros Organics.

Table 5 displays the commercial PPGs and PEG used and obtained from Alfa Aesar. Humic acid and Bovine serum albumin were purchased from Sigma Aldrich. All solutions were prepared with deionised (DI) water produced from an ELGA deioniser (PURELAB Option).

Table 5: MW of commercial grade oligomers used

Oligomer	Mw (Da)
Tripropylene glycol	300
Polypropylene glycol 400	400
Polypropylene glycol 750	750
Polypropylene glycol 1000	1000
Polyethylene glycol 1000	1000
Polyethylene glycol 1500	1500
Polyethylene glycol 2000	2000
Polyethylene glycol 3000	3000
Polyethylene glycol 4000	4000
Polyethylene glycol 6000	6000

3.2.2 Membranes

PET/PBT backing layer- Novatexx 2484 (120 µm) was supplied by Freudenberg Filter technologies (Germany). Flat sheet nanofiltration membranes DURAMEM® 500 and PURAMEM® S 600 where purchased from EVONIK. Table 6 displays the technical specification of the commercial nanofiltration membranes used in this project

Table 6: Technical specifications of flat sheet nanofiltration membranes

Type of membrane	MWCO	Operating pressure (bar)	Temperature range (°C)	Solvent	Membrane Material
DURAMEM®	500	20-60	20-50	Polar aprotic/protic	P84® polyimide ISA
PURAMEM® S	600	20-60	20-50	Non polar	P84® polyimide TFC

3.3 Polymer synthesis

3.3.1 Synthesis of self-doped sulfonated polyaniline

S-PANI was synthetized by radical polymerisation of aniline and metanilic acid in the presence of ammonium persulfate in acidic medium. This synthetic route is reported to produce more thermally stable S-PANI [143]. In a 2 L bottle immersed in an ice bath were dissolved 0.05 mol of metanilic acid and 0.05 mol of ammonium persulfate in 800 ml of HCl 0.1M, and the mixture was stirred. After 5 minutes 0.05 mol of aniline was added dropwise in 1h as shown in Figure 12. The reaction was allowed to stir for 6 hours and then decanted all night to allow precipitation of the polymer. The reaction mixture was washed exhaustively with water and then acetone until neutral pH of the washing solution was reached. The resulting green product was dried in vacuo at 50 °C for 24 hours. The chemical structure of the synthesised polymer is reported in Figure 13.

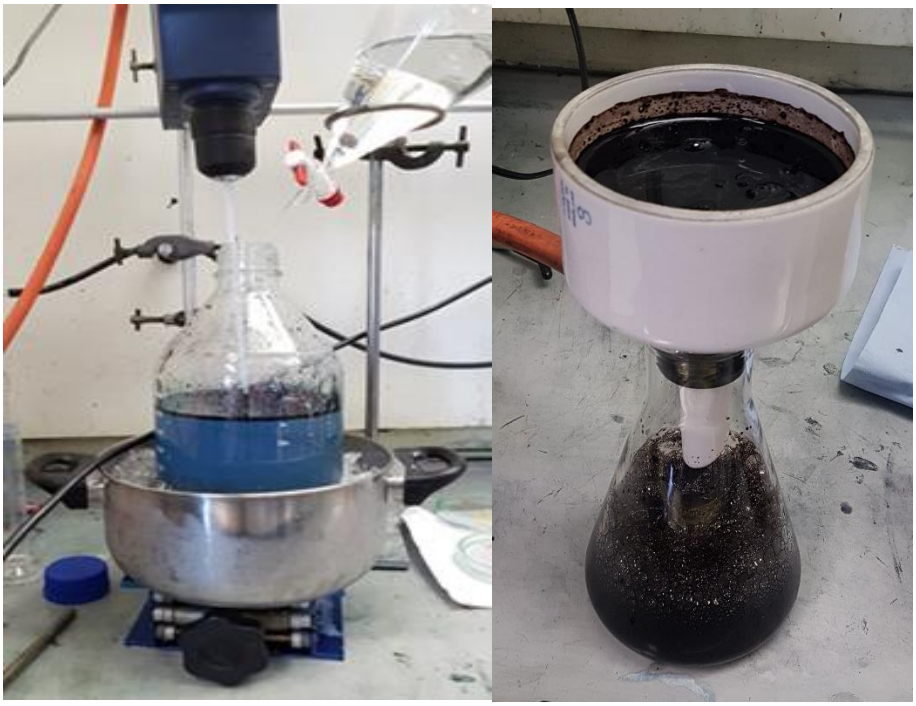

Figure 12: Apparatus showing (left) the synthesis of S-PANI by the dropwise addition of aniline to APS and metanilic acid in HCl 1M and (right) washing under vacuum of the powder.

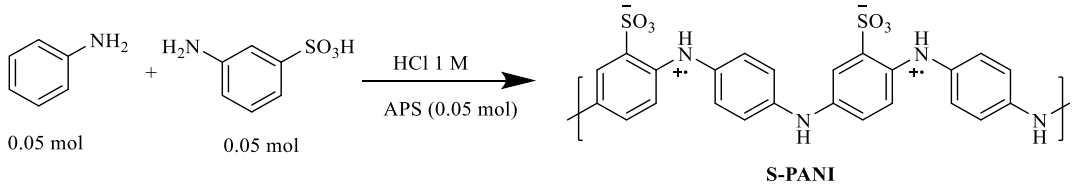

Figure 13: Radical polymerization of aniline and metanilic acid mediated by APS in HCl

3.3.2 Synthesis of polyaniline

Polyaniline was synthesized via chemical oxidative polymerisation [11]. In a 1 L bottle 18.23 mL of aniline was dissolved in 200.0 mL of HCl solution (1.0 M). In a separate reagent bottle, 45.63 g of oxidant agent APS was dissolved in 128.0 mL of HCl solution (1.0 M). The APS was slowly added into aniline solution using a peristaltic pump (20 mL h^{-1}). The solution was kept at 15 °C. This

reaction produces the PANI in the emeraldine salt form with a 60% yield. The product was washed extensively with DI water to remove the unreacted monomers and dried in vacuum oven at 50 °C for 12 hours. Each produced polymer batch was labelled IASP01, IASP02 etc.

3.4 Membrane fabrication

3.4.1 Preparation of polymer dope solution

3.4.1.1. S-PANI for preparation via non-solvent phase inversion in water

Table 7 summarises the optimisation study performed to select the concentration of polymer and composition of the dope solution. S-PANI was slowly added to the mixture of NMP, 4-MP and THF using a funnel in small portions over 5 min. The mixture was stirred at a low mixing speed (50-70 rpm) for 12 h to obtain a homogeneous solution and then left overnight to remove air bubbles, as shown in Figure 14.

Table 7: Screening of thickness, concentration, and composition for preparation of S-PANI membranes. MSP15, MSP18 and MSP18T were obtained from polymer batch IASP04. MSP20 and MSP23 were obtained from polymer batch IASP05, and SPWT01 was produced from polymer batch IASP06.

Membrane batch (notation)	Thickness (µm)	S-PANI wt%	Dope solution
MSP15	200	15	NMP/4-MP
MSP18	200	18	NMP/4-MP
MSP18T	200	18	NMP/4-MP/THF
MSP20	200	20	NMP/4-MP
SPWT01	250	20	NMP/4-MP
MSP23	200	23	NMP/4-MP/THF

3.4.1.2. PANI for preparation via non-solvent phase inversion in water

The above method was used to prepare PANI 20 wt% (1.5 g) dope solutions in NMP (5.5 g) and 4-MP (0.5 g). The mixtures were stirred at a low mixing speed (50-70 rpm) for 12 h to obtain a homogeneous solution and then left overnight to remove air bubbles.

3.4.1.3. S-PANI for preparation via non-solvent phase inversion in hexane

A solution of S-PANI (21 wt%) in NMP and 4-MP was prepared by adding the powder in small quantities over 1 hour and stirred overnight at 150 rpm. Different concentration of gel inhibitor and thickness were tested to optimise the composition of the dope solution as shown in Table 8. The polymer batch used to produce the membranes was IASP06. The membranes were casted using an adjustable casting knife and each batch produced was inspected for defects. Membrane coupons of 14.6 cm^2 were cut from each batch, labelled SPHX followed by a number corresponding to the batch number and a letter. For instance, the membrane coupon cut from batch MSPHX01 was labelled SPHX01A etc.

Table 8: Optimization of membrane fabrication conditions.

Membrane batch (notation)	**Thickness (µm)**	**S-PANI wt%**	**Dope solution**
MSPHX01	250	21	5.0 g NMP 0.5 g 4-MP
MSPHX04	250	20	5.5 g NMP 0.5g 4-MP
MSPHX05	250	20	5.0 g NMP 1.0 g 4-MP
MSPHX08	300	20	5.5g NMP 0.5 g 4-MP
MSPHX09	300	21	5.0 g NMP 0.5 g 4-MP
MSPHX10	300	21	4.5 g NMP 1.0 g 4-MP

MSPHX11	250	21	5.0 g NMP 0.5 g 4-MP

3.4.1.4. Incorporation of graphene oxide

Composite S-PANI/graphene oxide membranes were prepared by incorporating GO powder in the dope solution. The incorporation of GO into the S-PANI was performed by solution mixing. First the GO (0.15 g, 10 wt%) and S-PANI (1.35 g) are mixed together with a magnetic stirrer in solvent free conditions and then the mixed powder is added in small portions to a solution of NMP (5.5 g) and 4MP (0.5 g). IASP05 was used to produce one membrane batch.

Figure 14: preparation of a dope solution

3.4.2 Membrane preparation

All membranes were cast on a bench top laboratory caster. The Novatexx 2484 membrane backing layer was secured using scotch tape on a flat glass plate. An

adjustable casting knife was used to cast films using an adjustable film applicator (Elcometer 4340 automatic film applicator, Elcometer, UK).

3.4.2.1. Phase inversion in water

Membrane prepared from S-PANI (23 wt%) dope solution was casted using a casting knife of 200 μm. Evaporation time of 30 s was used before immersing the casted membrane solution into a DI water coagulation bath. The membrane was kept immersed in DI water at room temperature for at least 24 h and then rinsed with fresh water and stored in DI water for later chemical and thermal treatments. The membranes prepared from batch MSP23, MSP2301 etc. were labelled S-PANI. Membrane prepared from S-PANI dope solutions without THF were casted and directly immersed in DI water for 24 h.

3.4.2.2. Phase Inversion in hexane

Membrane prepared from S-PANI dope solution was casted using an adjustable casting knife with a thickness of 250 μm and the membrane was prepared via phase inversion using 1.5 L of hexane for the coagulation bath. The casted membrane was left in the solvent 24 h and after that stored in water. Membranes fabricated using hexane were labelled SPHX01 etc.

3.5 Characterization techniques

3.5.1 Powder analysis

3.5.1.1. Fourier transform infrared spectroscopy

The FTIR spectra of dry powders were obtained by using a Spectrum 100™ – FTIR Spectrometer (PerkinElmer, USA) fitted with an attenuated total reflectance (ATR) detector. A background scan was run prior to sample testing and spectra were recorded from 4000 to 650 cm^{-1} in transmission mode with a spectral resolution of 4 cm^{-1} and 32 scans.

3.5.1.2. UV-VIS spectroscopy

The powders were analysed by UV–vis spectrometry (UV-1601, Shimadzu, Japan). 100 mg of powder was dissolved in 100 mL of NMP to prepare 1.0 g L^{-1}

solution; the obtained solution was then diluted to $1.0 \times 10{-}2$ g L^{-1} by NMP. Spectra were recorded at wavelengths from 250 to 850 nm at room temperature.

3.5.1.3. Scanning electron microscope- energy dispersive X-ray (SEM-EDX)

The quantitative chemical composition of the powder was studied via SEM-EDX using a FSEM (JSM-6301F, JEOL, Germany). All samples were prepared 24 h in advanced and left under vacuum for one night.

3.5.2 Membrane analysis

3.5.2.1. Field emission scanning slectron microscopy (FESEM): membrane morphology

Membrane morphology was studied using FSEM (JSM-6301F, JEOL, Germany). All samples were prepared by freeze fracturing them in liquid nitrogen and drying them in vacuum overnight. Before the analysis was performed the samples were coated in chromium using a sputter coater (Q150T S, Quorum) under argon for 5 min.

3.5.2.2. Dynamic contact angle: membrane hydrophilicity

Membrane hydrophilicity was studied by dynamic contact angle analysis. (Contact Angle System OCA 15Pro, Dataphysics, Germany) as shown in Figure 15. The analysis was performed using sessile drop technique (4 μL) and data were recorded for 800 s and repeated 2 times.

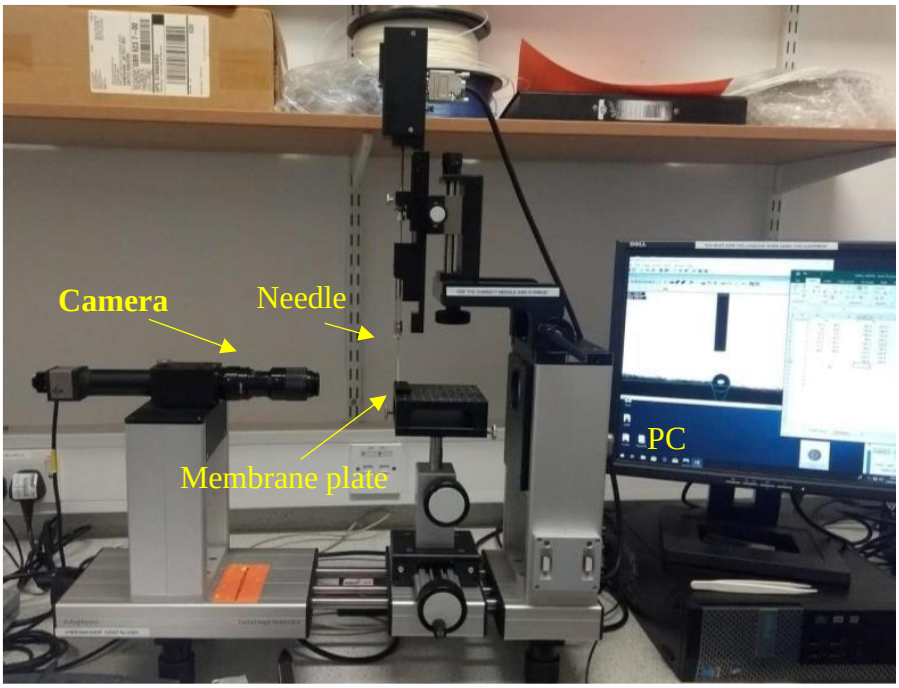

Figure 15: Equipment showing the OCA 15 PRO system used to perform contact angle of the produced membranes

3.5.2.3. Swelling degree

Swelling tests of the total mass solvent uptaken by the membrane were performed in water, 2-propanol, acetone and toluene. The swelling degree (SD) was calculated using the following equation:

$$Swelling\ Degree\ = \frac{m_{wet} - m_{dry}}{m_{dry}} \times 100 \qquad (6)$$

where m_{wet} is the mass of the swollen membrane after equilibrium and m_{dry} is the mass of the dry membrane.

3.5.2.4. Differential scanning calorimetry (DSC): thermal properties

Differential scanning calorimetry DSC thermograms of pure S-PANI membrane were recorded at a heating rate of and scans were done from 25 to 200 °C. Results are average of two membrane samples.

3.5.2.5. Four point probe conductivity meter: conductivity

The membrane surface conductivity was studied using a four-point probe conductivity meter (RM3000, JANDEL, UK). Each membrane sample was analysed twice.

3.5.2.6. Dynamic mechanical analysis (DMA) mechanical properties

The mechanical properties of the membrane were studied using a dynamic mechanical analyser (Mettler-Toledo, DMA1, STAR System) up to a temperature of 100°C with a heating rate of 1K min^{-1}. The membranes were cut into strips of 20 mm (L) x 5.0 mm (W) and secure on a clamp in dual cantilever mode.

3.5.2.7. XRD

X-ray diffractometry XRD was used to characterise the pure S-PANI membrane and the cross-linked membranes. XRD spectra were scanned on a STOE STADI P double setup, equipped with mythen detectors, using pure Cu-Kα1 radiation (λ= 1.54060 Å).

3.5.2.8. Cyclic voltammetry

Electrochemical performance of the membranes was measured by cyclic voltammetry with voltage range from 0.5 to -0.2, at a scan rate of 0.050 V/s. The experiments were carried out using a conventional three-electrode system, which consisted of the membrane (S-PANI, S-PANI GO etc.) electrode (working electrode), Pt electrode (counter electrode), and SCE (reference electrode). They were immersed in 0.05 M H_2SO_4 electrolyte solution. All experiments were conducted at room temperature.

3.6 Cross-linking of S-PANI membranes

3.6.1 Thermal cross-linking

Thermal cross-linking was performed in a vacuum oven (Thermo Scientific, VT 6025) at different temperatures for the desired amount of times. Membranes were cut in coupons of 14.6 cm^2 and placed between two glass plates to avoid curling and damage of the membrane structure. Table 9 reports cross-linking

temperature and time for S-PANI membranes. All thermal cross-linked membranes were labelled SPT followed by the temperature and cross-linking time.

Table 9: Optimization conditions for thermal cross-linking of S-PANI membranes. Membrane were obtained from the same batch MSP2301

Temperature (°C)	Time (h)	Membrane
155	1	SPT155_1
155	2	SPT155_2
155	3	SPT155_3
170	1	SPT170_1
170	2	SPT170_2
170	3	SPT170_3

3.6.2 Chemical Cross-linking

Chemical cross-linking of S-PANI membranes took place at 20° C and was performed as follow: A cross-linking solution of 0.2 M DCX in acetone/hexane (35/65 v/v%) mixture was used and the membranes were cross-linked following a procedure previously reported [13]. The membranes were kept in the cross-linker solution for the desired amount of time (, 3 and 6 days) and after crosslinking membranes were washed 2 times with acetone and store in water for future use.

S-PANI membranes were cross-linked in a 0.1 M solution of TCL in THF at room temperature for the desired amount of time (24 and 48 h). Membranes were then washed 3 times with THF and stored in water /isopropanol for future use.

After casting, S-PANI membranes were kept immersed in 600 ml of cross-linker solution containing 50 ml of GA (50 wt% solution) and 50 ml of HCL 12 M in water for phase inversion. A glass box equipped with a lid was used to contain the crosslinking solution. After 1 h 400 ml of acetone was added to the membranes and the box was sealed and left for 1,3 and 5 days until reaction

completion. After cross-linking membranes were stored in water. Figure 16 reports a proposed reaction scheme for the formation of chemically cross-linked membranes and displays cross-linking time for the membrane.

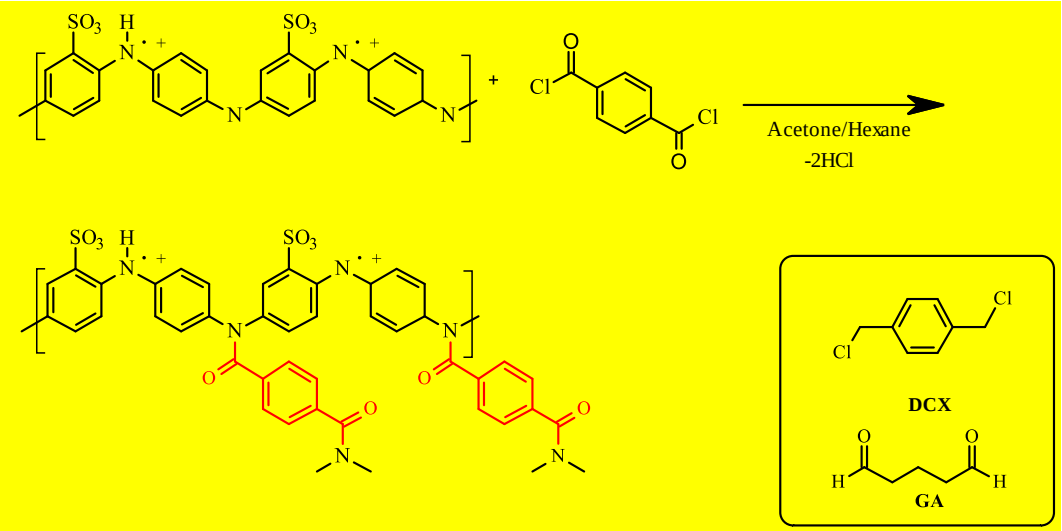

Figure 16: Example of reaction scheme for the chemical cross-linking of S-PANI with TCL. Chemical cross-linking with DCX and GA is reported for PANI here [13].

3.7 Membrane permeance and rejection

3.7.1 Dead-end filtration

A dead-end cell (HP 4750, Sterlitech, USA) was employed to measure solvent permeance and solute rejections of the prepared membranes. A schematic of the equipment is shown in Figure 17. The stirred cell has a membrane active area of 14.6 cm^2 and a processing volume of 300 ml. The membrane was cut in coupons using a stainless-steel porous disk as a template and the membrane cell is then sealed and placed in a water bath over a hot plate to keep the temperature constant at 25 °C. The driving force for the filtration was provided by nitrogen gas. The filtration began by gradually pressurising the cell at the chosen pressure. The permeate was collected in a becker and the permeate mass was recorded at specific intervals of time using a computer connected to digital mass balance (Sartorius LC3201D-00M, Germany). The permeate was collected until a steady

state flux was achieved to ensure consistent performance. The cell was then charge with fresh feed and pressurise at the chosen operating pressure to study permeance and rejection.

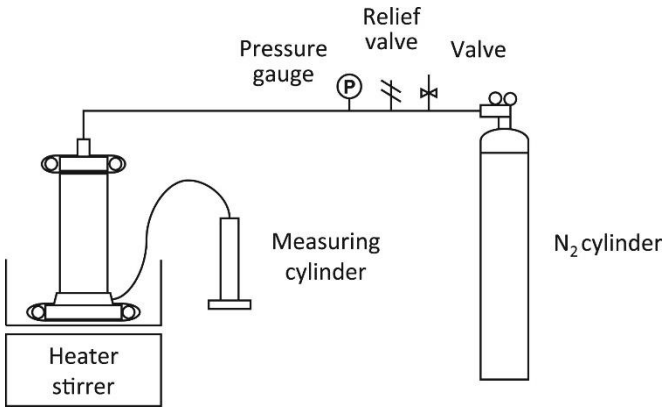

Figure 17: Schematic of the dead-end cell used to study membrane performance

3.7.1.1. Membrane solute rejection and determination of MWCO

(1) PEGs analysis

PEGs were used to determine membrane solute permeance and rejection in water and were prepared using the following concentrations: PEG 1000 (600 ppm) PEG 3000 (2400 ppm), PEG 4000 (2400 ppm) and PEG 6000 (2400 ppm). The PEGs concentrations were analysed using a reverse high-performance liquid chromatography (HPLC) apparatus (Agilent 1260 infinity series, Agilent Corporation, USA) consisted of an autosampler (G1329B) coupled with an evaporative light scattering (ELSD) detector. A flowrate of 1.0 mL min^{-1} was used with mobile phase acetonitrile /water (15/85). The separation was achieved using an Alltech Altima C8 column (150 mm length×4.6 mm I.D., 5 µm particle size, 80 Å pore size). The peaks in the chromatogram were analysed using an already established method [144, 145].

After preconditioning, 100 ml of PEG mixture was poured in the filtration cell and 50 ml of permeate were collected and analysed. This method is advantageous

because it allows the analysis of a range of different MWs with a single filtration avoiding costly and laborious repeated filtrations of single component solutions.

(2) PPG analysis

PPGs were used for the determination of the MWCO of nanofiltration membranes in water and organic solvents. PPG has the same polyether backbone as PEG, but the extra methyl groups increase its solubility in non-polar organic solvents when compared to PEG (Figure 18A and B) [146]. PPG mixtures were prepared by dissolving 4 g of each component in 1L of solvent. For each filtration, 50 ml of feed was added to the cell and half of with was permeated through the membrane at the chosen pressure. The collected permeate was analysed using the same HPLC apparatus used for the analysis of PEG mixture, consisting of a quaternary pump (G1311B), autosampler (G1329B), column oven (G1316A) and ELSD (GB1530001) equipped with a Poroshell 120 EC-C18 (4.6×50 mm 2.7 μm) column. An injection volume of 100 μL, a flow rate of 1 mL min−1 and a column temperature of 25 °C were used. The analysis conditions were a gradient elution of water and acetonitrile as reported in Table 10.

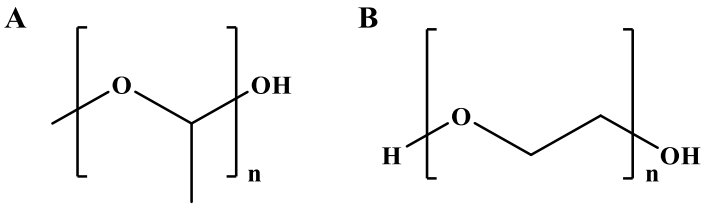

Figure 18: Molecular structure of (A) Polypropylene glycol (PPG) and (B) Polyethylene glycol (PEG)

Table 10: Solvent gradient used during the HPLC elution of PPG mixture

Time (min:s)	Water concentration (%)	Acetonitrile concentration (%)
0	95	5
2:30	80	20
42:30	0	100
47:30	0	100
50	95	5
57	95	5

(3) Bovine serum albumin (BSA) and humic acid (HA) spectrophotometric determination

UV-VIS analysis was used to analyse the permeate obtained from filtration experiments using BSA (1 g/L) and HA (1g/L) as feed. Table 11 shows the concentrations used to build the calibration curves to measure the unknown BSA and HA concentration of the permeate samples. The BSA analysis was performed recording spectra at 278 nm, and the HA analysis was performed at 254 nm. Highly absorbing samples such as the HA mixture were diluted 10 times to ensure linear response. A quartz cuvette was used and washed three times with DI water after each analysis.

Table 11: Standard concentration of the calibration curves for BSA and HA

BSA	HA
Concentration (g/L)	Concentration (g/L)
0.25	0.025
0.5	0.05
0.75	0.075
1	0.1

3.7.2 Fouling experiments

3.7.2.1. Cross-flow filtration: permeance and rejection

Flux of S-PANI membrane was measured using a cross-flow rig which consisted of a pump, a solution bottle and a membrane cell with an effective filtration area of 14.6 cm^2 as shown in Figure 19. Bovine Serum Albumin BSA (1g/L) was used to perform fouling experiments. The membranes were first pre-compacted at 2 bar with deionised water for 1 h and then the permeance was measured at 1 bar. The permeation flux of the foulant solution was calculated as Jp (L/m^2h) and a UV-Vis spectrometer (UV-1601, Shimadzu, Japan) was used to analyse the permeate samples at 278 nm.

3.7.2.2. Study of membrane low fouling ability: flux recovery

After filtration of the BSA solution the tested membranes were extensively washed with water using the same condition of the experiment (1 bar, 0.5 L/min) and the pure water flux (Jw1, L/m^2h) of the cleaned samples was measured again. In order to measure the fouling resistance ability of the synthetised S-PANI and cross-linked SPANI membranes, fouling indexes were calculated using the following equations:

$$FRR\ \% = \frac{Jw1}{Jw} \times 100 \quad (7)$$

$$TFR\ \% = \left(1 - \frac{Jp}{Jw}\right) \times 100 \quad (8)$$

$$RFR\ \% = \left(\frac{Jw1 - Jp}{Jw}\right) \times 100 \quad (9)$$

$$IFR\ \% = \left(1 - \frac{Jw1}{Jw}\right) \times 100 \quad (10)$$

Where FRR is the water flux recovery ratio, TFR is the total fouling ratio, RFR is reversible fouling ratio and IFR is the irreversible fouling ratio. Membranes

with a high value of FRR and a low IFR have better antifouling properties [20]. The flux recovery ratio of the membrane after 3 cycles (Fr) was calculated as follow:

$$Fr\ \% = \left(\frac{J}{J_0}\right) \times 100 \quad (11)$$

Where J_0 is the initial pure water flux of the membrane before any fouling occurs

Permeate was analysed using the above UV VIS spectrophotometric method.

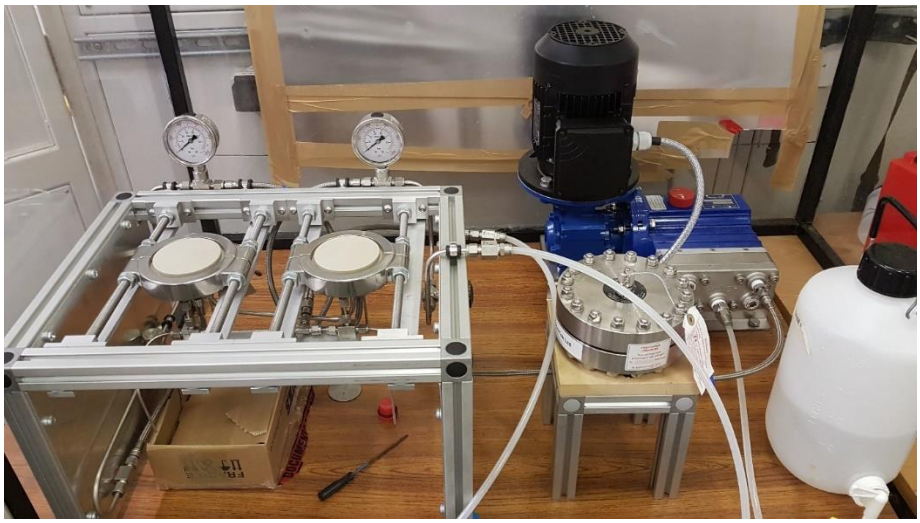

Figure 19: Representation of the cross-flow membrane cell apparatus used during fouling experiments

3.8 Catalyst recovery: benchmarking of commercial membranes in organic solvent systems

3.8.1 Palladium catalysed Suzuki coupling

All the reactions took place in a reaction carousel using tubes and round bottom flasks of different volumes as shown in Figure 20. Under nitrogen, a carousel tube containing a magnetic stir bar was charged sequentially with $Pd(OAc)_2$ (0.04 mmol), Xphos (0.048 mmol), 3-chloropyridine (2 mmol), phenyl boronic

acid (2 mmol), 1,3,5-TMB (0.1 mmol ,16 mg as NMR internal standard) and 10 ml of degassed n-butanol. The tube was capped, and the mixture was stirred at 25 °C for 15 minutes. A solution of $CsOH \cdot H_2O$ (3.4 mmol) in 2 ml of H_2O was added drop-wise to initiate the Suzuki reaction. A reaction scheme is showed in Figure 21. The tube was capped and the reaction mixture was stirred at 25 °C under nitrogen. After 90-100% conversion was reached, the reaction mixture was poured into a dead-end system and the filtration was carried out as reported in 3.7.1. 85-90% of the solution was collected as permeate and the catalyst was recovered from inside the cell using fresh butanol. The carousel tube was topped up again with fresh substrates (90% of initial concentration) and with the catalyst recovered from the membrane. The reaction was run again under nitrogen. Samples were taken at regular intervals and submitted to NMR analysis.

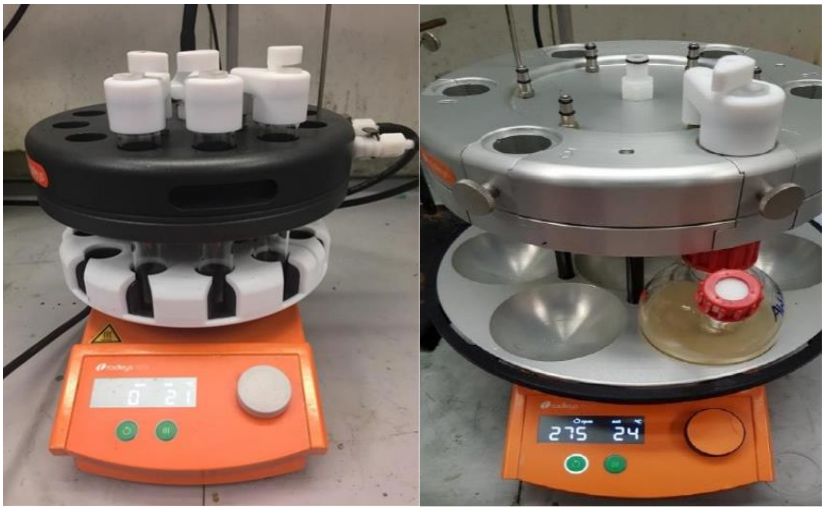

Figure 20: Reaction carousels used to carry out optimization and screening of the reaction conditions

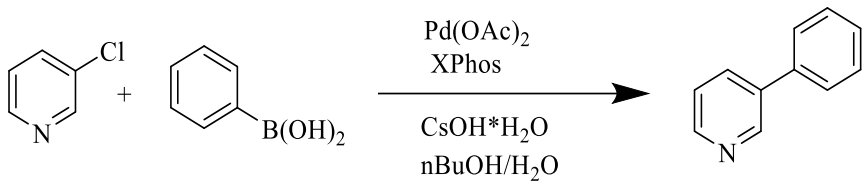

Figure 21: Reaction scheme of the Suzuki coupling of 3-chloropyridine and phenyl boronic acid

3.8.1.1. NMR analysis of permeate

At specific intervals, an aliquot was taken out from the reaction mixture and immediately quenched filtrating the mixture through a short plug (1-2 cm) of silica gel to remove the catalyst. All samples were collected in NMR tubes and submitted to analysis the same day. The samples were analysed in a 400 MHz Bruker spectrometer Conversion and yield of the reaction products are calculated using the peak of 1,3,5-trimetoxybenzene as the internal reference. Known peaks in the product (or starting material) are integrated against the known amount of standard. For example, when integrating against the aromatic peaks in the standard, the 1,3,5-trimethoxybenzene aromatic singlet was set to 0.3, therefore if 100% product had formed (i.e. 1 mmol), a 1H signal on the product would integrate to 1. If integrating against starting material, a 1H signal on the starting material would integrate to 1.2 if no starting material had been consumed.

The catalyst turnover number TON was calculated as follow:

$$TON = \frac{moles\ of\ product}{moles\ of\ catalyst} \qquad (12)$$

3.8.1.2. Uv-Vis analysis of $Pd(OAc)_2$ in the permeate

UV-VIS analysis was used to analyse the permeate obtained from filtration experiments of the Suzuki coupling reaction. The analysis of $Pd(OAc)_2$ was performed recording spectra at 400 nm. The calibration curve was built using 3 standards of 1mM, 2mM and 4mM $Pd(OAc)_2$ in BuOH.

3.8.2 Kinetic resolution of 1-phenylethanol catalysed by free lipase

To a double-necked round bottomed flask, 100ml of solvent (ethyl acetate or toluene) was added. Then, the flask was charged sequentially with Pseudomonas lipase (1g), 1-phenylethanol (5 mmol), vinyl acetate (25 mmol) and 1,3,5-TMB (1 mmol) as internal NMR standard was added. A reaction scheme is showed in Figure 22. The reaction took place at 25 ºC and was stirred at 275 rpm to avoid denaturation of the enzyme. The reaction was then left to complete for 24 hours. After the completion, the reaction mixture was poured into a dead-end system and the filtration was carried out as reported in 1.7.1. 85-90% of the solution was collected as permeate and the lipase was recovered from inside the cell using fresh solvent. The flask was topped up again with fresh substrates (90% of initial concentration) and with the lipase recovered from the membrane. The reaction was re-initiate and samples were taken at regular intervals and submitted to NMR analysis.

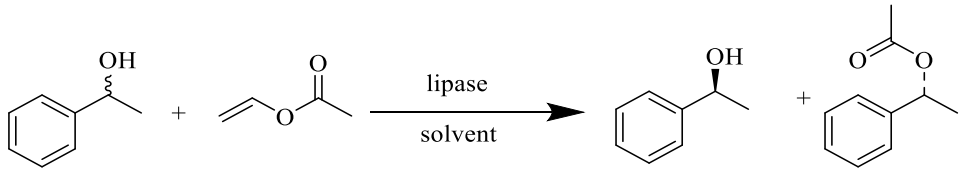

Figure 22: Reaction scheme of the kinetic resolution of 1-phenylethanol catalysed by free lipase.

3.8.2.1. UV VIS analysis of permeate Bradford Essay

This method was used to analyse the protein (enzyme) concentration of the permeate samples. The Bradford reagent was prepared first by dissolving 100mg of Coomassie Brilliant Blue G-250 in 50ml 95% ethanol. 100 ml of phosphoric acid was added to this and the volume was made up to 1Lwith DI. The solution was stirred for an hour to ensure the reagent was well mixed, and then stored in the dark at 4ºC. Before being used, the reagent was filtered. Standards of BSA ranging from 0.25 to 1.5 mg/ml were prepared using sodium chloride as the buffer. The analysis was performed as follow: 5 ml of Bradford's reagent was added to 0.1ml of each of the protein concentrations. 1ml of each of these

solutions were then added to blank cuvettes and placed in the spectrometer and analysed at 595nm. Similarly, 5ml of Bradford's reagent was added to 0.1ml of the permeate samples and the absorbance measured at 595nm. Using the calibration curve, the concentration of the permeate samples were determined.

Chapter 4

Benchmarking of industrial relevant reactions with commercial OSN membranes

4.1 Introduction

Organometallic catalysts and biocatalysts are fundamental tools to synthesise chemicals. Organic synthesis of pharmaceutical intermediates and high-value products often uses organometallic complexes as homogeneous catalysts that are difficult to remove from the final products and require high solvent volumes and energy. This not only generates waste and metal rich sludge but leads to the loss of valuable ligands increasing the overall cost of the process [4]. Despite the disadvantage given by the homogeneity of the reaction, this type of catalysts is efficient and able to catalyse reactions with high efficiency. An alternative to organometallic complexes is the use of enzymes to catalyse chemical processes as they can be obtained from sustainable resources such as plants/ bacteria, and present a low toxicity while catalysed the process with high stereo and chemo-selectivity [147].

Nanofiltration membranes have shown the potential to be an economically feasible and less energy consuming technique for the recovery of expensive catalysts and purification of products from organic reaction systems [6, 70, 148]. Furthermore, their use in separating enzymes has found application in the development of continuous enzymatic membrane reactors were the costly enzyme immobilisation is avoided and the enzymatic catalyst is retained and the products easily recovered [71].

Reactions are often influenced by membrane operating conditions such as temperature and pressure and the substrates might interact with the membrane materials or be adsorbed on its surface. Besides fouling in organic systems still represent the main limitation. Hence, well established and scaled up chemistry should be used to benchmark membranes. In this chapter it is reported the

investigation of i) the Suzuki coupling of biaryl compounds catalysed by and the $Pd(OAc)_2$XPhos complex and ii) the kinetic resolution of 1-phenylethanol catalysed by free lipase in organic solvents.

The Suzuki-Miyaura coupling is a wide applied synthetic route to prepare compound libraries for material chemistry and pharmaceuticals and often palladium-based catalyst are utilised because they efficiently allow the coupling of challenging electrophiles and bulky substrates [149, 150]. In particular, Buchwald ligands are now widely used with palladium to catalyse the coupling of many substrates [151]. They are crystalline materials with high air stability and thermal stability which make them easy to handle and use. Furthermore, their steric and electronic properties stabilise the palladium intermediates that are key species in the catalytic cycle, making the process highly efficient [152, 153]. So far nanofiltration membranes have been used to increase the activity of palladium based catalytic system by separating them from the post reaction mixture and reuse them multiple times. A relevant examples is the semi-continuous nanofiltration of $Pd(OAc)_2(PPh3)_2$ in different solvents where a total turnover number of 1200 was achieved after 5 reaction filtrations sequence [66]. Other examples report the separation of Pd coupled with ionic liquids [70] and both imidazolydenes and quaternary ammonium salts [4]. Solvent screening and optimisation was necessary to tackle the formation of palladium black which is considered responsible for de-activation of the catalytic system [154]. Indeed, membrane replacement was necessary after each cycle for limited stability under the reaction conditions. The coupling of arylpyridines and phenyl boronic acid mediated by $Pd(OAC)_2$ XPhos presents some advantages such as i) the ready availability of the starting materials, ii) the mild temperature conditions and iii) the low toxic solvent system making it an ideal candidate to investigate membrane performance and catalyst reusability.

The kinetic resolution is a process for the preparation of optically active compounds that is based on the different reaction rates of enantiomers in the

presence of a chiral catalyst [155]. The chiral catalyst is used to promote a selective reaction of one of the enantiomers over the other. The resolution of 1-phenylethanol is particularly studied and used because the chiral derivatives of 1-phenylethanol are used in the pharmaceutical and natural products industries [156, 157]. Biocatalysts, and in particular Lipases (glycerol ester hydrolases EC 3.1.1.3) have been successfully applied to kinetic resolutions as they show high selectivity, stability in non-aqueous media and improved product yield [158, 159]. Enzymes can be isolated from renewable sources and thus considered an environmentally friendly alternative [160].

Hence in this chapter, commercial nanofiltration membranes will be benchmarked against the chosen reaction systems to evaluate i) the performance of the membrane in the solvent systems, ii) the potential reuse of the organo-catalyst and of the biocatalyst and iii) the reaction parameters.

4.2 Suzuki coupling in a biphasic mixture

4.2.1 Reaction benchmarking in batch

The catalytic system - $Pd(OAc)_2$XPhos- was tested in the presence of $CsOH*H_2O$ as an inorganic base under nitrogen atmosphere to prevent oxygen contamination and the filtrations were carried out separately in a dead-end cell. As the reaction vessel is separated from the filtration unit the system is referred to as semi-continuous nanofiltration [66]. The results from the batch experiments are reported in Figure 23. The reaction, after 35 minutes of stirring at 25°C yielded full conversion of the 3-chloropyridine to 3-phenylpyridine (Figure 23 A). The reaction reached more than 50 % conversion in less than 10 minutes turning from intense yellow to dark red showing that the palladium shift from Pd (II) to active Pd(0) [161, 162]. Additional data were collected during the online NMR monitoring of the reaction (Figure 23 B) confirming the fast kinetic of the tested reaction system.

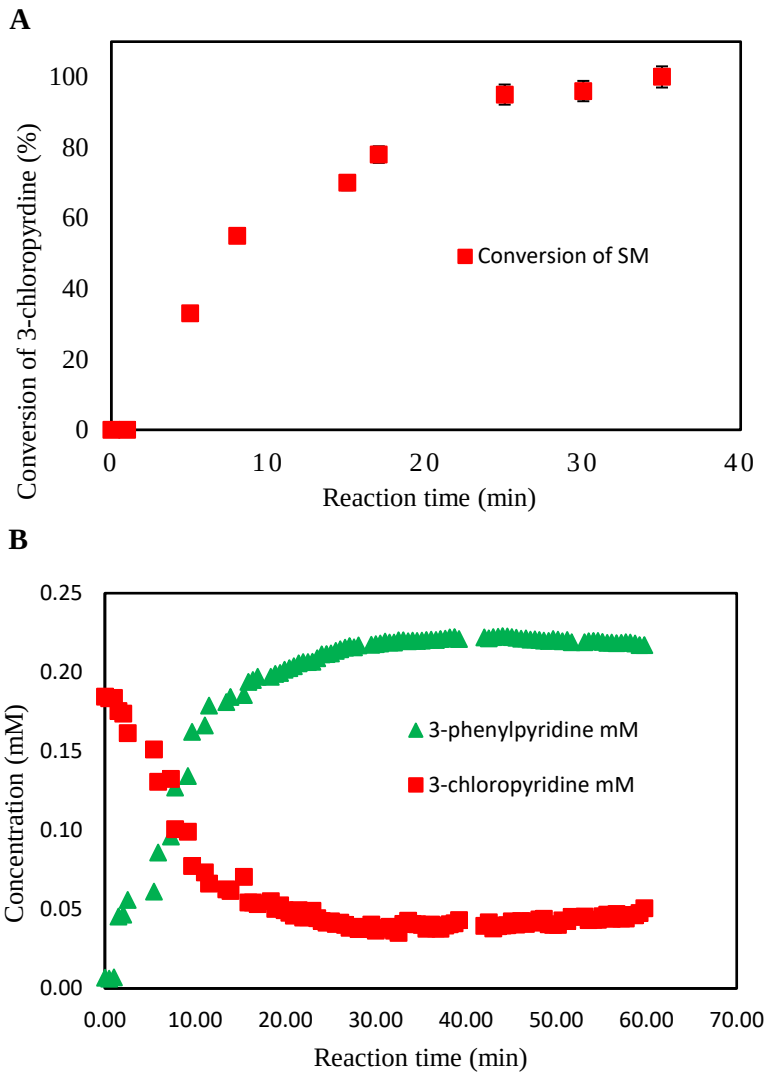

Figure 23: (A) Conversion % of 3-chloropyridine over time for reaction IASC65. Standard Reaction conditions: 1 eq. 3-choloropyridine, 1 eq. phenylboronic acid, 2% mol of $Pd(OAc)_2$. Offline NMR acquisition: data are average of 2 experiments. (B) Evolution of the 3-chloropyridine and 3-phenylpyridine concentration over time. Reaction conditions: 1 eq. 3-choloropyridine, 1 eq. phenylboronic acid, 2% mol of $Pd(OAc)_2$. Online NMR monitoring was performed at the Dynamic Reaction Monitoring facility (DReaM) at the University of Bath.

4.2.2 Membrane compatibility with reaction conditions

4.2.2.1. MWCO suitability

The membrane involved in the separation of the post reaction solution containing the catalyst, product and eventually unreacted substrates, was the DURAMEM

polyimide 84 with a MWCO of 500 Da. According to the manufacturer specifications, the membrane is stable in most of the organic solvents including polar protic therefore are usable in butanol. To efficiently retain the catalyst the MWCO of the chosen membrane should be lower than the MW of the catalysts. The $Pd(OAc)_2$XPhos complex has a total MW 701.22 g mol^{-1}, therefore, it could be hypothesised that DURAMEM 500 is able to retain the catalyst and allow the other lower MW components through the membrane.

4.2.3 Membrane performance and catalyst reuse

The results of the coupled reaction-separation related to the Suzuki coupling between 3-chloropyridine and phenylboronic acid are illustrated in Figure 24 A and B. Reaction 1 after 20 minutes of the progress of the reaction yielded 100 % conversion. After permeating 90 % of the post-reaction mixture through D500 at a pressure of 35 bar, the retentate rich in catalyst and ligand was recycled to the reaction carousel. Reaction 2 and Reaction 3 represent the re-initiation step after filtration and they also run for 20 mins, each yielding 50 % and 5 % respectively of the expected product. The initial TON of 50 decreased of the 75% and 98% in Reaction 2 and Reaction 3. This indicates a substantial loss of catalytic activity that was first attributed to the prolonged filtration time (up to 6 hours) that caused de-activation of the catalyst during the time spent in the dead-end cell. However, the NMR online monitoring of the reaction re-initiated by the addition of fresh substrates without filtration step showed that palladium de-activation was still happening as illustrated in Figure 24 B. After Reaction 2 the catalyst is not able to retain its catalytic activity and the conversion of 3-chloropyridine drop from 100 % in Reaction 1 to 5% in Reaction 3 and 17% in reaction 3 without filtration. It was also found that the reaction mixture changed colour becoming darker, most likely for the decomposition of the catalyst in palladium black.

A

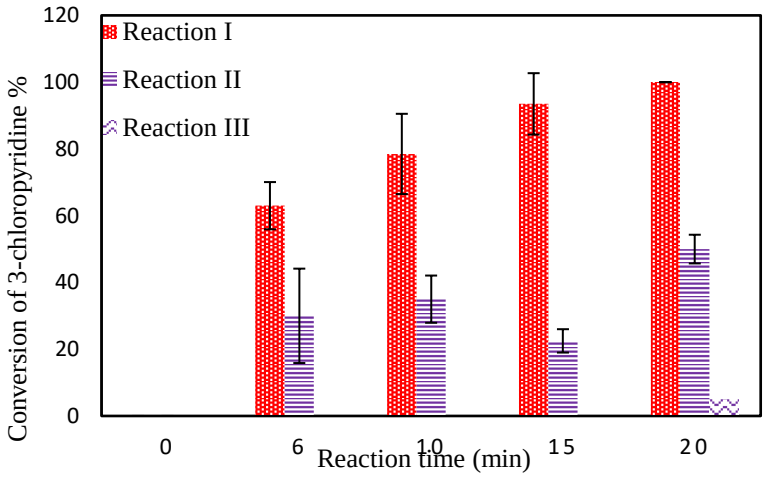

B

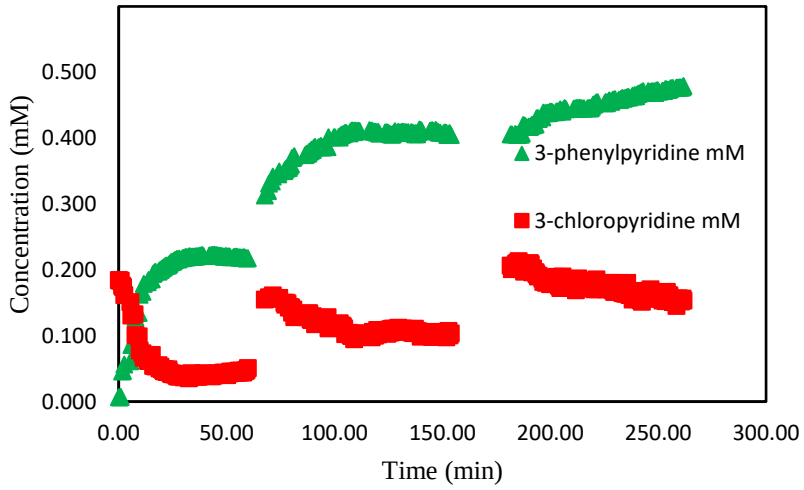

Figure 24: (A) Illustration of the conversion of 3-chloropyridine over time before the dead-end filtration (Reaction I), re-initiation after the first filtration (Reaction II) and re-initiation after the second filtration (Reaction III), Standard reaction conditions: 1 eq. 3-choloropyridine, 1 eq. phenylboronic acid, 2% mol of $Pd(OAc)_2$, Offline NMR acquisition: data are an average of 2 experiments. (B) Evolution of 3-chloropyridine and 3-phenylpyridine concentration over time in standard conditions and re-initiation without dead-end filtration of the post- reaction mixture. Online NMR acquisition was performed at the Dynamic Reaction Monitoring facility (DReaM) at the University of Bath.

The performance of the D500 membrane is reported in Table 12. The mean permeance for the pure n-butanol/H_2O system at 35 bar is 0.08±0.03 which is

then 1.4 and 4.5 times lower after the first and second filtration cycle. Furthermore, the same membrane disk was used in each reaction-filtration experiment. Thus, the decreasing in permeance is most likely attributed to the deposition of the de-activated palladium/ palladium black species[148] onto the membrane surface. Nevertheless, the analysis of the permeate confirmed a 100% rejection of the palladium in each run showing that the catalyst de-activation was not due to the loss of small palladium species through the membrane.

Table 12: Performance of D500 membrane in n-butanol/H_2O 5:1 and during filtration of the post-reaction mixture.

Filtration cycle	Conditions	Permeance ($Lm^{-2}h^{-1}bar^{-1}$)	Rejection
Pure solvent	35 bar, 25 °C,	0.08±0.03	N/A
I	35 bar, 25 °C	0.06±0.05	100%
II	35 bar, 25 °C	0.018	100%

4.2.4 Fouling Characteristics

Fouling of the D500 membrane was investigated using SEM-EDS to determine the nature of the species that builds up onto the membrane surface. As illustrated in Figure 25, the section of the D500 membrane shows a substantial accumulation of a black deposit on the centre of the membrane top surface and crystalline accumulation on the membrane edges. The mapping of the fouled membrane reports the accumulation of both organic and inorganic species. Surprisingly, the elements present in higher percentage are, after carbon, oxygen and nitrogen, cesium and boron. Besides, palladium is found to be just 3.7% of the total mapping of the fouled D500 membrane. It is well known that, the formation of the adsorbed layer is generally quickly followed by the build-up of a thicker fouling layer, the cohesion of which is due to interactions developed between solutes. Inorganic components with less affinity toward the membrane material can be entrapped in the organic layer and thus participate to the global fouling [163].

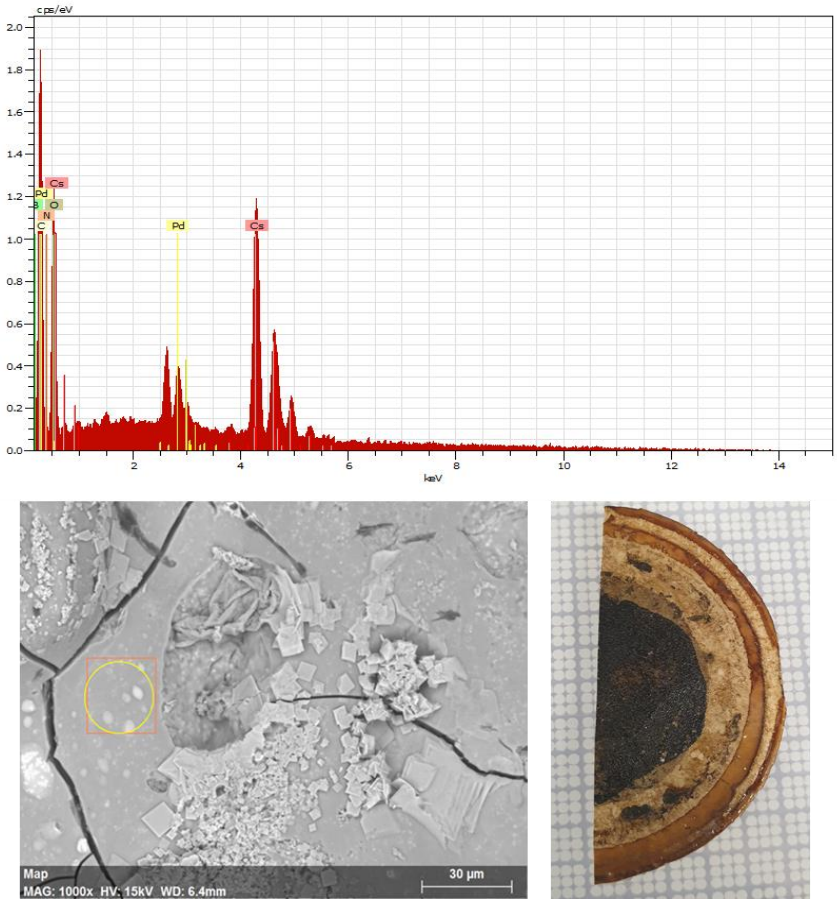

Figure 25: EDS spectrum and mapping of fouled D500 membrane after 3 cycles of filtrations of PdXPhos catalysed Suzuki coupling

4.2.4.1. Investigation of catalyst de-activation in batch mode

The semi-continuous nanofiltration of the $Pd(OAc)_2$XPhos system showed a decreasing in the conversion of 3-chloropyridine due to catalyst de-activation and loss of membrane performance due to fouling. It was found that fouling was related to catalyst de-activation due to the accumulation of palladium black onto the membrane surface, hence, catalyst deactivation was investigated in batch to improve the activity of the palladium in the biphasic reaction. Two different approaches were then considered to avoid deactivation of the catalyst during the reaction: i) increasing in the palladium loading and ii) keeping the excess of one of the reagents. Figure 26 shows the results from re-initiation using two different

loading of catalyst. To obtain the same conversion after re-initiation it was necessary to use a much higher catalyst loading (5%) However the solution became much darker because of an increasing amount of palladium black. This suggests that the catalytic activity of the catalyst was not primarily influenced by the catalyst load and that this would also negatively affect the membrane fouling. Because of the high cost of the catalyst and ligands, this solution could be efficient on a lab-scale condition but limited a potential scale-up of the system.

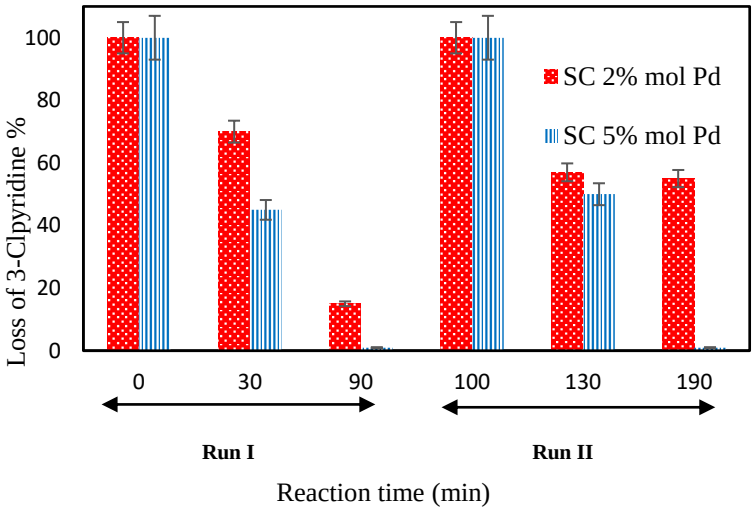

Figure 26: % loss of 3-chloropyridine for 2%mol of Pd catalyst and 5% mol of Pd catalyst. Reaction is re-initiated by adding fresh substrates after reaching complete conversion, the crude mixture is not filtrated with membranes.

Figure 27 illustrates the data obtained from the reaction performed using an excess of the starting material. The graph shows the evolution of the concentration of the concentration (mM) of 3-chloropyridine and 3-phenylpyridine over time for a total of 4 reactions. The catalyst is reused 4 times by re-initiating the reaction at 60 min, 180 min and 240 min keeping the 3-chloropyridine always in excess. The catalyst TON keeps increasing as more product is formed each time, reaching a value of 140 after 400 minutes of off-line monitoring of the reaction.

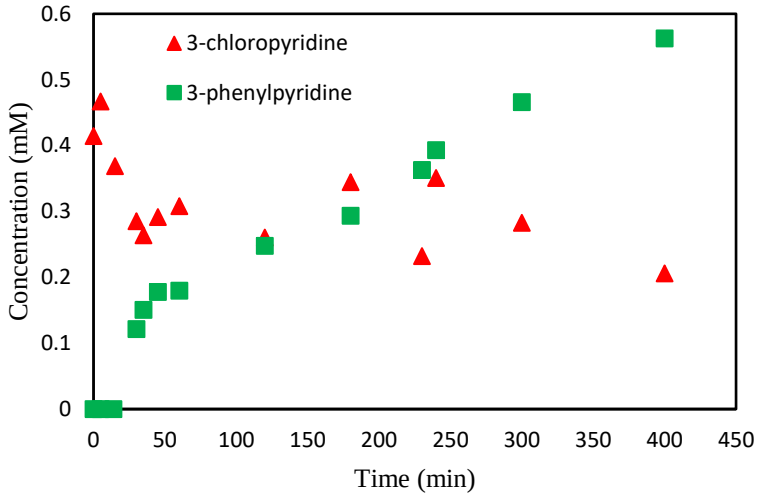

Figure 27: Concentration (mM) of 3-chloropyridine and 3-phenylpyridine over time. Reaction conditions: 2 eq. 3-Chloropyridine, 1 eq. phenylboronic acid. The reaction is initiated by $Pd(OAc)_2$. The catalyst is reused 3 times by re-initiating the reaction at 60 min, 180 min and 240 min with 1.7 eq. of CsOH, 1 eq. phenylboronic acid and 2 eq. of 3-chloropyridine. Offline acquisition.

4.3 Kinetic resolution in organic solvents

4.3.1 Conversion and kinetics of reaction in toluene and ethyl acetate

The kinetic resolution of racemic 1-phenylethanol in the presence of vinyl acetate as acyl donor and catalysed by lipase was carried out at 20 °C in two different solvents: toluene and ethyl acetate. The results from the batch experiments are reported in Figure 28. The reaction in toluene, after 24 hours yielded 50 % of the product which is the maximum conversion of the racemic 1-phenylethanol. The reaction in ethyl acetate reached 43 % conversion after 24 hours.

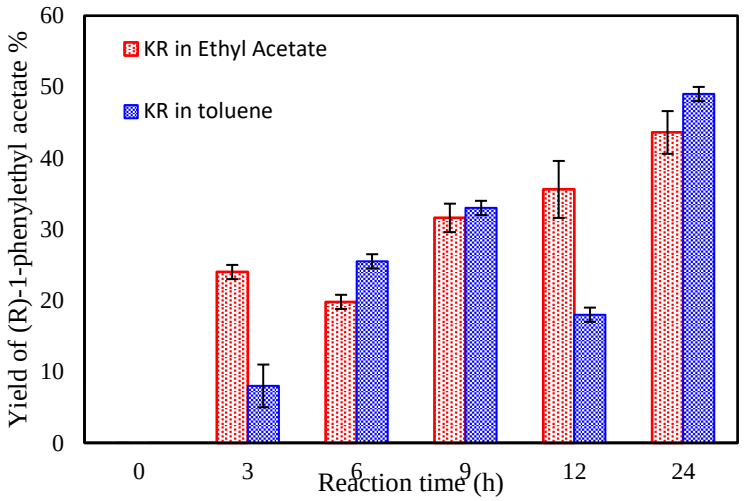

Figure 28: Conversion % of (R)-1-phenylethyl acetate over time for reaction IAKR01 in toluene and IAKR02 in ethyl acetate catalysed by lipase. Offline NMR acquisition: data are an average of 2 experiments.

4.3.2 Filtration in dead-end cell and lipase reuse

After 24 hours the reaction mixture was transferred in the dead-end cell and 90% of it was permeated through the membrane. The free lipase was recovered and between each reaction-filtration, it was assumed 10% of enzyme loss. The same membrane was used in each filtration cycle and removed from the cell at the end of the 2 completed cycles to avoid drying out of the membrane and keep it in good working conditions. The selectivity and permeance of the D500 and PS600 at 35 bar are reported in Table 13. PS600 used in toluene showed initial solvent permeance of 1.5 **L** $m^{-2}h^{-1}bar^{-1}$ that drop of almost 15% in Cycle II. However, the highest permeance decline was that of D500 used in ethyl acetate which showed initial permeance of 3.3 **L** $m^{-2}h^{-1}bar^{-1}$ at 35 bar that dropped of almost the 93% reaching a value of 0.23 **L** $m^{-2}h^{-1}bar^{-1}$ Cycle II. As both membranes were used in Cycle I and Cycle II under the same reaction conditions, the permeance decline of D500 could be attributed to membrane instability or enzyme adsorption onto the membrane surface. Figure 29 shows PS600 and D500 before and after filtration. The former appears almost intact and a layer of

the enzyme is visible on the edges, however, D500 changed colour after Cycle II and become dark brown. This suggests a remarkable instability of the D500 toward the solvent conditions. Nevertheless, both D500 and PS600 showed 100 % rejection of lipase after cycle 1 and cycle 2.

Table 13: Performance of D500 membrane in Ethyl acetate and PS600 membrane in toluene during filtration of the post- reaction mixture.

Filtration cycle (35 bar, 20 °C)	Permeance ($Lm^{-2}h^{-1}bar^{-1}$)	Rejection
Pure Toluene	1.5±0.03	N/A
I	1.24±0.05	100%
II	1.3	100%
Pure EA	3.3	N/A
I	0.96	100%
II	0.86	100%

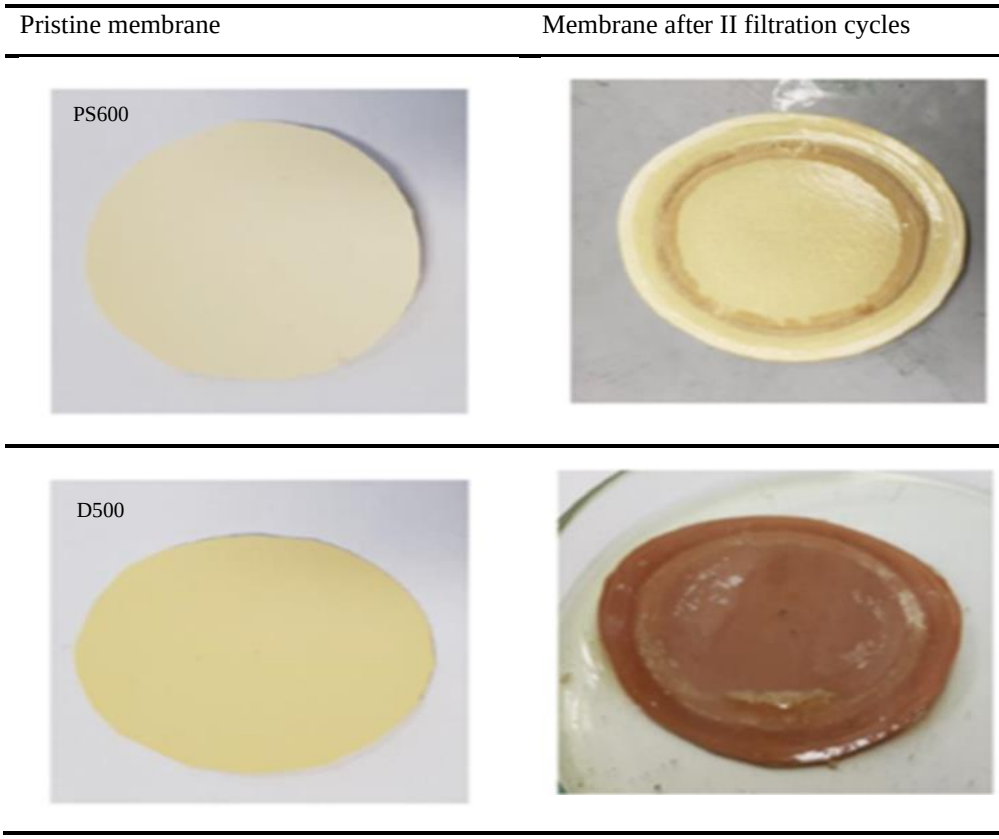

Figure 29: Visual stability of commercial PS600 and D500 after dead-end filtration in toluene and ethyl acetate respectively

Figure 30 reports the results from the coupled KR in toluene-filtration and KR in ethyl acetate-filtration. Both Reactions I reached almost 50 % conversion but only KR in toluene yielded the S product in high yield - 43% in Reaction II and 47 % in Reaction III-. In contrast, KR in ethyl acetate yielded only 27% and 23 % of the S product. Furthermore, the 1H NMR spectrum of the permeate after Cycle I and Cycle II (data are shown in the appendix) reports a side product along with the R-phenyl ethanol and (S)-1-phenyl ethyl acetate. The side reaction might be attributed to the use of ethyl acetate as solvent of the reaction. It is well known that the acyl groups from acylating agents can affect the enantioselectivity of the lipase catalysed reaction [164], and this is could be responsible for the lower yields and the side-products presents in the permeates of reaction II and III. During the prolonged filtration time, the ethyl acetate might

compete with the active sites of the enzyme reducing its selectivity toward the reaction [165].

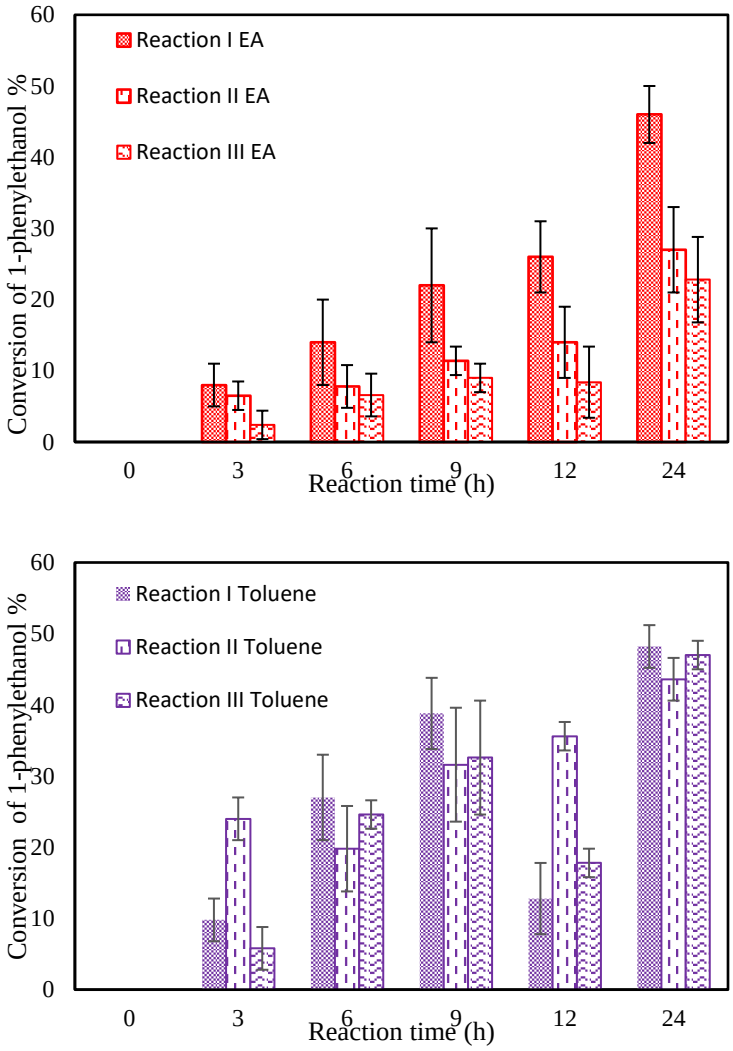

Figure 30: Illustration of the conversion of 1-phenylethanol over time before the dead-end filtration (Reaction I), re-initiation after the first filtration (Reaction II) and re-initiation after the second filtration (Reaction III), Standard reaction conditions: 25 eq. 1-phenylethanol, 5 eq. vinyl acetate, 1.0 g lipase, Offline NMR acquisition: data are an average of 2 experiments.

4.4 Conclusion

In this chapter, it was investigated the performance of commercial D500 and PS600 membrane during i) the separation of $Pd(OAc)_2$XPhos from the biphasic

Suzuki coupling and ii) the separation of lipase from the kinetic resolution in organic solvents. It was found that the semi-continuous nanofiltration of the Suzuki reaction at 35 bar gave 100 % conversion of the 3-chloropyridine after 20 minutes and re-initiated after the addition of fresh substrates reaching 50% and 5% conversion. The Buchwald ligand dissociates from the organometallic complex, forming palladium black which builds up onto the membrane surface along with the hydroxide base which is no longer soluble in the biphasic system after the catalyst deactivation. From filtration experiment and NMR online monitoring it was found that the deactivation was not influenced only by the prolonged filtration time. Further batch experiments showed that an increase in the load of palladium of up to 5% could completely convert 1 equivalent of the 3-chloropyridine in the expected product in both first and second run, however, because of the biphasic system and limited solubility of the complex, the membrane fouling could be negatively affected. An excess of the initial substrate was necessary to keep the $Pd(OAc)_2$XPhos activated during the off-line monitoring of the reaction. The lipase-mediated kinetic resolution was studied in a semi-continuous nanofiltration system using two different membranes; PS600 for the reaction in toluene and D500 for the reaction in ethyl acetate. It was found that the enzyme successfully catalysed the reaction in toluene with 50% conversion during the first reaction-filtration run and 43% and 47% in the subsequent re-initiations. Furthermore, the PS00 showed stable performance during filtration and it was found almost clear from solutes adsorption on its surface. Conversely, the reaction performed in ethyl acetate yielded different products because of a possible competing acylation mechanism between the used solvent and the vinyl acetate. Overall, this work demonstrates that for the studied organo-catalysed and bio catalysed reactions, the nature of the solvents, the substrate reactivity, the nature of the catalysts combined with the membrane tendency to fouling play a crucial role in the development of a durable and efficient nanofiltration-coupled reaction system.

Chapter 5

Self-doped sulfonated polyaniline membrane: fabrication, fouling resistance and properties

5.1 Introduction

Separation technologies require high-performance membranes to overcome fouling and the inability to resist in the presence of harsh organic solvents. In the last twenty years, many studies have presented PANI as a desirable membrane material because of its thermal and chemical stability, chemical doping, non-toxicity and rather cheap cost with respect to other materials [11, 12, 114]. Many recent examples report PANI as a polymer in the fabrication of both UF [166] and NF [12, 13, 25, 42] membranes. In addition, due to its versatility and the possibility to prepare electrical responsive films, PANI membranes for in-situ fouling removal have been developed demonstrating the control over neutrally charged molecules under applied external stimulus [11, 25, 167].

PANI is doped to achieve better solubility and improved conductivity but often this leads to potential leaching during filtration with loss of mechanical stability and deterioration of membrane performance. However, PANI contains activated aromatic rings, thus it is possible to introduce substituents by electrophilic substitution [168] and convert it in self-doped derivatives through synthesis. Instead of external doping, the acidic groups are covalently bonded to during synthesis and act as permanent dopants. Sulfonated polyaniline (S-PANI) is a self-doped polymer with improved properties and processability with respect to PANI [16]. The ionic polymer has a six-member ring doping structure with the sulfonic group and the imine nitrogen in the *ortho* position with respect to each other [169]. The sulfonic group is charged and protonates -dopes- the imine nitrogen with a mechanism analogous to the HCL protonation with PANI [105]. Due to the strong delocalisation the charges are continuously re-localise along the polymer backbone giving S-PANI two important properties: electrical

conductivity as parent PANI and a zwitterionic surface. The second one refers to the presence of both positive and negative charges in the same molecules and has been exploited in membrane fabrication to prepare membranes with super hydrophilic characteristics [18, 19, 86]. Sulfonation improves the solubility of PANI in aqueous solutions due to the hydrophilicity of the functional group and does not lose its doping at high or low pH, remaining constant and therefore ensuring stability during chemical and electrochemical processes.

However, in strong polar aprotic solvents, the polymer tends to aggregate in gel-like structures. For this reason, when it is processed in combination with other polymers as a composite membrane, it is used with ammonia solution that de-dope the polymer and prevents the formation of gels in organic solvents [19]. In the protocols reported in the literature to prepare composite low fouling membranes, the polymer synthesis involves two steps: PANI is synthesised via chemical polymerisation and ii) the sulfonation step occurs [18, 19, 86]. The polymer is then de-doped and incorporated in the membrane solution before casting and phase inversion in water. It was then hypothesised that i) S-PANI membrane can overcome acid leaching and instability of PANI membranes and that the ii) self-doping could be exploited to prepare fouling resistant membranes as it enhances surface potential and promotes charge-charge interactions with the solutes.

It is well known that the membrane properties can be adjusted by cross-linking them using either chemical or thermal methods or a combination of both. Thermal cross-linking is a method to prepare membranes with a shrunk structure and recently, a method to prepare NF PANI-PAMPSA membrane via low temperature thermal cross-linking has been proposed [25]. Chemical crosslinking is used for fine-tuning the structure properties of polymers used in membranes, not only improving chemical stability but also affecting the permeance and the pore size [13]. The mechanism of action is the formation of stable bonds among the polymer chains, which allow them to be efficiently

packed and overcome their high free volume and rigidity. An advantage of performing chemical cross-linking is that it can be controlled by changing concentration and cross-linking time. Previously the effect of DCX and GA on nanofiltration properties of PANI have been shown [13], however, the anionic sulfonic groups are bulky therefore their steric hindrance as well as their charge could affect the membrane formation process increasing the porosity. Hence the effect of the self-doping sulfonic group during the cross-linking of S-PANI will be investigated. Furthermore TLC is a cross-linker that have been used to modify the properties of other polymers [44], but this is the first report showing the effect of TCL as a cross-linker for PANI or S-PANI. TCL is highly reactive to amino compounds [170] and as such could be an effective cross-linker for S-PANI by targeting the amine sites.

Hence this chapter covers the preparation of novel membranes using pure S-PANI. The low fouling S-PANI membrane is synthesised via non-solvent phase inversion and its morphology, performance and antifouling properties are compared with PANI membrane. To further improve the solvent resistance of S-PANI membrane, the effect of DCX and GA as chemical cross-linkers will be investigated. Thermal cross-linking at different temperatures is also studied. Furthermore, we report for the first time the effect of TCL in cross-linking self-doped S-PANI. Permeance and rejection of the developed S-PANI membranes is measured in a dead-end cell using pure water and a solution of different molecular weight polyethylene glycols. Solvent stability is tested in a range of solvents in both static (immersion test) and dynamic mode (in-filtration test). The low fouling behaviour of S-PANI membranes is evaluated in a crossflow cell using BSA as model foulant. Ultimately the conductivity of both pure S-PANI membranes, and composite S-PANI/graphene oxide membranes is characterised and the performance of the two membrane systems is compared.

5.2 Synthesis of self-doped sulfonated polyaniline S-PANI

To fabricate S-PANI membranes, the polymer was synthesised via radical polymerisation using APS as radical initiator as reported in the method section 3.3.1. The obtained green powder was characterised to determine if sulfonation has occurred and the degree of doping. PANI was also synthesised and characterised to compare its properties with the sulfonated derivative.

5.2.1 FTIR characterisation

FTIR confirmed the chemical structure of S-PANI and PANI membranes (Figure 31).The PANI spectrum has two characteristic peaks at 1449 cm^{-1} and 1554 cm^{-1} corresponding to the benzenoid (B band) and quinoid form (Q band) of PANI [171]. The band at 1279 cm^{-1} is assigned to both C-H and C-N stretches whereas the para-disubstitution characteristic of PANI is reflected by the peak at 810 cm^{-1} of the C-H bending out of plane [172]. The FT-IR spectrum of S-PANI has additional peaks at ~1030-1070 cm^{-1} (S=O stretching) and another at 707 cm^{-1} (S-O stretching). The peak at 825 cm^{-1} has been assigned to the tri-substitution of the benzene ring. Characterization results are in agreement with the literature [19].

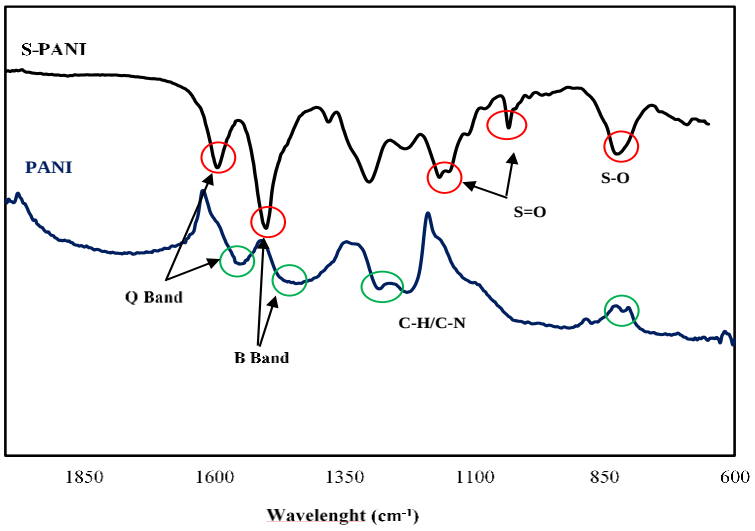

Figure 31: Vibrational spectra of S-PANI and PANI

5.2.2 UV-VIS analysis

UV-VIS spectroscopy was used to observe and compare the optical properties of PANI and S-PANI. Figure 32 shows the resulting absorbance spectra of the two polymers in NMP. S-PANI has two humps at 342 nm and at 655 nm which correspond to the B-Band and the Q-band respectively. The hump at 342 nm (B-Band) derives from the π→π* transition associated with π electrons of benzenoid rings whereas the absorption in the visible range at 655 nm (Q-band) is due to the excitation of an electron from the highest occupied orbital of benzenoid rings to the lowest occupied orbital of the quinoid ring. PANI presents a shift of the same B Band at 355 nm and the Q band is shifted at 630 nm. As reported in the literature, these results suggest the electronic delocalisation is higher in S-PANI where the SO_3H groups have a self –doping effect on the quinone structure [20].

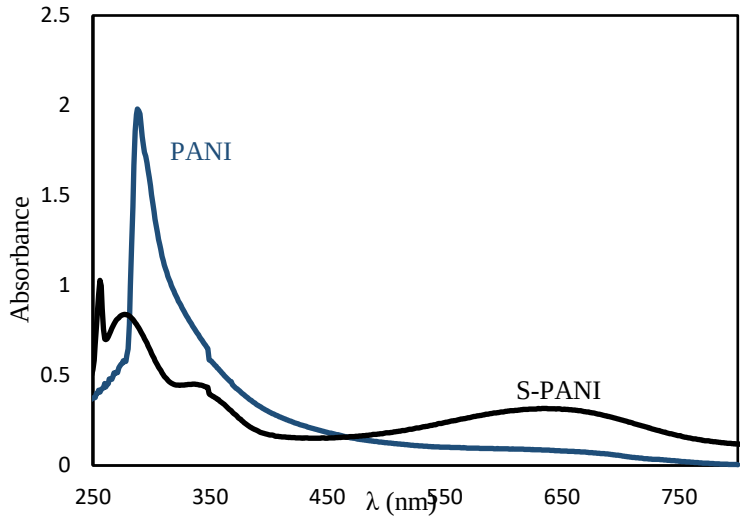

Figure 32: UV-VIS spectra of PANI powder and S-PANI powder in NMP (0.01 g/L)

5.2.3 SEM EDX

SEM-EDX analysis was used to determine the degree of sulfonation of the S-PANI powder. Both PANI and S-PANI are conducting polymers that can be converted from insulators to conductors through acid doping. PANI oxidation state can be controlled by external protonic doping, however, in S-PANI, the addition of sulfonic groups on its benzenic structure introduce a covalently bond acid group that make the polymer self-protonated or self-doped [17]. The calculated S:N ratio for the synthesised S-PANI is 0.45 (Table 14) corresponding to a fully doped S-PANI with both positive and negative charges. In this oxidation state, S-PANI acts as a zwitterionic polymer with high hydrophilicity and reported low fouling tendency [18]. SEM images of the powder are reported in Figure 33 and shows S-PANI powder consisting of a spherical-like structure.

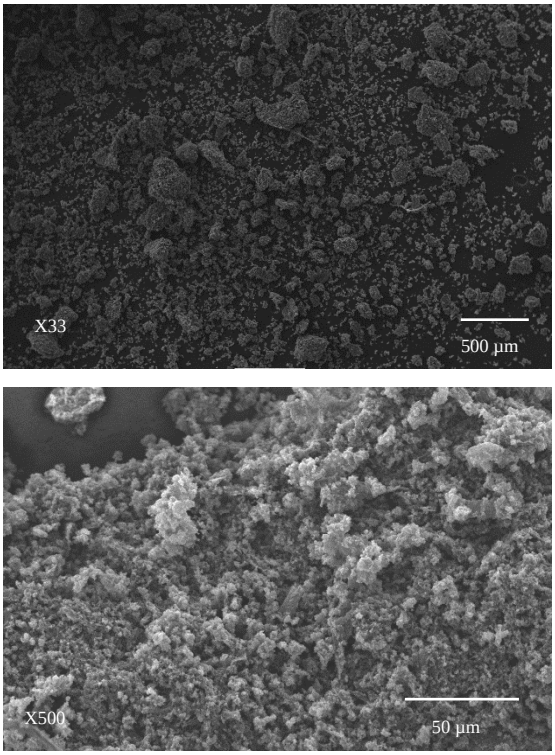

Figure 33: SEM images of S-PANI powder at 2 different magnifications

Table 14: Atomic % and weight% of S-PANI powder

IASP01			IASP02		
Element	Weight %	Atomic %	Element	Weight %	Atomic %
C	67.4±0.76	76.2±0.80	C	67.2±0.59	76.5±1.29
N	11.2±0.60	10.9±0.59	N	10.1±1.47	9.92±1.35
O	9.17±0.47	7.78±0.40	O	9.5±0.94	8.11±0.75
S	9.02±0.31	3.82±0.13	S	10.3±1.46	4.4±0.66
Cl	3.10±0.11	1.19±0.04	Cl	2.79±0.38	1.08±0.15

5.3 Preparation of S-PANI membranes

5.3.1 Optimisation of membrane fabrication conditions

Table 7 reports the different parameters investigated in the preparation of S-PANI membranes. After an initial screening of polymer concentration,

membrane thickness, and composition of the dope solution a 23% w/w load of polymer concentration in a mixture of NMP/4-MP and THF was selected as an optimal dope solution. It has been reported that the use of the additive in the dope solution could help forming a denser active layer. Previous studies have reported that THF is the best additive when used in combination with NMP to prepare PANI PAMPSA membranes. 4-MP was added in the dope solution to prevent the polymer to gel. MSP15, MSP18 and MSP1T were unstable and disintegrated when cut in coupons for filtration experiments, most likely because of the weak interaction with the support layer.

5.3.2 Characterisation of (UF) S-PANI membranes

5.3.2.1. Membrane morphology

The morphology of PANI and S-PANI is reported in Figure 34. Cross-sections of PANI and S-PANI membranes differ with the number and size of the macro-voids and cavities; PANI has a porous layer with regular small cavities on the top and bigger voids on the bottom and S-PANI presents big and dispersed macro-voids. The morphology of S-PANI membrane is in agreement with other studies where the inclusion of the hydrophilic moiety increased the water diffusion rate during phase inversion and causes the formation of large macro-voids [21, 173].

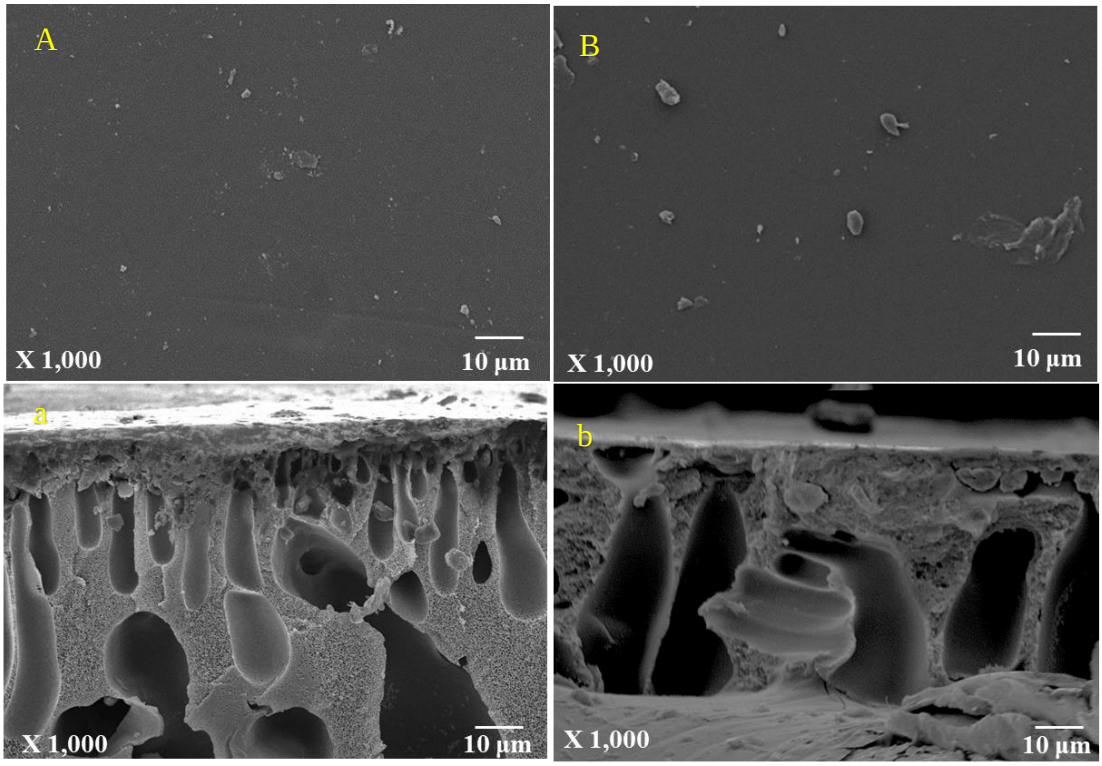

Figure 34 : SEM surfaces and cross-sections of (a,A) PANI and (B,b) S-PANI membrane

5.3.2.2. Contact angle

To assess the surface hydrophilicity, the wettability of the prepared S-PANI membranes was investigated via sessile drop technique and compared with the wettability of PANI membrane. Figure 35 illustrates the change in contact angle as a function of time for PANI and S-PANI that present an initial contact angle of 73±10° and 73±2° respectively. For S-PANI, the contact angles rapidly decrease reaching a value of 42±6° after 600 s, whereas PANI exhibits a contact angle of 61±8. The higher reducing rate and therefore the lower contact of S-PANI can be attributed to a membrane with low surface energy and good hydrophilicity. The sulfonation improves the wettability of the membranes suggesting that S-PANI could be potentially used as anti-fouling material and prevent the adhesion of organic matters on the membrane.

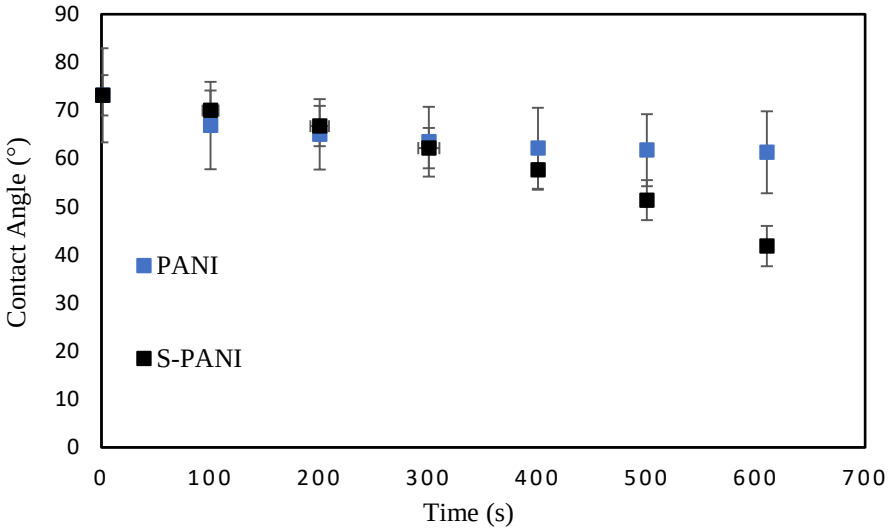

Figure 35: Contact angles as a function of time for PANI and S-PANI membranes

5.4 Cross-linking of S-PANI membranes

5.4.1 Thermal cross-linking

The initial attempt to prepare thermally cross-linked S-PANI membranes began with the investigation of the optimal temperature and time required to cross-link them.

The DSC thermogram in Figure 36 shows an endothermic peak in the range of 110-180 °C that was attributed to chain cross-linking during the heating process. Thus, to optimise the thermal cross-linking, two different temperatures were chosen: 155 °C and 170 °C for 1, 2 and 3 h (see Table 9 in method section) and the effect of the cross-linking time on membrane filtration and solvent stability were studied.

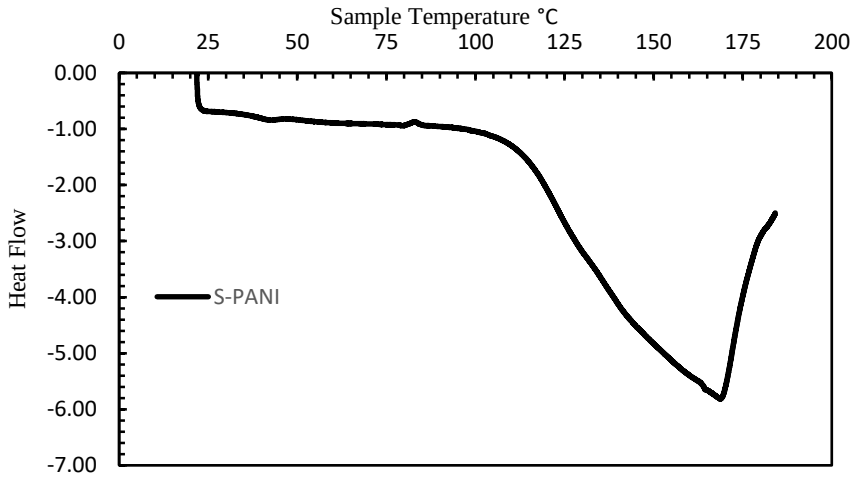

Figure 36: DSC thermogram register from 20 to 100 °C of S-PANI membrane.

5.4.1.1. Mechanical properties and solvent stability of thermally cross-linked membranes

Figure 37 reports the variations of storage E' and a loss E'' modulus for the S-PANI membranes. It can be detected by measuring the change in flexibility of a bar of a polymer upon heating. The DMA measures the storage modulus which represents the degree of stiffness of a material. At 55 °C E' modulus shows a step decrease, indicating a decrease in stiffness, while the loss modulus shows a peak, indicating an increase in molecular motion. This double feature is typical of the glass transition and indicates a physical change between a metastable glassy state and a viscous or rubbery state upon temperature change. Therefore, it could be hypothesised that during cross-linking at high temperatures the mechanical properties will change and, as indicated by the decreasing in E', the membrane would be less robust.

It was observed that the membrane at 170 °C for 3 h cross-linking time became very brittle and it was impossible to handle in further filtration experiment. SPT170_1, SPT170_2 and SPT155_3 were unstable when tested in the dead-end cell at pressures above 2 bar in water. Conversely, SPT155_1 and SPT155_2 were able to withstand pressures of 5 and 10 bar during filtration, therefore,

lower cross-linking temperature and less cross-linking time were necessary to avoid excessive brittleness of S-PANI membrane. Prolonged exposure to high temperatures appeared to worsen membrane chemical properties. In addition, SPT155 and SPT170 membranes showed no relevant improvement in their solvent stability with respect with pure S-PANI i.e. thermal cross-linking was not effective in producing solvent stable membranes.

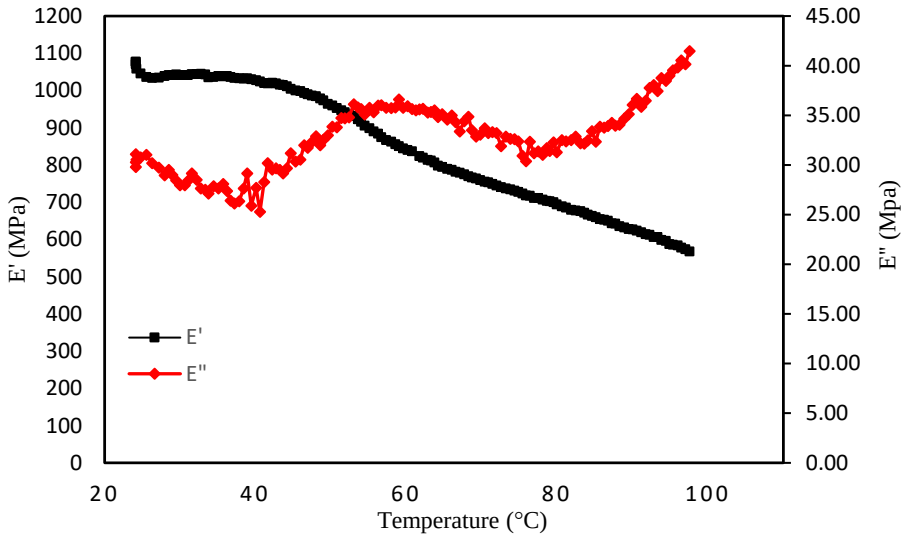

Figure 37: Variations with temperature of storage (E') and loss (E'') modulus of S-PANI membranes.

5.4.2 chemical cross-Linking: synthesis of S-PANI GA, S-PANI DCX and S-PANI TCL membrane

Cross-linking at different times was studied to optimise the reaction conditions. Initially, to check if cross-linking occurs, 1cm square of the membrane was immersed in DMF and THF for 10 minutes. The unstable membranes readily dissolved in the solvents giving a blue intense solution. The optimised cross-linking time was found to be 3 days for S-PANI DCX, 5 days for S-PANI GA and 24 h for S-PANI TCL.

5.4.2.1. FTIR of chemical cross-linked membranes

FT-IR analysis shows a comparison between the cross-linked S-PANI with pure S-PANI membrane (Figure 38). There is no significant difference between the S-PANI membranes cross-linked with DCX, TCL and GA due to the overlapping of those bands with the S-PANI ones. The spectrum of S-PANI TCL has, however, two additional peaks at 1600 cm^{-1} (amide C=O stretching) and 1200 cm^{-1} (C-N stretching for tertiary amide) that confirms the cross-linking reaction [44]. Cross-linking was further confirmed by solvent stability tests.

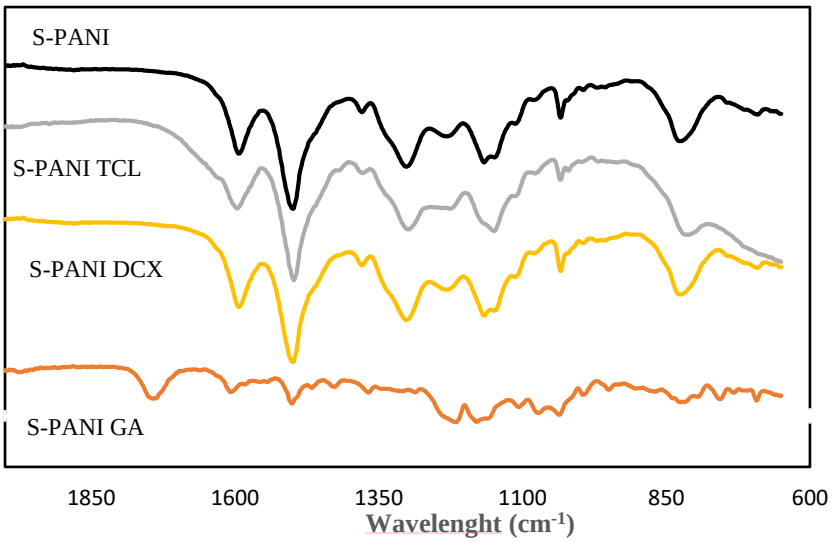

Figure 38: Comparison of S-PANI, S-PANI GA, S-PANI DCX and S-PANI TCL to characterise membranes after cross-linking

5.4.2.2. XRD analysis

The XRD method was used to analyse S-PANI membrane and the cross-linked membranes. The XRD pattern of membranes prepared with GA, DCX and TCL are displayed in Figure 39. Polyaniline and its derivatives are semi-crystalline in nature and the x-ray diffractograms of the membranes show three evident peaks with different sharpness (width) according to the degree of orientation of the polymer chains in that particular crystal plane [174]. The cross-linked

membranes show three similar peaks with different intensities meaning a consistent orientation of the crystalline domains in the same direction of the pure S-PANI and indicating that cross-linking does not greatly affect the crystal structure of polymer. The peak of S-PANI at 2Θ=22.2°, that is attributed to the periodicity parallel to the polymer chains [175], become slightly broader for cross-linked membranes. This implies that the crystal structures of S-PANI gradually turn into a disorder structure with the cross-linking which could be ascribed to shrinkage of intersegmental spaces [176].

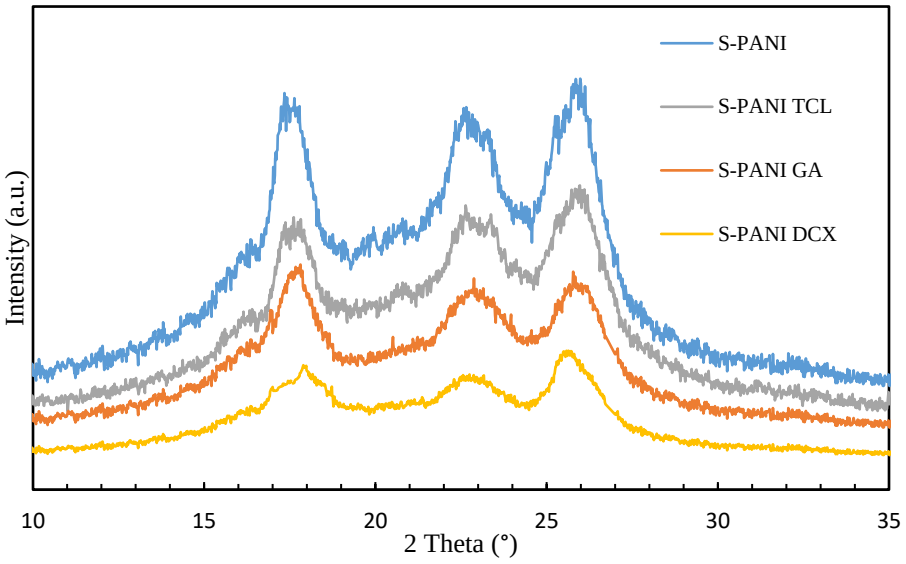

Figure 39: XRD patterns of S-PANI membrane and S-PANI membranes cross-linked with GA, TCL and DCX.

5.4.2.3. Morphology of chemically cross-linked membranes

SEM was used to study the morphology of S-PANI and chemically cross-linked S-PANI membranes and compare them with pure PANI. Figure 40 displays the top cross-sections and surfaces of all chemically cross-linked membranes. All the membranes show a smooth surface with no obvious pores or patterns. The small particles present on all the top surfaces are most likely impurities deriving from the sample preparation process. All cross-sections present an asymmetric structure with a porous bottom layer and a denser top skin layer. The S-PANI

GA membrane (Figure 40 A) has a narrower bottom finger-like structure in difference to the other cross-linked membranes (Figure 40B and Figure 40C) that present large voids and cavities. This difference in the structure can be attributed to the inclusion of the cross-linker solution in the coagulation bath, causing a delayed de-mixing of the polymer [177] (see section 2.3 for the method). Yet the macro voids present in the studied PANI, S-PANI, S-PANI TCL and S-PANI DCX membranes can be related to the better affinity between NMP used in the casting solution and water, which caused the instantaneous de-mixing [11]. Cross-sections of S-PANI DCX and S-PANI TCL show that the former has a porous sublayer with a regular pattern of large cavities and the latter is in contrast denser with a few dispersed cavities.

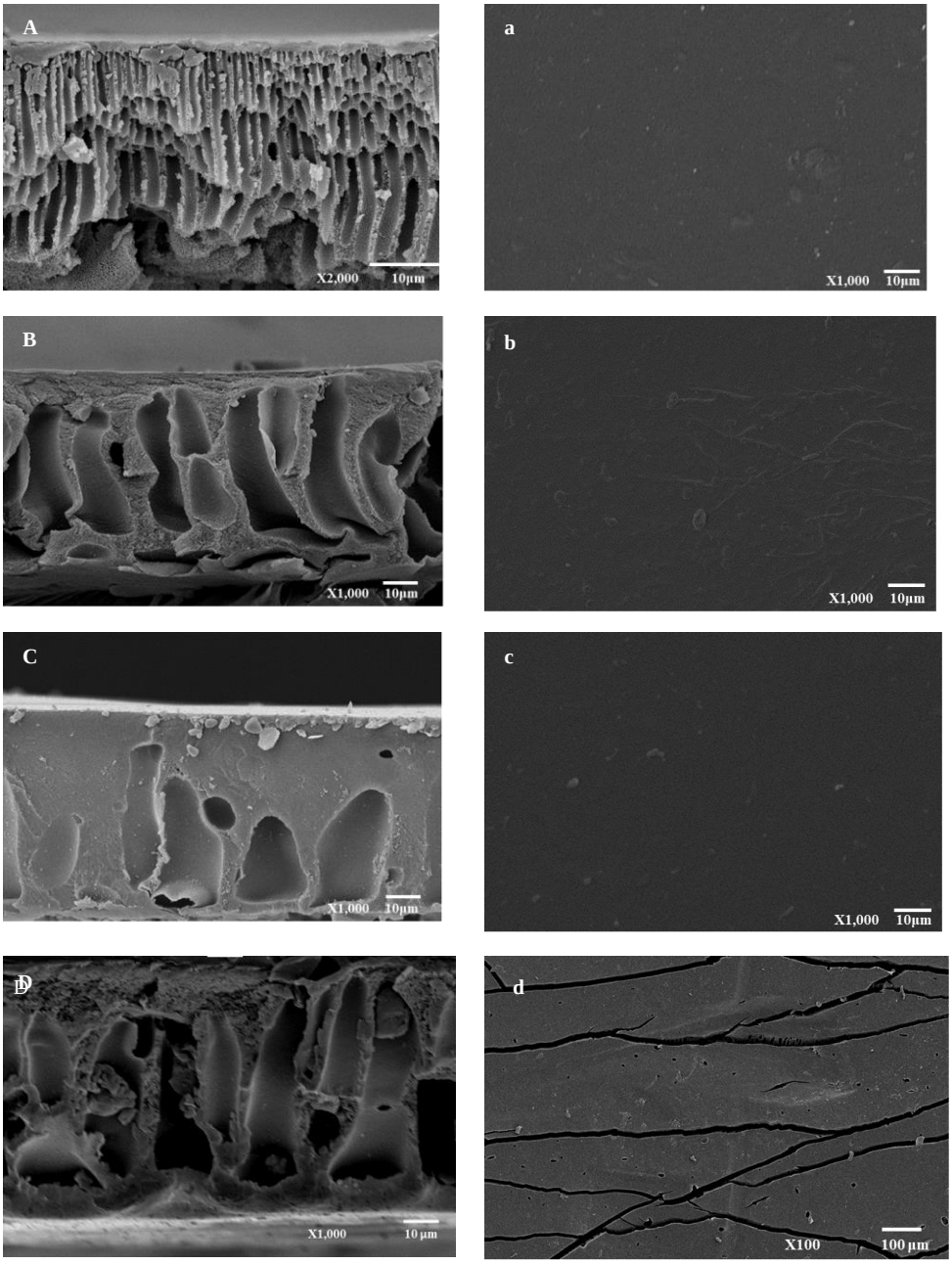

Figure 40: Cross-section SEM images of (A) S-PANI GA (B) S-PANI DCX and (C) S-PANI TCL and (D) SPT170.Top Surface SEM images of (a) S-PANI GA, (b) S-PANI DCX and (c) S-PANI TCL and (d) SPT170

Figure 41 shows cross-sectional images of the top surface layer of the S-PANI and chemically cross-linked S-PANI membranes taken at higher magnification.

The top layer of (A) S-PANI, (C) S-PANI DCX and (D) S-PANI TCL consists of a layer of densely packed irregular nodular structures. These nodular structures aggregate and become more porous and irregularly distributed along the bulk in the pure S-PANI membranes, but they remain densely packed in the cross-linked membranes. A magnification of 10,000x and 50,000x was necessary to study the top layer of (B) S-PANI GA membrane, which consists of spherical structures that rearrange in narrow-finger like voids.

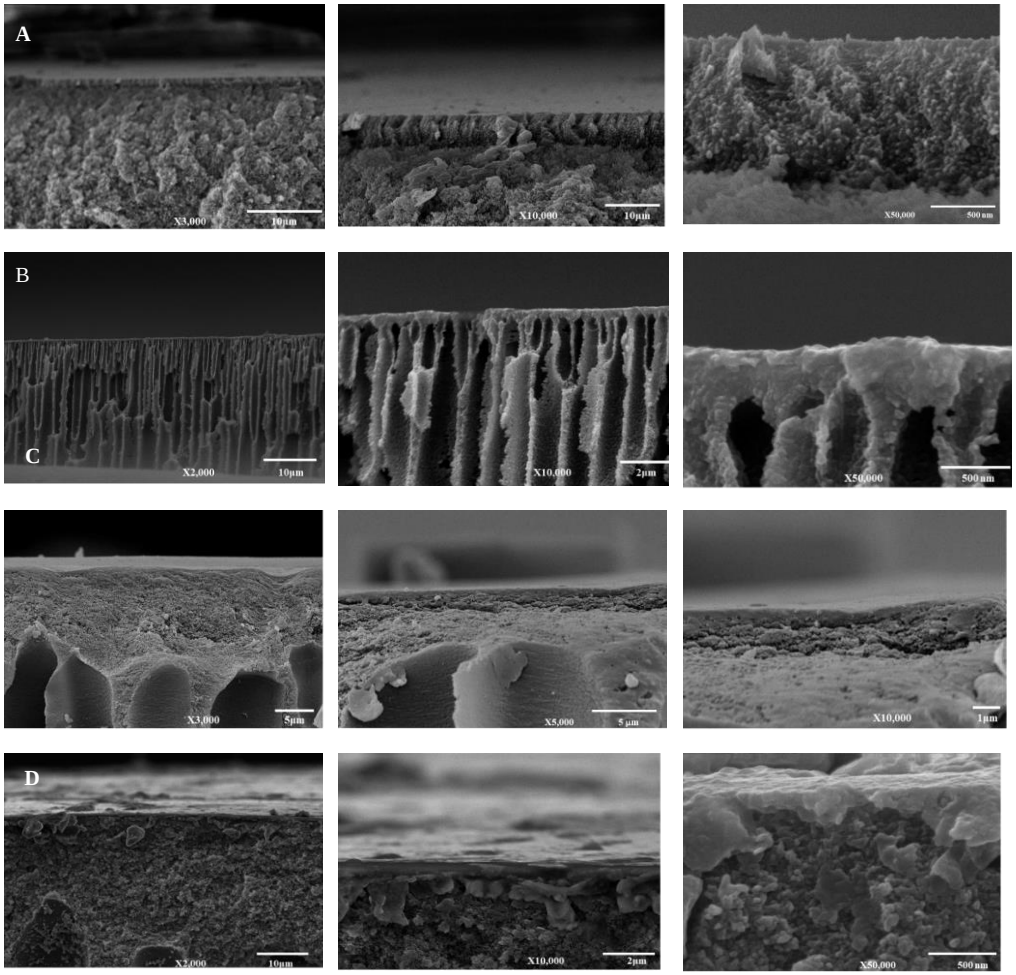

Figure 41: Cross-section SEM images of the top surface layer of (A) S-PANI (B) S-PANI GA (C) S-PANI DCX and (D) S-PANI TCL.

5.4.2.4. Stability in organic solvents: visual stability study

Stability in organic solvents was evaluated using an immersion test in different solvents. Figure 42 shows the effect of DMF and DMAc on membranes stability.

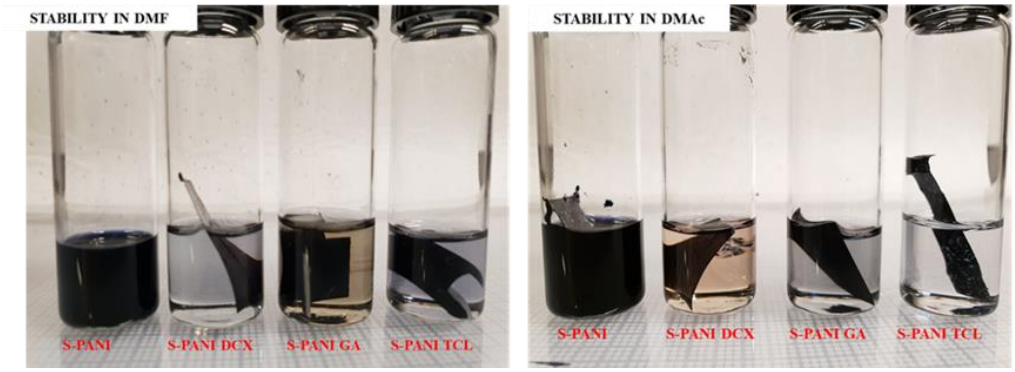

Figure 42: Effect of DMF and DMAc on membrane stability. Picture is taken after half an hour from immersion in solvents.

S-PANI is directly dissolved in DMF and DMAc, giving a vivid blue solution, whereas S-PANI GA, S-PANI DCX and S-PANI TCL appear to be more resistant to the harsh polar aprotic solvents giving a slightly darker solution after 10 minutes. Therefore, the dissolution of the membrane was quantify through solvent resistant tests [178] to determine the effect of cross-linking on S-PANI membranes. Table 15 reports the % weight loss for each membrane after soaking the samples for 1 month in DMAc, DMF, EtOH, toluene, ethyl acetate and acetone. The test in different solvents confirms the superior chemical stability of S-PANI GA, S-PANI DCX and S-PANI TCL. The improved solvent stability is due to the formation of interchain bonds in the polymer that 1) change the physical network by creating fix points and 2) limit the molecular chain movements making the whole membrane less prone to dissolve.

Table 15: % Weight loss data for S-PANI membranes and S-PANI GA, S-PANI TCL and S-PANI DCX membranes in different organic solvents. Data were collected after 1 month of soaking in the chosen solvent.

Membrane	Weight loss in solvent					
	DMAc	DMF	EtOH	Toluene	EA	Acetone
S-PANI	11.0 %	15.0 %	0.0%	0.0%	0.0%	0.0%
S-PANI GA	0.40 %	0.58 %	0.0%	0.0%	0.0%	0.0%
S-PANI DCX	0.60 %	0.47 %	0.0%	0.0%	0.0%	0.0%
S-PANI TCL	0.38 %	0.88 %	0.0%	0.0%	0.0%	0.0%

These results show that S-PANI can be chemically cross-linked to prepare high solvent stable membranes for applications where chemical stable membranes are required but their availability is limited [32]. The solvent stability could be exploited in reactions like the Suzuki coupling and kinetic resolution where hydroxide bases or harsh reaction conditions require robust and durable membranes.

5.4.2.5. Membrane surface hydrophilicity; effect of chemical cross-linking

Surface hydrophilicity data of chemically cross-linked membranes are reported in Figure 43. The cross-linked membranes present initial contact angles of 71±4° (S-PANI DCX), 70±7° (S-PANI GA) and 70±3° (S-PANI TCL). The overall trend for all membranes is a very small decrease in the contact angles after 600 s meaning that the cross-linking increased the H_2O transport resistance and slower the reducing rate over time. The trend for all cross-linked membrane is similar to that of pure PANI membrane. This suggests that the main factor affecting the wettability of cross-linked membranes is the slower penetration of the water drop because of the tighter pore size rather than the presence of the sulfonic group.

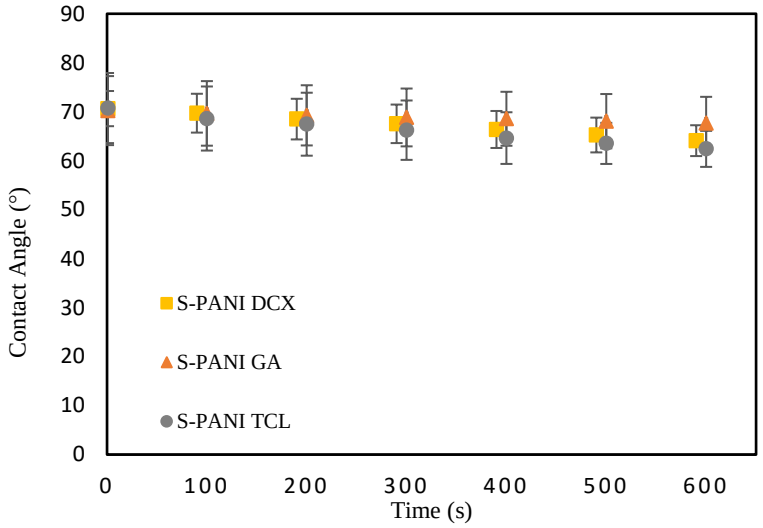

Figure 43: Contact angles as a function of time for S-PANI DCX, S-PANI TCL and S-PANI GA membranes

5.5 Investigation of membrane performance

5.5.1 Water flux and PEGs rejection of S-PANI membrane, thermally cross-linked S-PANI membrane and chemically cross-linked S-PANI membrane in dead-end cell

Figure 44 shows the pure water flux decline for all membranes at 2 bar. At least 1h was required for all membranes to reach a steady flux. Compaction of polymeric membranes and consequent flux decline is a well-known issue in pressure-driven processes [179]. It can further be observed that PANI shows a higher flux decline and less resistance to compaction in comparison to S-PANI. S-PANI has a stable pure water flux of 117±20 L $m^{-2}h^{-1}$ and PANI has a water flux of 165±35 L $m^{-2}h^{-1}$. These values are an agreement with the literature [20] and can be placed in the ultrafiltration range.

For the cross-linked membranes, S-PANI GA and S-PANI TCL show the greatest flux decline reaching values of 22±8 L $m^{-2}h^{-1}$ and 13±4 L $m^{-2}h^{-1}$ respectively, which can be considered in the range of tight ultrafiltration. S-PANI DCX has an initial lower flux and the flux decrease below 1±0.5 L m^{-2} h^{-1}. As reported in 5.4.2.5 chemically cross-linked membranes showed a lower

surface free energy and therefore a higher H_2O transport resistance that is reflected in the flux decline to very low values. Fluxes of thermally cross-linked membranes are lower than pure PANI and pure S-PANI but all very different. It looks like SPT155 cross-linked for 1h has a lower permeance with respect of the same SPT155 cross-linked for 3hours. This could be explained as loss of membrane mechanical stability at prolonged exposure to high temperature. Nevertheless, the SPT155X3 was less brittle than the other thermally cross-linked samples but still not reusable multiple times as the chemically cross-linked membranes.

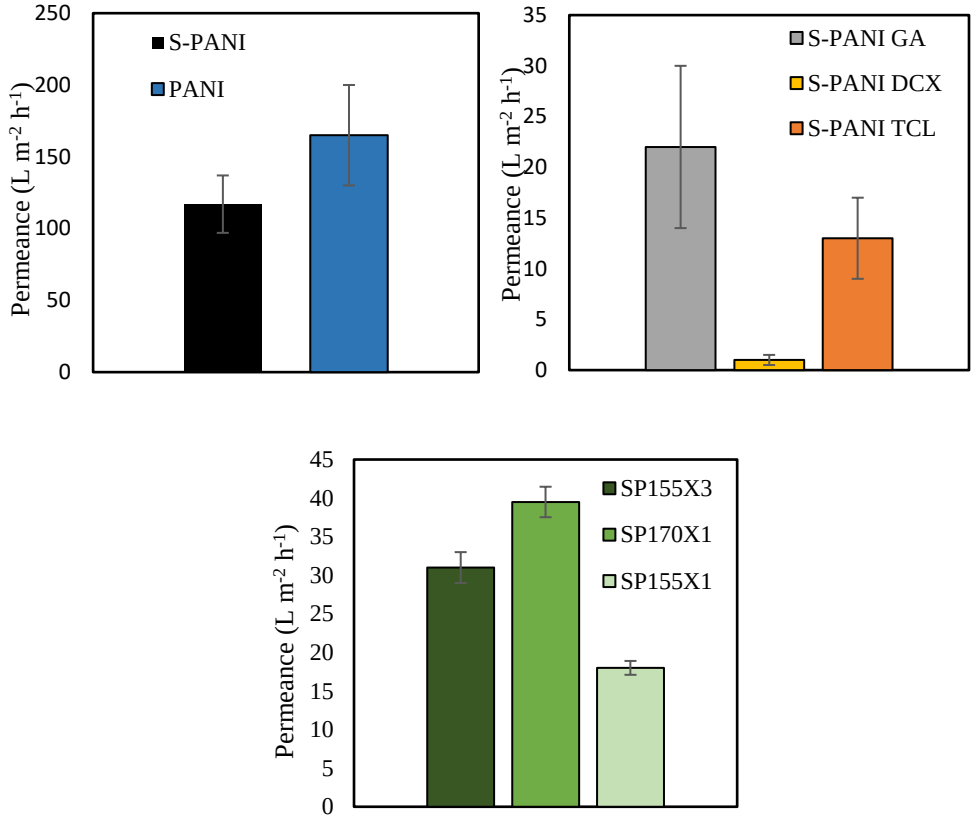

Figure 44: Pure water fluxes for S-PANI (average of two membrane samples of batch MSP2300 and MSP2302),PANI (average of two membrane samples of the same batch MP20) S-PANI TCL and S-PANI DCX (average of two membrane samples from batch MSP2302), S-PANI GA (average of two membrane samples from batch MSP2303 and thermally cross-linked S-PANI membranes (data are average of two membrane samples of batch MSP2301) conditions: dead-end cell 2 bar and 20 °C.

Figure 45 shows the performance curves of S-PANI membranes and chemically cross-linked S-PANI membranes tested with different PEGs in dead-end cell. S-PANI rejects only 12% for the oligomer with the highest molecular weight (PEG 5000) at 2 bar. The membrane was tested at a different pressure to evaluate its stability to elevated pressure resulting in 3 bar maximum operational conditions. This suggests that S-PANI has potential applications in the UF/tight UF range, similar to PANI [34], and that the addition of sulfonic groups is a chemical

modification that affects the hydrophilic properties but has no effect on the membrane pore size.

In comparison, the cross-linked membranes, S-PANI DCX and S-PANI TCL, were able to reject the higher MW PEG (5000 Da) of 56 and 48% respectively. These membranes showed an improve filtration stability with maximum operating pressures of 10 bar. S-PANI GA showed the best performance with a 93 % rejection of the PEG 5000 and a maximum operating pressure of 30 bar. In addition, the MWCO for this membrane was found to be 1800 and S-PANI GA was the only membrane that could be fully characterised in terms of MWCO. Crosslinking forms stable bonds among the polymer chains, which allows them to be efficiently packed and overcome their high free volume and rigidity. Examples of chemical cross-linking of PANI with DCX and GA [13] and aniline with TCL [44, 170] have been reported. In the case of PANI, chemical modification produces a nanofiltration membrane with high solvent resistance. In contrast, the results from this work show that S-PANI DCX and S-PANI TCL has an improved solvent resistance but most likely presents potential applications in the tight UF range. The cross-linking with GA successfully produced a membrane with a tighter pore size and almost 90 % rejection of all tested PEGs.

Nevertheless, all the chemically cross-linked membranes showed enhanced stability in several solvents, especially harsh polar aprotic solvents such as DMF, with respect to S-PANI. Overall, the chemical treatment makes the membrane more stable in solvents due to the formation of strong covalent bonds but, as hypothesised, the big sulfonic groups prevent the shrinking of the membrane pore size. As stated in 5.4.1, thermal cross-linking at different temperatures produced brittle membranes with lower solvent resistance and scarce stability during filtration. Indeed, the PEGs rejection profile revealed that the SPT155 and SPT170 were not able to reject larger PEGs most likely because of leaking during the filtration test.

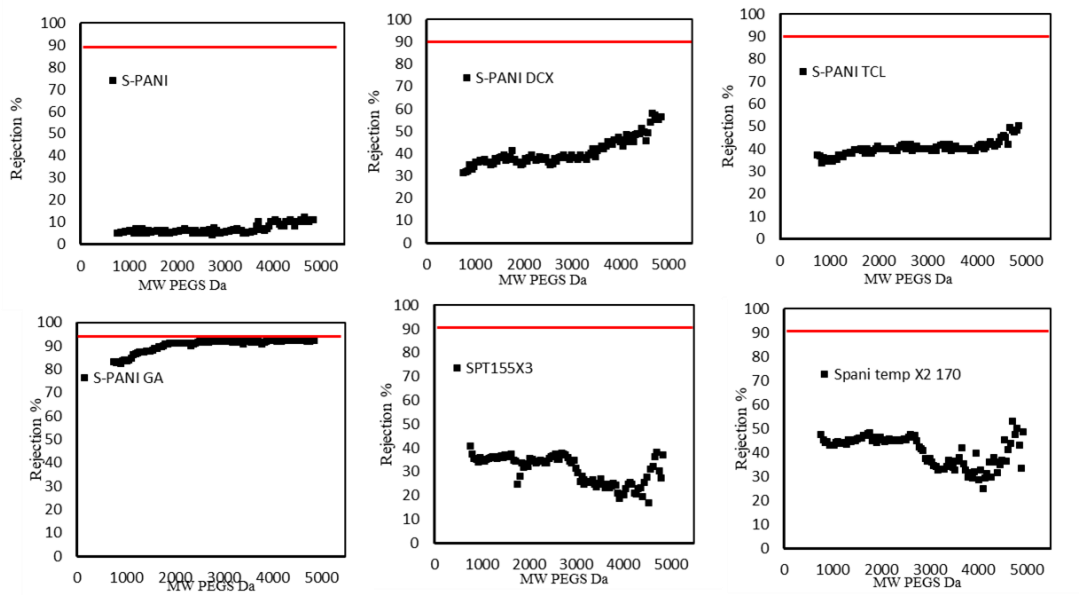

Figure 45: Rejection curve of (A) S-PANI and chemically cross-linked S-PANI membranes: (B) S-PANI DCX, (C) S-PANI TCL and (D) S-PANI GA. Operation conditions are 1 bar, 25 °C, dead-end filtration. The red line at 90% marks the MWCO.

5.5.2 Solvent stability study: investigating DMF resistance of chemically cross-linked S-PANI membrane in the dead-end cell

Aprotic solvents such as DMF, DMSO etc. are primarily used as industrial solvents to process polymer fibers, films, and surface coatings and as a crystallization medium in the pharmaceutical industry [180]. Visual studies have shown that chemically cross-linked S-PANI membranes have improved solvent stability in harsh aprotic solvents. Hence, we further assessed this stability during filtration in DMF re-using the same membrane sample after 1 week. For this filtration study, 7 months old membranes were chosen. Figure 46 shows DMF permeance over time from two different runs of the chemically cross-linked membranes. During the first run, the permeate was only slightly coloured and the flux did not increase over the 2 hours of the filtration. S-PANI GA, S-PANI TCL and S-PANI DCX showed stable permeance of 6.1 L m^{-2} h^{-1} bar, 6.9 L m^{2} h^{-1} bar and 8.4 L m^{-2} h^{-1} bar respectively. During the second run, the permeate did not change colour and interestingly all the membranes showed a

lower permeance. S-PANI GA was 4.2 L m^{-2} h^{-1} bar^{-1} and S-PANI DCX was 4.8 L m^{-2} h^{-1} bar^{-1}. S-PANI TCL showed the lowest value of 0.6 L m^{-2} h^{-1} bar^{-1}. In summary, these results showed the excellent chemical resistance and stability of chemically cross-linked S-PANI membranes in DMF.

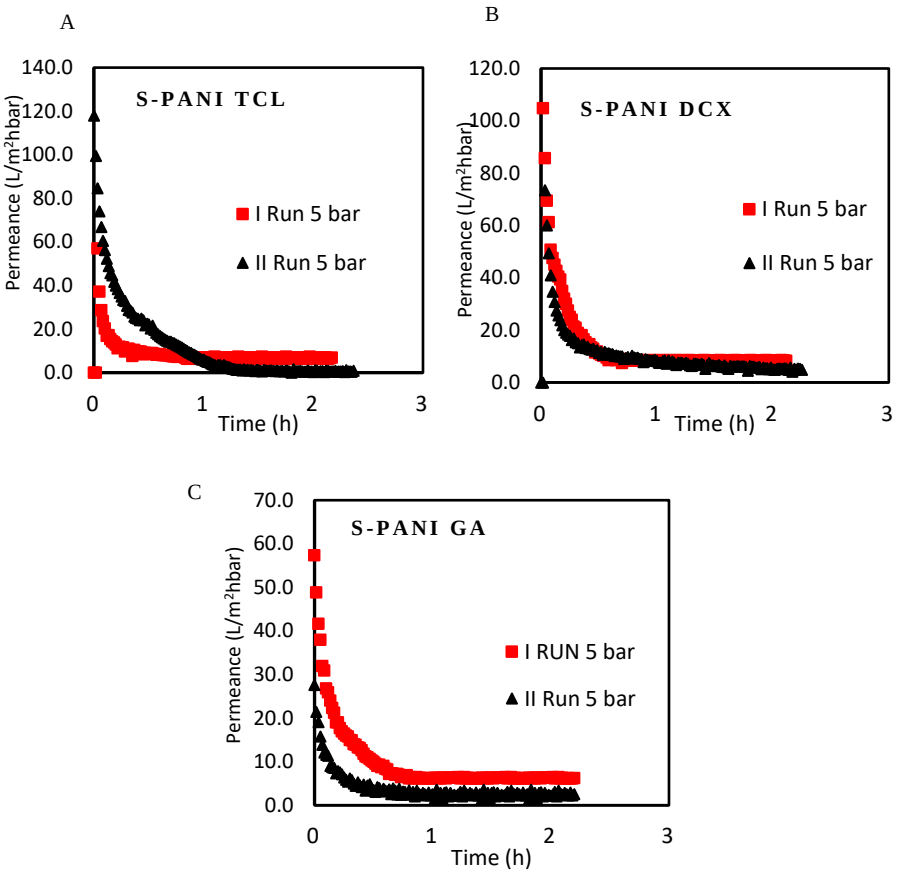

Figure 46: DMF permeance over time of (A) S-PANI TCL, (B) S-PANI DCX, (C) S-PANI GA. Operation conditions are 5 bar, 25 °C, dead-end filtrations. The same membrane sample was used twice.

5.5.3 Fouling study: comparing the fouling resistance of S-PANI, PANI and S-PANI GA membrane in cross-flow

As reported in 2.3.5, membrane fouling in biocatalytic and homogeneous catalytic processes, reduces the production rates and increases the complexity of membrane operations. Backwashing and chemical cleaning or frequent replacement of the membranes are widely applied solutions to overcome fouling,

that, however, increases the overall process costs. The effect of the incorporation of the sulfonic group during synthesis on membrane potential antifouling ability was investigated using BSA as a model foulant in cross-flow. For long-term stability test in cross-flow, pure S-PANI, PANI and S-PANI GA (best chemically cross-linked S-PANI) membranes were selected.

Experiments were performed using one membrane and running pure water for 1 h (Jw). Then the membrane was fouled with 1g/L of BSA solution and the flux decline was recorded for 1 h. The cleaning step was performed washing thoroughly the membrane with pure water for half an hour and the flux recovery was recorded (JwI). The fouling-cleaning cycle was repeated twice (Jw II and Jw III). Figure 47 reports the time-dependent flux values of S-PANI, PANI and S-PANI GA membranes. Fouling indexes calculated for the first cleaning cycle are reported in Table 16. S-PANI showed very good antifouling behaviour during the first cycle in cross-flow with a FRR of the 87±7% which was larger than the 40±2% FFR of PANI. During the first cycle, S-PANI showed also low irreversible fouling IFR value of 13±4% which was much lower than the IFR of 60±4% of PANI. Usually higher values of FRR and lower IFR describe a membrane with good antifouling properties [6]. S-PANI GA showed similar results with very low IFR (17±5 %) and RFR (16±6 %) and an FRR of 83±2%.

Results from this experiment show that protein adsorption is significantly reduced at the S-PANI surface compared to PANI membrane. It has been reported that the zwitterionic surface formed a hydration layer which stops the BSA absorption [6]. Both S-PANI and S-PANI GA membranes performed better during the first cycle showing a TFR of 39 ±2 and 33±6%, in contrast with PANI, which presented a very poor flux recovery and a high TFR% of 61±5%. Overall after 3 continuous fouling and cleaning cycles S-PANI shows Fr of 60 % starting from an initial flux value of 107±2 l/m^2h, PANI shows Fr of 41% starting from 84±2 l/m^2h and S-PANI GA showed Fr of 50% with an initial flux of 14±3 l/m^2h. Overall the performance of the PANI membranes improved after sulfonic groups

were introduced demonstrating that S-PANI membranes can be of potential use as low-fouling membranes in UF processes without the need for additional treatments or complex preparation. In addition, the tested chemical cross-linked S-PANI membrane showed a good antifouling performance demonstrating that S-PANI could be used as low fouling polymer to fabricate solvent resistant tight UF membranes.

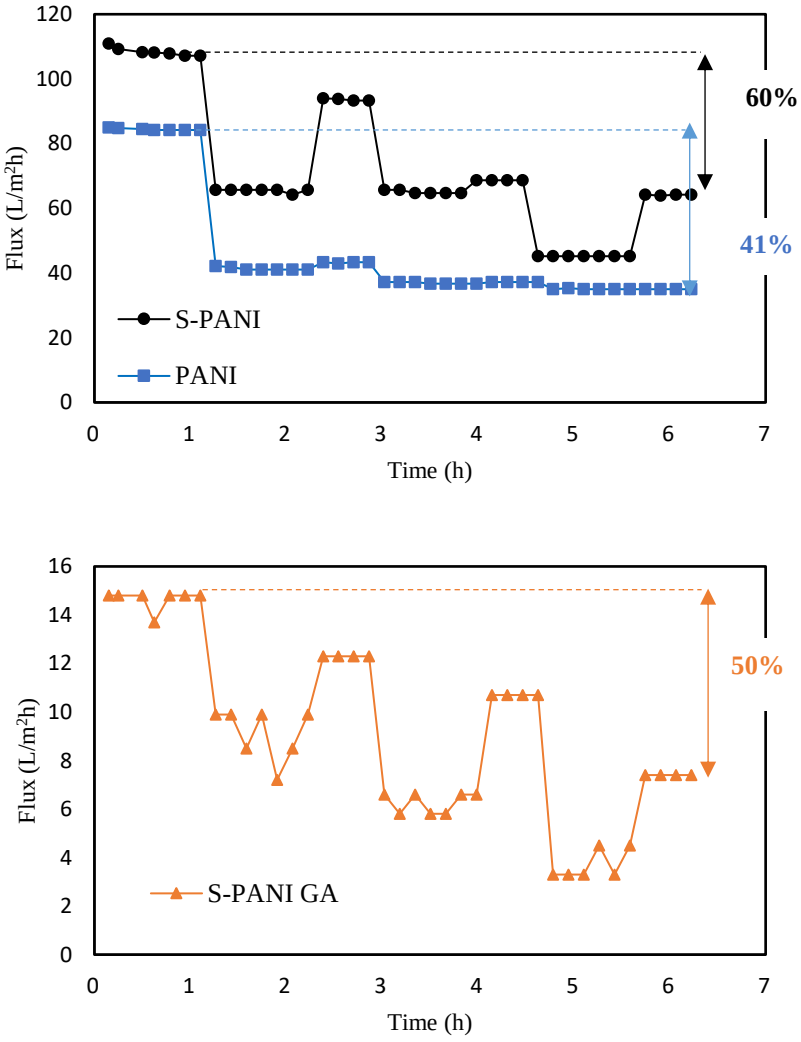

Figure 47: Time dependent flux of S-PANI, PANI and S-PANI GA membranes tested in cross-flow with BSA

Table 16: Fouling indexes for S-PANI and PANI membranes related to the first cleaning-fouling cycle.

	FRR %	TFR %	RFR %	IFR %
PANI	40±3	61±5	2±1	60±4
S-PANI	87±7	39±2	25±4	13±4
S-PANI GA	83±2	33±6	16±6	17±5

5.6 The conductivity of S-PANI membranes and synthesis of composite S-PANI/graphene oxide membranes

The separation characteristics of conducting polymers in form of a membrane can be electrochemically modulated and changes in the local chemical environment lead to changes in the membrane properties such as hydrophilicity, volume swelling, permselectivity and solute partitioning [98]. In this view, PANI membranes doped with different acids or blended with conducting particles have been studied and the most recent examples can be found in here [41, 181]. Hence, we hypothesise that S-PANI can be used in similar electro-responsive systems with the advantage of being fouling resistant and highly solvent stable. In addition, we incorporated graphene oxide GO into the pure S-PANI membrane to compare the two systems in terms of conductivity and membrane performance.

Blending nanoparticles with polymers is a well-known method to improve the permeability and antifouling ability of membrane [182]. In the case of conducting particles such as GO, the membrane acquires conducting characteristics that can be exploited to enhance the separation performance [183]. GO has also some ideal properties [184] such as excellent chemical and physical stability and the presence of carboxyl and hydroxyl groups that makes it well dispersible in water and polar organic solvents, and therefore improve the feasibility in membrane fabrication. Therefore, GO was chosen as a conducting

additive to i) compare the conductivity of a blend membrane with pure S-PANI membrane, ii) compare the selectivity and permeability of the two membranes.

5.6.1 Electrochemical properties

Preliminary studies to evaluate the electrochemical properties of S-PANI and investigate the potential to prepare responsive membranes were therefore carried out on a pure S-PANI membrane and a composite S-PANI-GO membrane. The conductivity and the presence of electrochemical transitions was evaluated using a four-probe conductivity meter and cyclic voltammetry as reported in method 3.5.2.5. Results from these experiments are reported in Table 17 and Figure 48.

Table 17: The conductivity of the prepared S-PANI-GO and S-PANI membranes was tested using a 4-probe conductivity meter by applying a current of 10 mA. The data are an average of 2 membrane samples. Data from PANI EB and PANI doped with PAMPSA are also reported.

Membrane type	**Conductivity (S/cm)**
S-PANI-GO	0.66±0.07
S-PANI	$4.44*10^{-11}$
PANI ES[11]	$5*10^{-2}$
PANI PAMPSA	$2.07*10^{-5}$

S-PANI shows a very low conductivity and no redox peak during the cyclic voltammetry (A) is detected, meaning that the prepared S-PANI membranes is mostly an insulator. S-PANI-GO shows the highest conductivity of all membranes; however, no redox peak can be seen in the voltammograms at wider potential windows. The absence of redox peaks in the S-PANI-GO voltammograms could be attributed to the small area of the active electrode surface (1 cm^2) and the fact the GO was not homogeneously dispersed onto the membrane surface as displayed in Figure 49 and Figure 50.

PANI membranes doped for 24 hours in HCl shows a conductivity value that is nine orders of magnitude higher than pure S-PANI. It has been reported, that despite the initial high surface conductivity HCl doped PANI membranes

suffered from low conductivity because of acid leaching during filtration [129]. Bigger acid dopants such as PAMPSA do not leach out in water but the membrane is not stable in solvents and the conductivity is lower than HCl doped PANI. PAMPSA possesses sulfonic groups like S-PANI that are distributed along the polymer chains and not covalently bonded to the polymer: their addition affects the steric and the electronic properties. During the formation of the membrane, the conductivity is influenced by the distribution of the polymeric chains. The material rearranges in the solvent forming domains with non-homogeneous properties. Furthermore other factors might have contributed in decreasing the conductivity: i) the addition of sulfonic group causes a loss of planarity of the rings [132, 185] and ii) the electron density of the rings is less because of the withdrawing effect of SO_3 [185].

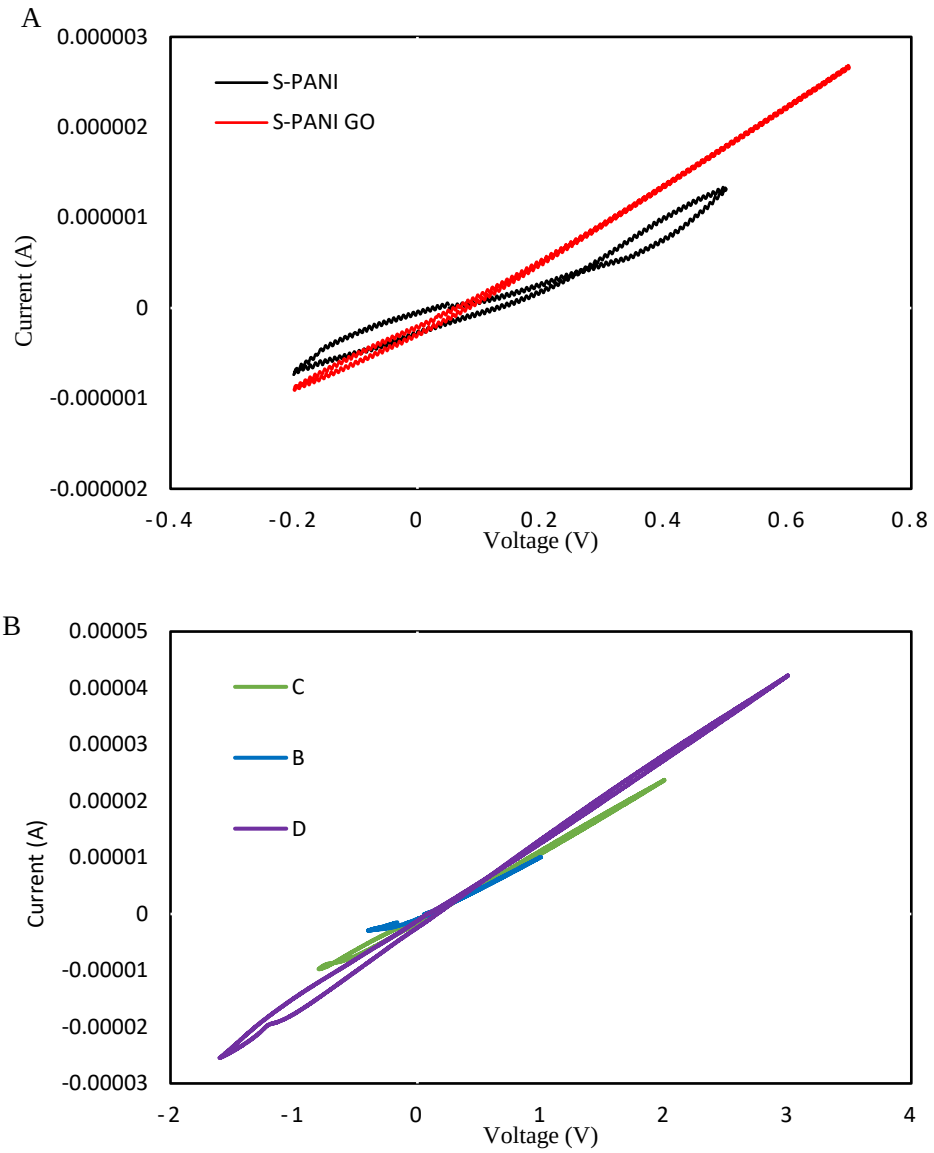

Figure 48: Cyclic voltammetry of (A) S-PANI and S-PANI/GO membranes from -0.2 V to X0.8V. and (B) additional voltammograms of S-PANI GO membranes taken at wider potential windows.

5.6.2 Characterisation of S-PANI-GO membrane

Despite the negative preliminary electrochemical evaluation, the chemical structure, hydrophilicity, morphology and membrane performance of the S-PANI-GO membranes were characterised to compare the properties with the pure S-PANI membranes. Figure 49 shows the top surface and bottom surfaces

of the prepared S-PANI and S-PANI GO membranes. No difference is spotted in the pictures of the top surfaces as S-PANI is a dark green powder and has the highest concentration in the dope solution. The bottom surface reveals that S-PANI GO forms a less uniform layer when casted onto the support, probably because of the aggregation of the GO particles and less uniform distribution of the solution onto the support [183, 186].

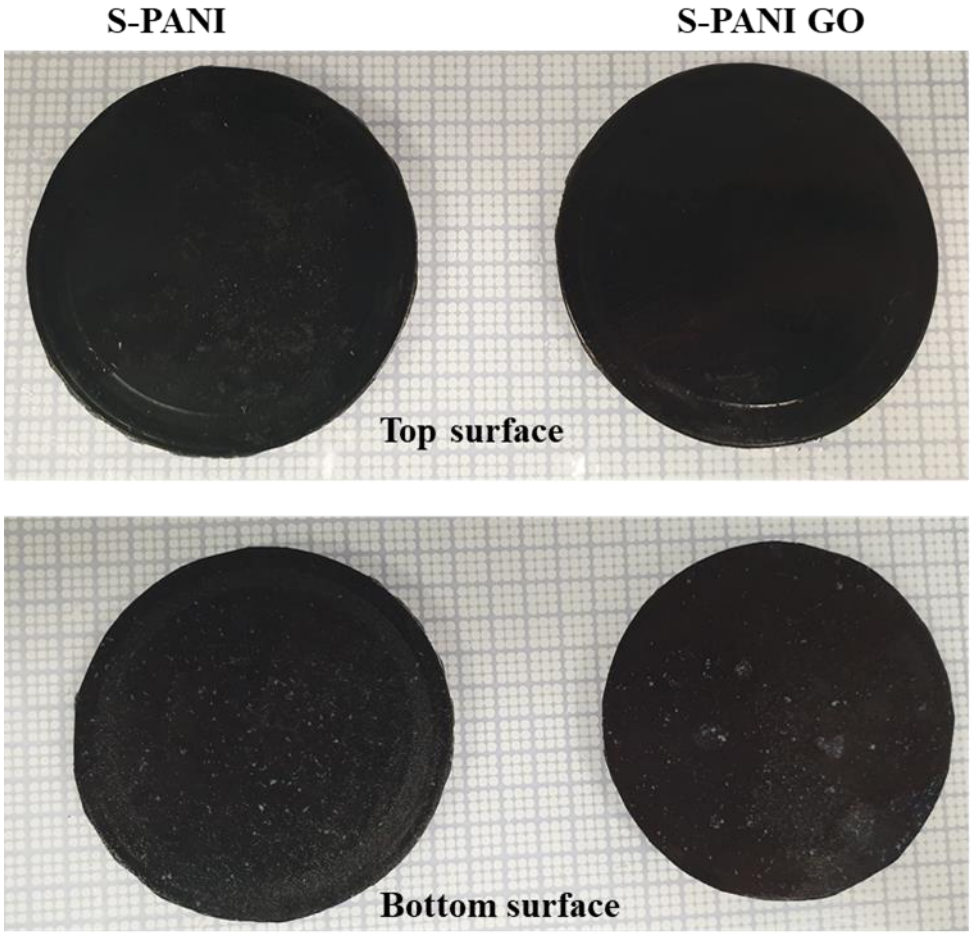

Figure 49: Picture of the top surface and bottom surface of S-PANI and S-PANI GO membranes.

The chemical structure of the prepared S-PANI/GO membrane was characterised via FTIR a (full spectra are reported in Appendix). Surface hydrophilicity and pure permeance of the membranes are reported in Table 18.

The higher contact angle of the S-PANI GO and the lower permeance could be again attributed to irregular aggregation of GO particles which could lead to pore plugging [186].

Table 18: Properties of S-PANI/GO and S-PANI membranes

Membrane	**Contact angle**	**Permeance at 1 bar**	**Cross-linking**
S-PANI/GO	60±7	22±4 L $m^{-2}h^{-1}$	Cross-linked with TCL, membrane is brittle
S-PANI	51±5	80±6 L $m^{-2}h^{-1}$	Cross-linked with DCX, TCL, GA.

Figure 50 reports the SEM surfaces and cross-sections of S-PANI-GO membranes. The top surfaces show a rough surface and irregular GO agglomeration observed at 6500x magnification. This supports the theory of the irregular dispersion of GO onto the membrane. The cross-section morphologies exhibit an asymmetric porous structure with a finger-like layer and denser sublayer with macrovoids.

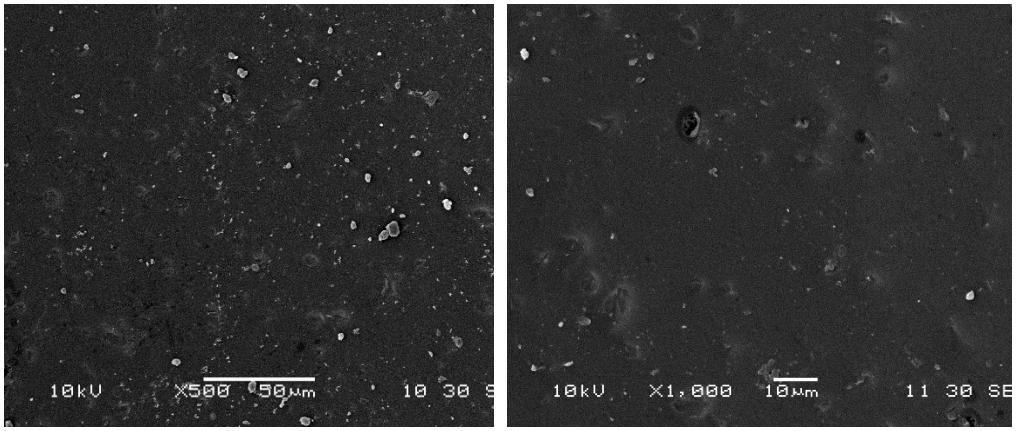

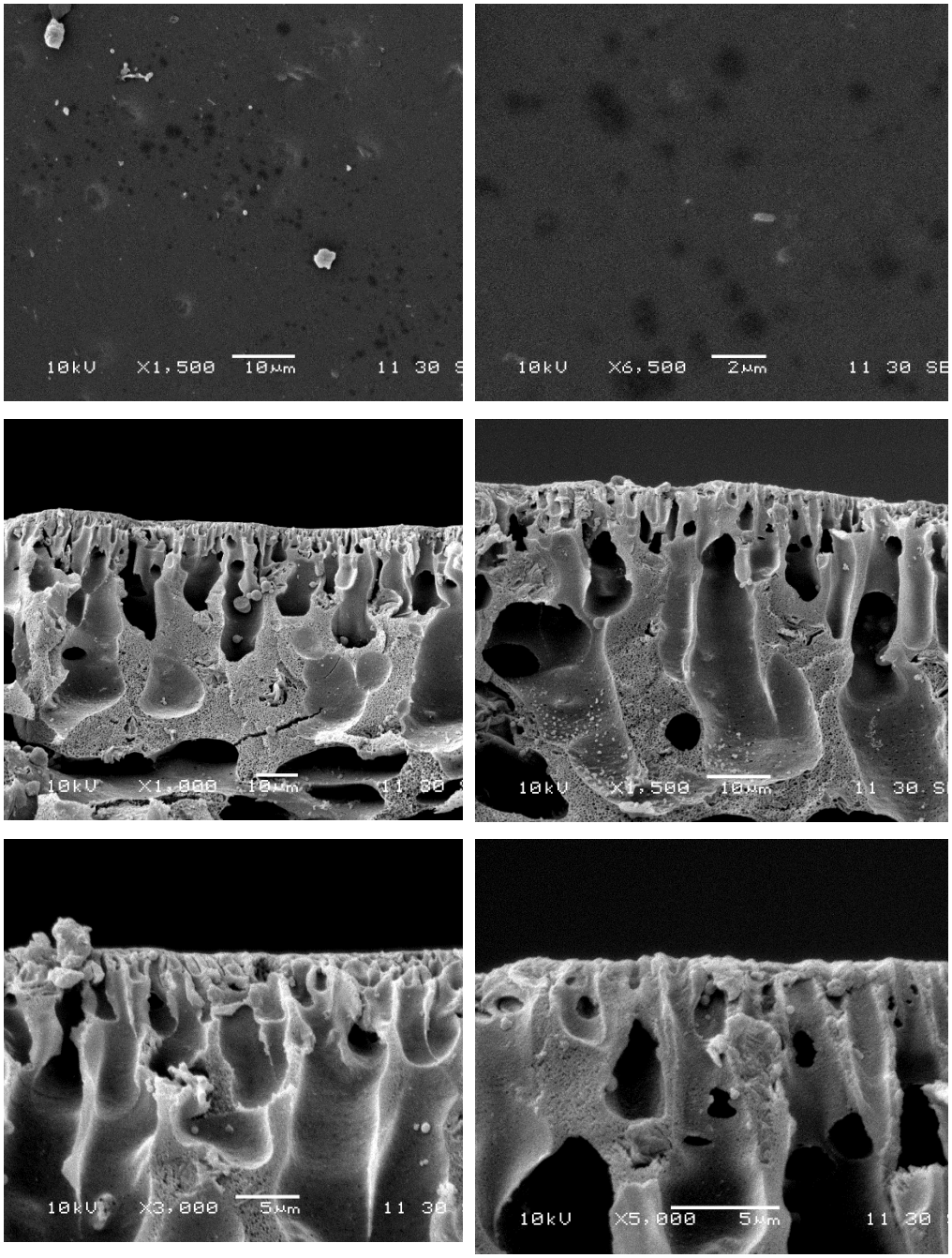

Figure 50: SEM Surfaces and cross-sections of S-PANI/GO membranes

5.6.3 Conclusions

This chapter reported the fabrication and characterisation of a new family of self-doped sulfonated polyaniline (S-PANI) membranes improving the performance

of PANI membranes including acid leaching, fouling and solvent stability issues. The pure S-PANI membranes were prepared via phase inversion from a solution of doped S-PANI, NMP, 4-MP and THF and were further cross-linked via thermal treatment and chemical treatment using DCX, GA and TCL. The produced membranes were compared to pure PANI membrane to determine performance, antifouling and hydrophilicity. The effect of cross-linking of self-doped S-PANI membranes in terms of membrane performance and properties compared to uncross-linked S-PANI membranes has been investigated. In addition, the electrochemical properties of the S-PANI membrane were studied to investigate the potential of S-PANI membrane as novel stimuli responsive systems.

Pure S-PANI membrane showed similar morphology, flux, rejection and operating pressure as PANI. The thermal treatment produced membranes with poor mechanical stability and short membrane lifetime. On the other, chemical cross-linking successfully yielded long-term solvent (DMF) stable membranes with excellent reusability, improved PEG-rejection and ability to operate at high pressure (20 bar), showing the potential of chemically cross-linked S-PANI membranes.

The flux recovery ratio and other flow indices showed significant improvement of fouling resistance of the S-PANI and S-PANI GA membranes compared to PANI membranes demonstrating that protein adsorption could be significantly reduced using the self-doped S-PANI. Furthermore, chemical cross-linking can further improve the solvent resistance whilst retaining low fouling properties. These newly developed S-PANI membranes show excellent solvent stability and high fouling resistance. However, the cross-linking was not able to tight the pore size of the membranes to the NF range to separate molecules of MW<1000 Da.

The preliminary electrochemical studies showed that the conductivity of the membranes is very low and that the addition of conducting particles such as 10%

of graphene oxide seems to improve the conductivity of the membrane surface, but no redox process is detectable during cyclic voltammetry.

Chapter 6

Preparation of nanofiltration S-PANI membranes

6.1 Introduction

In Chapter 5 it was reported that chemical crosslinking successfully improved the chemical resistance of S-PANI membranes, however, the steric hindrance of the sulfonic groups do not let the polymer chains to be efficiently packed and overcome their high free volume and rigidity. S-PANI GA showed the lowest MWCO of 1800 Da in the tight UF range and it was found that adding the cross-linker *in situ* during the phase inversion influenced the cross-sectional morphologies of the membrane. This effect on membrane morphologies as well as performance has led us to investigate alternative routes to shrink the pore size of the membrane.

Previous works [57, 187-190] have focused on achieving control on the pore size by changing the chemical potential between the coagulation bath and the casting solution by using additives during the phase inversion technique. It has been reported that for semi-crystalline materials, using additives could slow down the phase inversion liquid-liquid de-mixing and the membrane is formed via crystallization, which reduces the pore size[190]. As stated in 2.3.3.2, a solution containing the polymer, a solvent and additives is prepared until homogeneity is achieved. Then the solution is casted into a thin film and immersed for the desired time in a non-solvent bath. Upon immersion, solvent and non-solvent mix spontaneously according to their mutual affinity and the polymer solidifies [51]. Phase diagrams have been used to analyse the thermodynamics of the membrane precipitation process and helped to understand membrane formation. A ternary diagram for instantaneous de-mixing and delayed de-mixing is shown in Figure 51. At t<1 s, the composition path crosses the binodal line, hence liquid-liquid de-mixing starts immediately after immersion (Figure 51a). In the second case, all the compositions directly beneath the top layer are in the one-phase region and still miscible, which means that no de-mixing occurs

immediately after immersion but only after a while when more nonsolvent has diffused into the polymer solution so that the binodal can be crossed (Figure 51b). Hence, it is possible to have a tailored morphology for a specific separation according to the de-mixing rate: instantaneous (more porous membrane) or delayed (asymmetric membrane) [53].

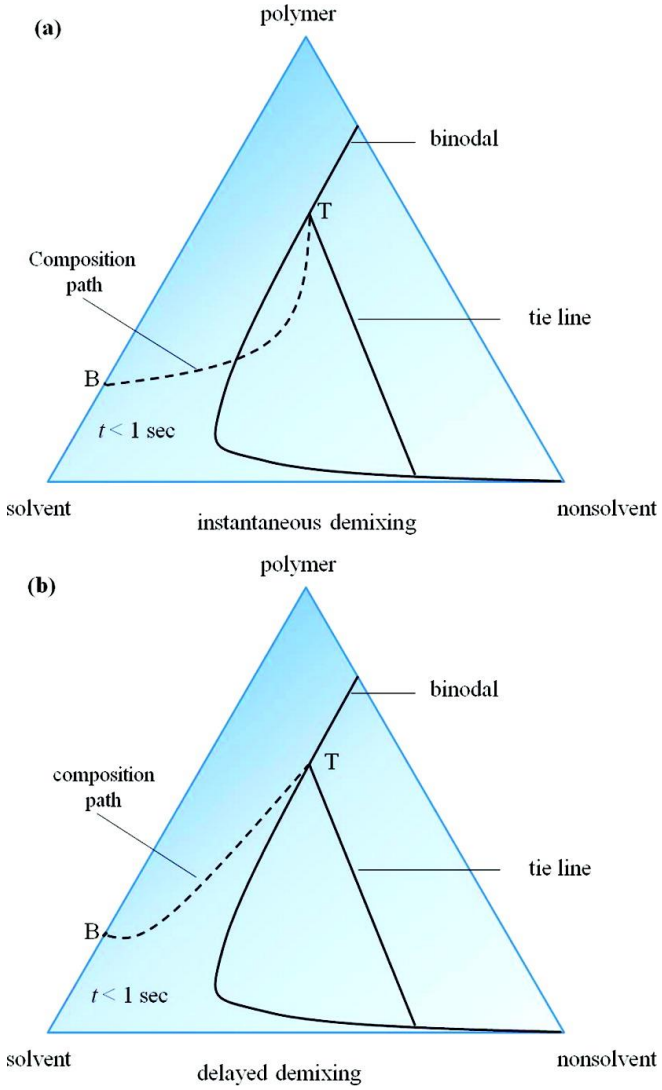

Figure 51: Composition paths of a casted film immediately after immersion (t < 1 s) showing (a) instantaneous demixing and (b) delayed demixing; T and B represent top and bottom of the film, respectively [191]

In a work from 2003 [192], it is reported a highly mechanically stable PANI film prepared via phase inversion in hexane. Interestingly, the PANI film had a much denser morphology than those prepared in water resulting in a 12 times higher Young modulus than conventional PANI. According to a previous work [193], hexane can suppress finger like macrovoids because of a change in the rate of precipitation. Therefore, a denser spongy structure is formed over a porous with

macrovoids. A possible mechanism for the formation of a polymer membrane in n-hexane has been reported by *Cheng et al.*in their study of formation of asymmetric PMMA membranes [52]. After casting and immersion into a n-hexane bath, an integral skin is formed because of the delayed de-mixing, and then liquid-liquid phase separation occurs because of the diffusion of the n-hexane (non-solvent) into the casting solution. The final stage is the formation of a spongy sublayer.

Therefore, we hypothesise that we could prepare S-PANI membranes with shrunk pore size by changing the composition of the coagulation bath in phase inversion. As the current membranes prepared with this method have not been evaluated in solvents, the chemical properties and the separation performance in water and in solvents of different polarity will be comprehensively characterised.

6.2 Membrane preparation: synthesis of SPWT and SPHX membrane

S-PANI 21 wt% dope solutions were casted at 250 nm and then immersed in hexane or water for 24h. Figure 52 shows the resulting membranes obtained after phase inversion: SPWT membranes (Figure 52A) had a shiny and smooth top surface, whereas SPHX membranes (Figure 52B) appeared with a rougher surface.

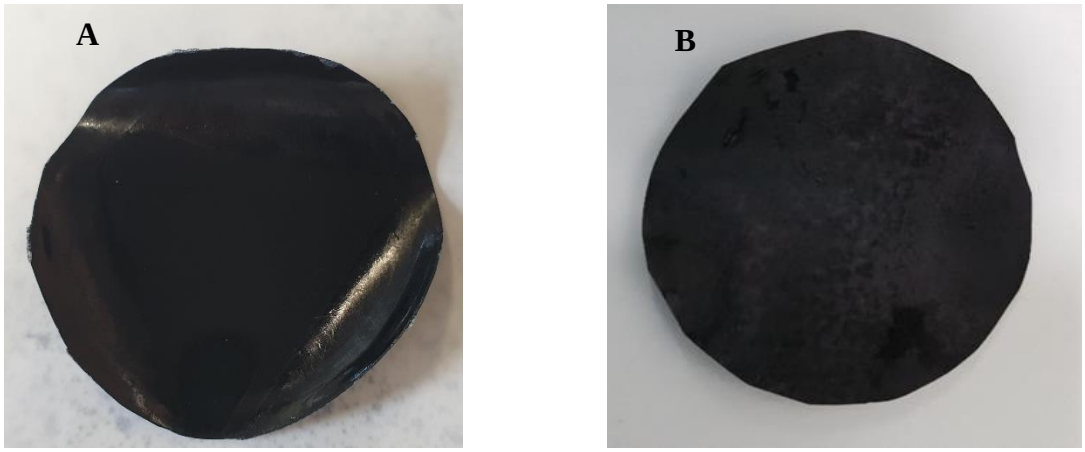

Figure 52: Top surfaces of (A) SPWT and (B) SPHX membrane

6.3 Effect of coagulation bath on membrane morphology

SEM was used to investigate the effect of the coagulation bath during the phase inversion process on membrane morphology. Figure 53 shows surfaces and cross-sections of SPWT and SPHX respectively taken at 500, 1000 and 1500 magnification. SPWT presents a smoother surface with no clear evidence of a specific pattern. Conversely, SPHX presents a much rougher surface. The main difference in the membrane morphology can be clearly spotted by cross-sectional images. SPWT presents a porous top layer with many macrovoids almost regularly distributed along the membrane cross-section. Interestingly cross-sections of SPHX exhibit a very different morphology with a mostly denser structure and micropores distributed all over it. The membranes have been casted using a casting solution of the same polymer concentration and solvent ratio and the main difference in the fabrication method is the use of a coagulation bath of different polarity. SPHX have been prepared in a non polar solvent and SPWT in a polar solvent. The difference in morphologies can be attributed to the different affinity between solvent and non-solvent in the fabrication step. The great affinity of NMP (solvent) and water (non-solvent) causes instantaneous de-mixing and formation of macrovoids hence SPWT has

a morphology similar to other PANI membranes prepared in similar conditions [11, 12, 25]. The solubility parameter difference $\Delta\delta_{S-NS}$ between the solvent system of the casting solution and the non-solvent system of the immersion bath is a first indication of their mutual affinity. The $\Delta\delta_{S-NS}$ -values of NMP with water is reported to be 35.38 [194] . However there are no reported values for the pair hexane -NMP, but similar studies have confirmed the lower affinity between the two solvents and a slower precipitation rate, hence the spongy structure [52, 195]. It is also reported that for a slower precipitation rate, the density of the obtained casted films is usually higher However, a first qualitative inspection revealed that a 14.6 cm^2 coupon of the SPHX membrane was thinner and lighter than the same SPWT coupon and the average weight of a 2X2 cm^2 SPWT sample was 21±4 while 18±4 for a SPHX sample. As it was difficult to derive a conclusion on the formation of the SPHX membrane and the properties of the resulting film, further swelling tests were carried out to establish a relationship between the obtained membrane morphology and the solvent uptake.

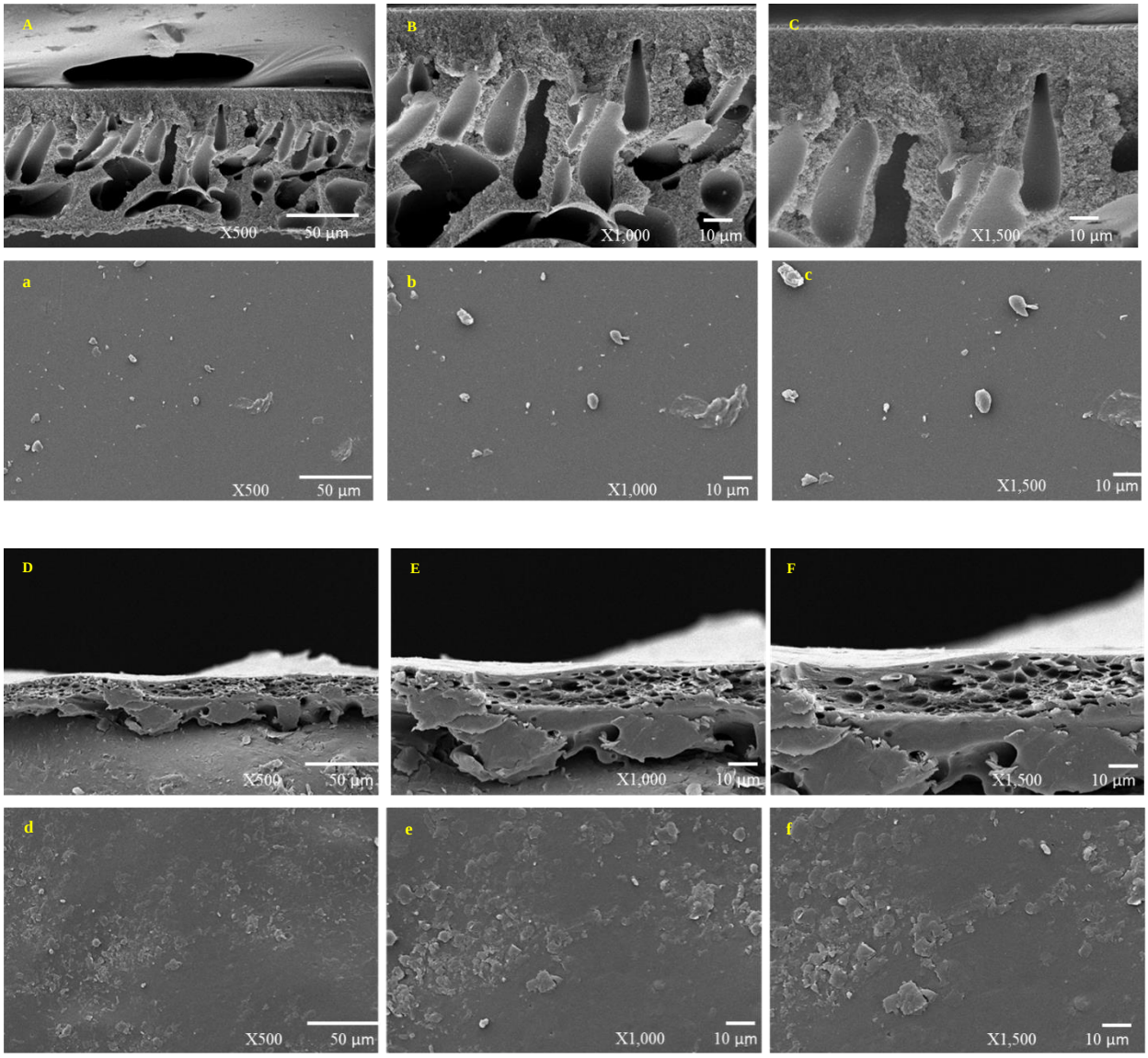

Figure 53 SEM surfaces and cross-sections at different magnification of (A-C) SPWT and (D-F) SPHX.

6.3.1 Membrane hydrophilicity

SPHX and SPWT were characterised for their hydrophilicity via dynamic contact angle analysis. Figure 54 reports the decrease of contact angle over time for both membranes. S-PANI is a hydrophilic polymer because of the sulfonic groups covalently attached to the polyaniline backbone and the consequent self-doped effect makes the polymer charged [16, 196]. SPHX has an initial contact

angle of 78 °, which is higher than the initial contact angle of SPWT of 63°. After 200 s the contact angle change to 49° for SPWT and 63° for SPHX. Considering that SPHX membranes did not undergo any post-modification, the difference in the initial contact angles is most likely attributed to the marked surface roughness of SPHX membrane highlighted from SEM analysis, rather than a change in the chemical composition of the membrane.

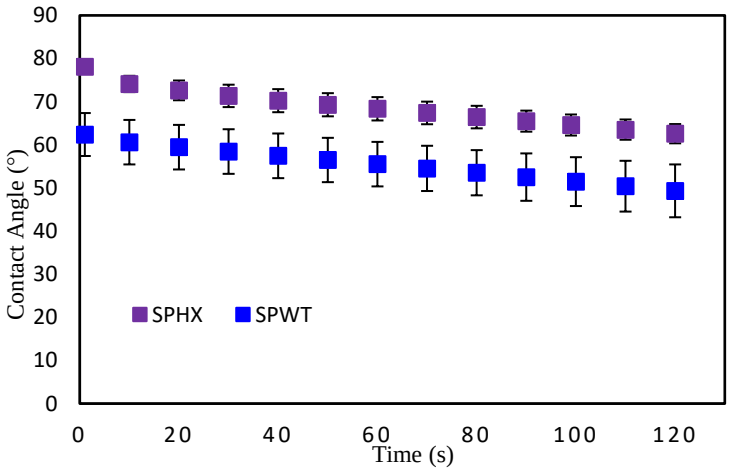

Figure 54: Contact angle over time of SPWT and SPHX membranes. Data are average of 3 samples.

6.4 Solvent stability of SPHX and SPWT membrane and study of the swelling behaviour

Figure 55 and Table 19 give the comparison of the swelling degree of the SPHX and SPWT membranes for four different solvents ranging from the polar water to the non-polar toluene. SPHX membrane has almost a constant swelling degree at higher solubility parameters whilst SPWT exhibits an increasing swelling trend at higher solubility parameters. The swelling is caused by the slow diffusion of solvents into polymer chains leading to a swollen membrane [197]. In porous membranes, macroscopic swelling could lead to an increase in the polymer volume with the closure of the porous structures and subsequent abatement of the flux and increase of the MWCO of the membrane. In dense

membranes, a large sorption of molecules can induce swelling in the matrix leading to an increase in the free volume. Higher mobility of the polymer chains reduces the discriminating power of the membrane and hence an increase in MWCO. From the data reported in Table 19 it is clear that SPWT, which presented a porous structure, has a much higher swelling degree at increased solvent polarity with 71±4 % of swelling degree in water. Conversely, the low swelling degree of SPHX membranes at more polar solvent (8±1 % in water) can be attributed to the denser structure of this membrane.

Table 19: Swelling degree in different solvents of SPHX and SPWT membranes. Results are the average of two experiments.

Membrane	**Swelling degree (%)**	**Solvent**
SPWT	71±4	water
	64±10	2-propanol
	51±33	acetone
	20±3	toluene
SPHX	8±1	water
	7±5	2-propanol
	6±4	acetone
	0.4±0.2	toluene

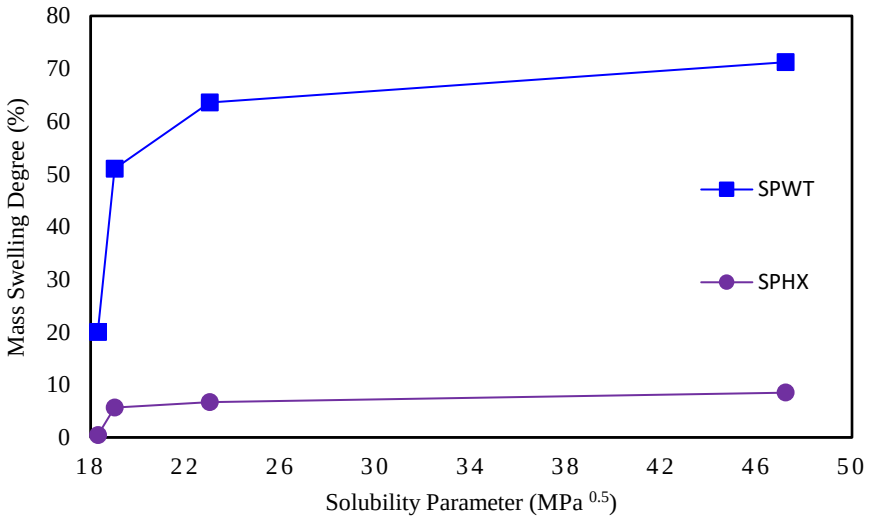

Figure 55: Mass swelling degree of SPHX and SPWT membranes plot against Hansen solubility parameters[54, 198]

6.5 Investigating nanofiltration performance in dead-end cell

6.5.1 Water flux and PEGs/PPG rejection

The performance of the produced SPHX membranes were studied using a dead-end cell. Figure 56 shows the MWCO curves obtained from rejection experiments using PEGs in water. The SPHX membrane has an excellent rejection of 99% of PEGs with MW ranging from 1000 to 5000 Da, whereas SPWT has only 10% rejection of the same PEGs. Interestingly, the operating conditions of the two membranes are also different: SPWT membrane showed a maximum operating pressure of 5 bar but SPHX membrane could withstand pressure up to 40 bar. Figure 57 reports the MWCO curve for SPHX membrane tested in water using PPGs of MW ranging from 308 to 1179 Da. The PPG method was used to determine the rejection ability of the molecules of the SPHX membrane at lower MW. The general trend is a rejection of 80% to 89 % for 300 Da and 950Da respectively. From the data, the SPHX membrane prepared by phase inversion in hexane has a MWCO of 1005 Da.

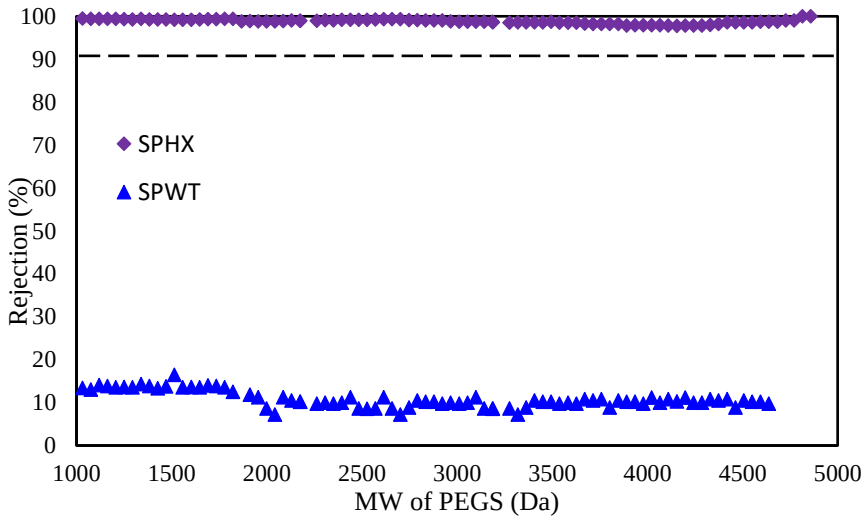

Figure 56: Typical MWCO curves for SPHX and SPWT membrane in water using PEGs. Filtration conditions: 25 °C and 20 bar for SPHX membrane and 25° and 1 bar for SPWT membrane. Data are averages of 2 membrane samples from batch MSPHX01 and SPWT01

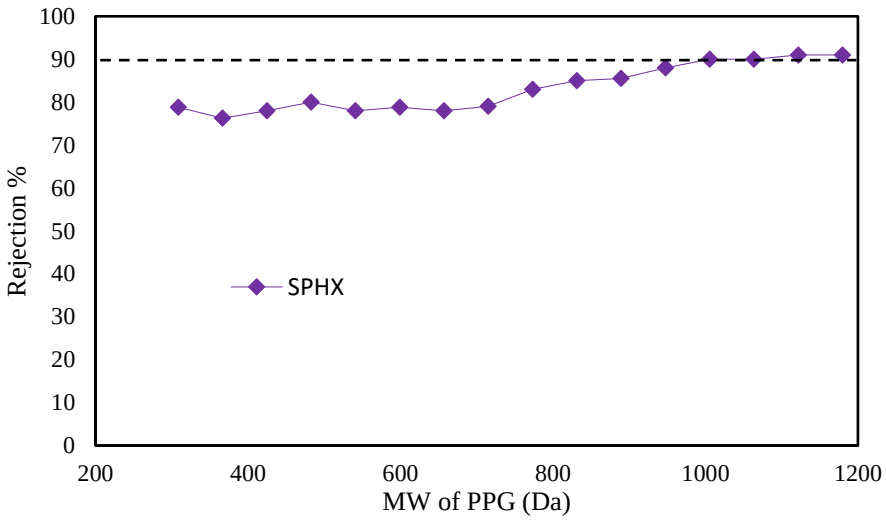

Figure 57: MWCO curve for a typical SPHX membrane in water using PPGs. Filtration conditions: 25 °C and 20 bar Data are average of 2 membrane samples from batch MSPHX01

6.5.2 Rejection of PPGs in solvents and the effect of the swelling degree on membrane performance

The stability and the performance of the SPHX membrane were evaluated in toluene, 2-propanol and acetone. The membrane has previously shown excellent stability when immersed in those solvents for a week with no trace of coloured deposits in the solution. Other solvents such as DMF, DMAc and THF turned blue when the membrane was immersed for less than 1 h. Therefore, Figure 58 reports the data from the rejection of PPGs in toluene, 2-propanol and acetone. The rejection in three solvents is lower than the rejection in water, specifically 30 % and 34 % less in toluene and acetone and 61 % less in 2-propanol. The permeate collected from the filtration experiments did not change colour and the membrane could be reused in the same solvents at the same operating conditions. No apparent damage was observed during the repeated use of the membrane. Finally, the SPWT membrane tested in solvents and water showed very low rejection -below 20 %- of PPGs (data are available in the appendix).

Furthermore, the differences in rejection in the solvents could be related to the swelling degree of the membrane in the chosen system as shown in Figure 59. For an increasing degree of swelling and Hansen solubility parameter, the PPGs rejection of SPHX membrane does not follow a linear trend. The swelling degree of the SPHX membrane in water is the highest (8%) and the highest is the PPGs rejection. However, the SPHX membrane swells similarly in 2-propanol and acetone (7 % and 6% respectively) but the rejection is 2.8 and 1.5 times lower. In toluene, the swelling degree of SPHX membrane is only 0.4 % which is also the lowest value, but the PPG rejection is 1.5 lower than the water results. The performance of the SPHX membrane can be further explained as a combination of its different swelling degree as well as the nature of the rejected solutes. Previous studies have shown that the degree of rotational freedom around the PPGs backbone affects solutes rejection in different solvents [146, 199]. PPGs in water exist in a solvent impermeable, tight-coil configuration stabilised by side-chain hydrophobic interaction [200], however, according to the polar character of the solvents the PPGs chain might open up and rotate to a preferred orientation to permeate through the membrane. In water the SPHX membrane swells and this could reduce the discriminating power of the membrane, however the tight-coil PPG conformation is rejected better. In toluene the SPHX membrane does not swell remarkably and the uncoiled PPG is less rejected. Yet other factors, both physical and chemical, are probably influencing the performance of the SPHX membrane in 2-propanol.

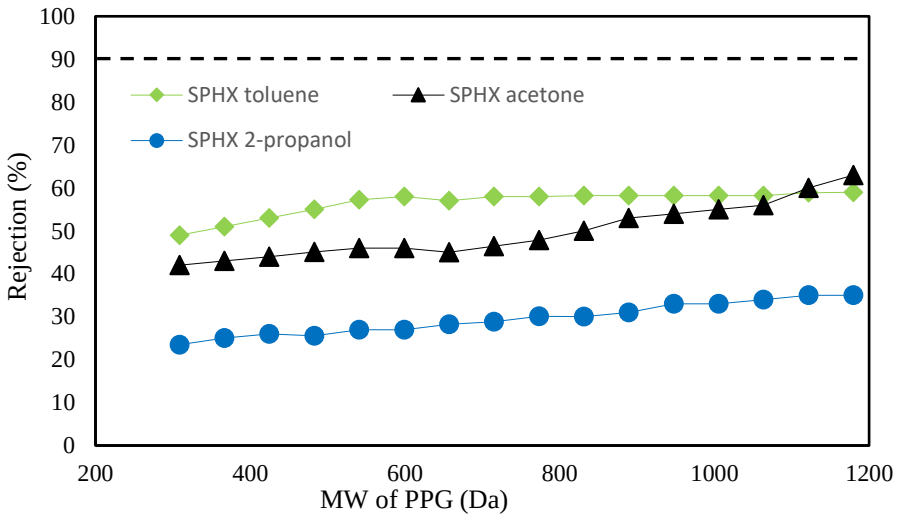

Figure 58: Rejection curves for SPHX membranes in toluene, acetone and 2-propanol. Operating conditions are 30 bar and 25°. Data are average of 2 membrane samples from batch MSPHX11

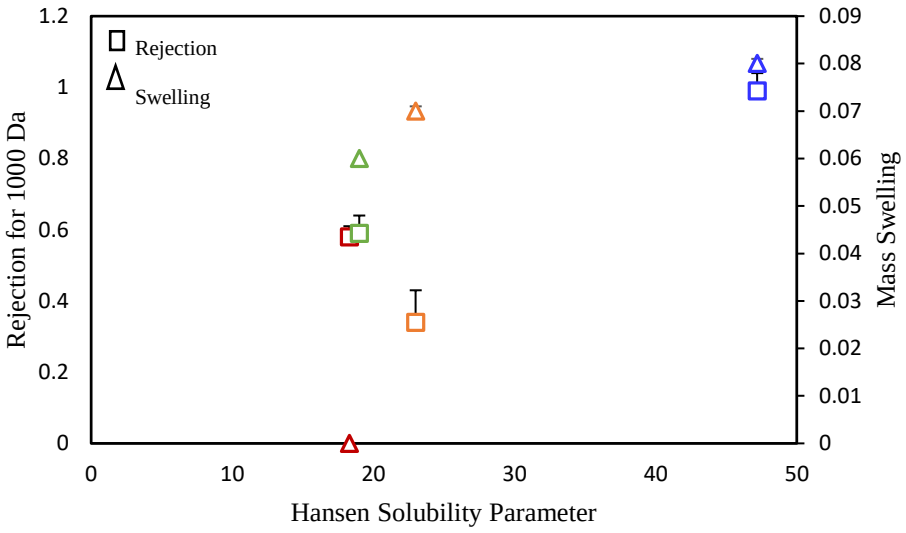

Figure 59: Correlation between i) PPGs rejection of SPHX membrane in toluene, acetone, 2-propanol and water and ii) the mass swelling degree of the membrane in the same solvents plot against the Hansen solubility parameters.

Finally, Figure 60 summarises the permeance in water and solvents for both SPWT and SPHX membranes. The porous SPWT membrane shows high permeance in water with maximum operating conditions of 5 bar and 2.5 bar for the membrane tested in toluene, 2-propanol and acetone. SPHX membrane shows lower permeance because of the denser structure and could withstand high operating pressure of up to 40 bar.

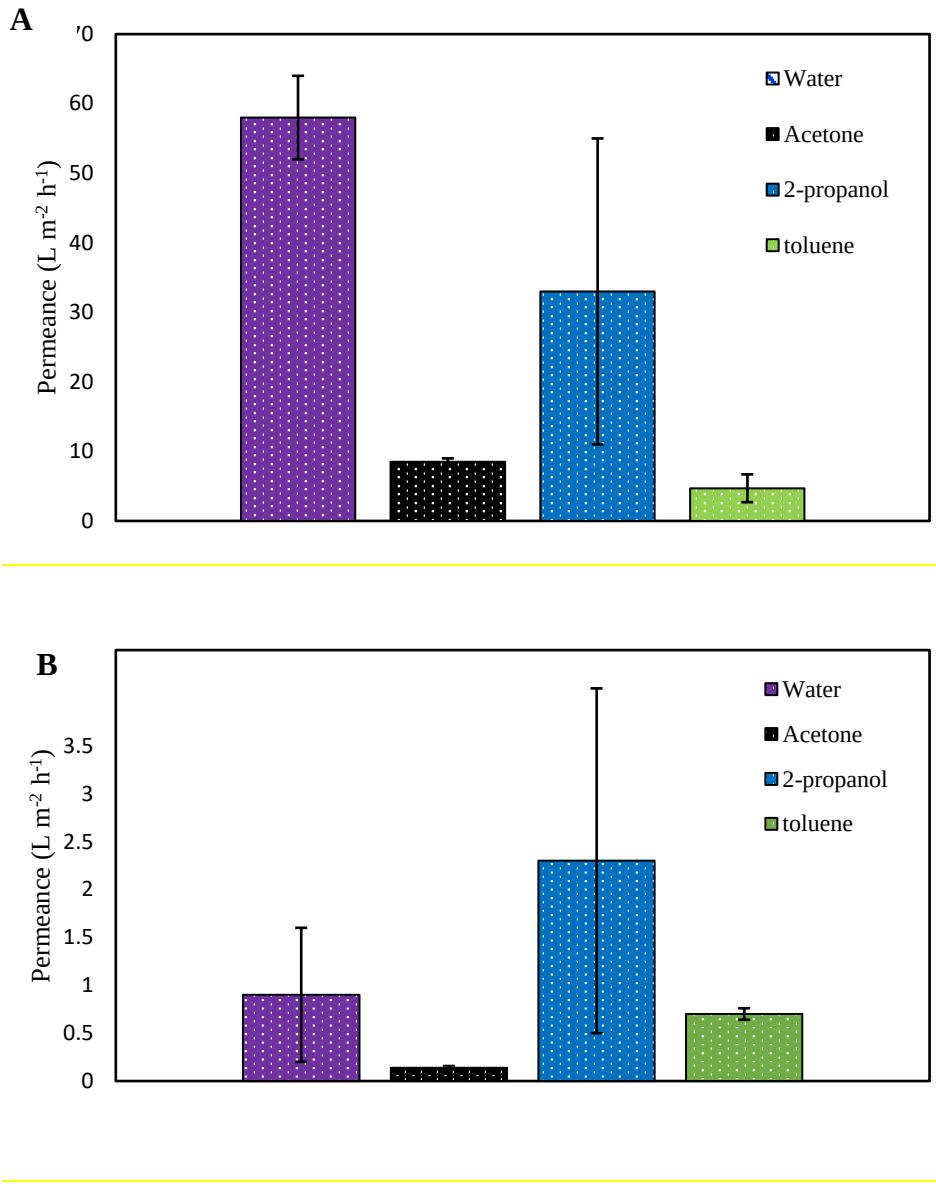

Figure 60: Permeance of (A) SPWT and (B) SPHX membranes in different solvents. Filtration conditions were i) 2 bar for SPWT and ii) 20 bar for SPHX. Data in water are average of 2 membrane samples from batch MSPHX01 and SPWT01 (filtration in water), MSPHX11 and SPWT01 (filtration in solvents).

6.6 Conclusion

Herein, we report for the first time the preparation of nanofiltration self-doped sulfonated polyaniline membrane via phase inversion in a hydrophobic

coagulation bath. The membrane was prepared from a solution of 20% w/v of S-PANI, casted and immersed in hexane for 24 h (SPHX). The physical properties and performance of the membrane were compared with a reference S-PANI membrane prepared via phase inversion in water (SPWT). The use of hexane successfully densified the structure of the bulky S-PANI polymer, in contrast with the membrane prepared in water, which showed a porous large finger-like macro-voids structure. The membrane prepared in hexane showed superior rejection of polyethylene glycols (PEG) and polypropylene glycols (PPG) in water, a MWCO of 1005 Da and operating pressures up to 20 bar when compared to the reference SPWT membrane, showing an overall robustness and stability in filtration conditions. Additionally, the SPHX membrane was reusable in toluene, acetone and 2-propanol at least three times with no loss in mechanical stability at a maximum pressure of 30 bar. Conversely, the SPWT membrane showed poor rejection in water, poor mechanical stability when tested in solvents (i.e. disintegrated after the first run) and maximum operating pressures of 2.5 bar. In summary, the use of a hydrophobic coagulation bath was proved effective for preparing tighter sulfonated polyaniline membranes with additional solvent stability at high pressures. Overall, this study offers an attractive and simple strategy to shrink membrane pore size and obtain nanofiltration sulfonated polyaniline membranes. The synthesised SPHX membrane shows potential for practical applications such as the recovery of enzymes or enlarged organometallic catalysts

Chapter 7

Conclusion and recommendations for future work

7.1 Benchmarking of industrial relevant organic reactions with commercial OSN membranes

7.1.1 Conclusions

In Chapter 4, two industrial-relevant reactions were investigated in a semi-continuous nanofiltration system namely i) the palladium catalysed Suzuki coupling carried out in a biphasic mixture and ii) the lipase-mediated kinetic resolution in toluene and in ethyl acetate. The performance of the DURAMEM 500 and PURAMEM S600 membranes were benchmarked against the reaction systems to study performance and stability in the organic solvents, membrane fouling and catalysts deactivation. It was found that D500 could be used in the biphasic solvent-water system, however, the inorganic hydroxide bases insoluble in the organic solvents reach their solubility limit and contribute to membrane fouling. Furthermore, the highly stabilising Buchwald ligand does not efficiently bind to the Pd complex leading to deactivation and formation of palladium black. Optimisation and monitoring of the reaction were necessary to keep palladium in the active form. Free lipase in organic solvents was efficiently retained from D500 and PS600, showing potential for free enzyme kinetics in organic solvents. PS600 in toluene showed excellent selectivity and membrane stability with no evidence of major catalysts adsorption onto the membrane surface. D500 in ethyl acetate showed low stability, furthermore, the solvent competes as acyl donor with the catalysts active sites leading to side reactions and decrease in product yield.

7.1.2 Future work

The reactions systems object of the study showed good reproducibility in batch however the lipase-mediated kinetic resolution was easier to characterise and study in the dead-end cell filtration. The biphasic palladium catalysed Suzuki coupling suffered from catalysts deactivation and insolubility of the inorganic

base in the organic phase which lead to increased membrane fouling in the dead-end cell. To better understand the mechanism of the reaction, the electrochemical characterisation of the palladium species present in solution would add useful information to the data obtained from the online reaction monitoring. Cyclic voltammetry experiments at different palladium/ligand concentration could be performed to study the de-activation step and minimise the formation of the palladium black in the solution. The XPhos ligand is considered a robust and highly efficient catalyst, but its reuse is limited by its high solubility in the reaction medium and low MW, therefore a better understanding of the catalytic cycle could improve the overall performance of the studied semi-continuous nanofiltration system.

Furthermore, the filtration of the Suzuki reaction mixture has been performed in dead-end mode to avoid unnecessary use of the chemicals, however, cross-flow filtration is the next step to test the optimised palladium system-with the excess of the 3-chloropyridine and to study fouling. The use of more fouling resistant commercial membranes to study organic and inorganic fouling should be considered in a future work. The lipase-mediated kinetic resolution in toluene is also a good candidate to be tested in a semi-continuous cross-flow membrane system. However, continuous systems in which the reactants are continuously pumped to the membrane cell should be tested to monitor the effect of removing the products while the reaction is happening to better understand the kinetic of the reaction.

7.2 Self-doped sulfonated polyaniline membrane: fabrication, fouling resistance and properties

7.2.1 Conclusion

This chapter reported the fabrication and characterisation of S-PANI membrane, the chemical and thermal cross-linking of the membrane and the preparation of composite S-PANI/graphene oxide membrane. The membranes were synthesised from S-PANI powder and prepared through non-solvent phase

inversion and their subsequent modification with organic cross-linkers and thermal treatment. Pure S-PANI membrane showed similar morphology, flux, rejection and operating pressure as PANI. Thermal treatment produced membranes with poor mechanical stability and short membrane lifetime. In contrast, chemical cross-linking successfully yielded long-term solvent (DMF) stable membranes with excellent reusability, improved PEG-rejection and ability to operate at high pressure (20 bar), showing the potential of chemically cross-linked S-PANI membranes. Fouling of S-PANI, PANI and S-PANI GA membranes was investigated using BSA in cross-flow. The flux recovery ratio and other flow indices showed significant improvement of fouling resistance of the S-PANI and S-PANI GA membranes compared to PANI membranes. Both S-PANI and S-PANI GA membranes performed better during the first fouling-cleaning cycle showing a TFR of 39 ±2 and 33±6 %, in contrast with PANI, which presented a very poor flux recovery and a high TFR of 61±5 %. This demonstrate that the performance of the PANI membranes improved after sulfonic groups were introduced and that the chemical cross-linking with GA did not negatively affect the fouling resistance despite the slight increase of contact angle. The prepared S-PANI membranes are robust and durable, show low fouling properties, and have strong potential to favourably extend the lifetime of membrane processes and reduce the operational costs and frequent chemical cleaning. Furthermore, the conductivity of the non-cross-linked S-PANI membrane was studied and a composite membrane S-PANI membrane was prepared using graphene oxide as conductive filler. The preliminary electrochemical studies showed that the conductivity of the membranes is very low and that the addition of conducting particles such as 10% of graphene oxide seems to improve the conductivity of the membrane surface but no redox process is detectable during cyclic voltammetry.

7.2.2 Future work

The low conductivity and the absence of redox peaks in the S-PANI and S-PANI-GO membranes limited the investigation of an electrical-responsive

membrane based on self-doped PANI. However, future work can focus on characterising the self-doped sulfonated polymer and the membrane exploiting electrochemical impedance spectroscopy (EIS) which has already been used for studying redox processes of conducting polymers. By EIS the redox processes taking place on the electrode surface (S-PANI) can be monitored as a function of the applied dc-potential and it is possible to obtain information of charge-transfer and diffusion processes. Having more control and understanding of the electrochemical species involved helps comprehend if the electro-responsiveness is feasible and how it will affect solute separation.

Many synthetic routes are available in literature to prepare the polymer with a good conductivity, however, when S_PANI is processed into a membrane, this is partially lost due to the non-homogeneous rearrangement of the polymer chains. In the future, different synthetic routes to prepare the polymer should be explored optimising the following parameters: monomer addition, type of initiator and S:N ratio. The use of NMP could inhibits the conductivity because of the formation of weak bonds with the polymer therefore, other solvents combinations should be investigated.

Despite the low conductivity, the S-PANI-GO membrane could be used as UF membrane with improved fouling resistance due to the combined effect of the sulfonated groups and the nanofiller. Future work should address this and the membrane fouling using different model foulants such as humic acid, and sodium alginate, and rejection experiments should be performed to complete membrane characterisation. In addition, a screening of GO concentrations and incorporation methods would be beneficial to assess membrane mechanical properties and the change in conductivity, surface properties and fouling at different filler concentration.

Finally, the developed membranes show a low fouling behaviour and an excellent resistance to harsh chemical environments which could be further assesed in one of the reaction systems studied in Chapter 4. In particular, the

chemically-cross-linked membranes could be used for the filtration of lipase in solvents because of their tighter pore size and stability during filtration. Bio-fouling and compatibility with the reaction conditions of the S-PANI GA, S-PANI DCX and S-PANI TCL membrane can be part of a future work on studying the properties of these novel membranes.

7.3 Fabrication of nanofiltration self-doped S-PANI membranes

7.3.1 Conclusion

In this chapter, it was reported the fabrication of nanofiltration S-PANI membrane by modifying the nature of the coagulation bath during phase inversion. Specifically, water was replaced with the hydrophobic non-polar solvent hexane. The use of hexane as coagulant resulted in the suppression of the spongy structure with finger-like macrovoids typical of UF S-PANI and in the formation of a denser layer. SPHX membrane formed in hexane and SPWT membrane formed in water were both synthesised from a 20% w/v S-PANI in NMP/4-MP. The two membrane systems were characterised to determine the differences in physical properties and performance. Pure water studies show that SPHX is a dense membrane with a molecular weight cut-off of 1005 Da in water. The stability and the performance of the SPHX membrane were evaluated in toluene, 2-propanol and acetone. It was found that the rejection in solvents was lower than the rejection in water, 30 % and 34 % less in toluene and acetone and 61 % less in 2-propanol; but no apparent damage was observed during the repeated use of the membrane. SPWT showed performance in the ultrafiltration range with very low rejection -below 20 %- of PPGs. Overall the reported method allows for the preparation of S-PANI based membrane with NF properties without the use of any thermal and chemical cross-linking. Thus, reducing significant chemical usage and process time.

7.3.2 Future work

The SPHX membrane was prepared exploiting a change in the chemical potential between the membrane dope solution and the coagulation bath which allowed to obtain a denser NF membrane. The mechanism of formation of this membrane

system prepared in non-polar solvents is not well understood and further studies focusing on changing polymer concentration, solvent/ non solvent pair to investigate membrane formation and resulting morphology should be carried out.

The low permeance is the main drawback that could limit its applicability in water and solvents. A way to address this issue is to explore different combinations of water/solvent or solvent/solvent for the coagulation bath.

Furthermore, the fabrication method was developed and evaluated only for the self-doped S-PANI but other polymer or blends of polymer could be tested to confirm its wide applicability. Some work using PAMPSA doped PANI has already been done and it is shown in Appendix C of this thesis.

Chapter 8

References

[1] E. Drioli, A. Brunetti, G. Di Profio, G. Barbieri, Process intensification strategies and membrane engineering, Green Chemistry, 14 (2012) 1561-1572.

[2] T.S. Letcher, Janet L.: Patterson, Darrell Alec, Chemical Processes for a Sustainable Future Royal Society of Chemistry, 2014.

[3] M. Galizia, K.P. Bye, Advances in Organic Solvent Nanofiltration Rely on Physical Chemistry and Polymer Chemistry, Frontiers in Chemistry, 6 (2018).

[4] D. Nair, J.T. Scarpello, I.F.J. Vankelecom, L.M. Freitas Dos Santos, L.S. White, R.J. Kloetzing, T. Welton, A.G. Livingston, Increased catalytic productivity for nanofiltration-coupled Heck reactions using highly stable catalyst systems, Green Chemistry, 4 (2002) 319-324.

[5] M.G. Buonomenna, Membrane processes for a sustainable industrial growth, RSC Advances, 3 (2013) 5694.

[6] M. Janssen, C. Müller, D. Vogt, Recent advances in the recycling of homogeneous catalysts using membrane separation, Green Chemistry, 13 (2011) 2247-2257.

[7] W. Guo, H.-H. Ngo, J. Li, A mini-review on membrane fouling, Bioresource Technology, 122 (2012) 27-34.

[8] D. Rana, T. Matsuura, Surface Modifications for Antifouling Membranes, Chemical Reviews, 110 (2010) 2448-2471.

[9] S. Shirazi, C.-J. Lin, D. Chen, Inorganic fouling of pressure-driven membrane processes — A critical review, Desalination, 250 (2010) 236-248.

[10] B. Van der Bruggen, L. Braeken, C. Vandecasteele, Flux decline in nanofiltration due to adsorption of organic compounds, Separation and Purification Technology, 29 (2002) 23-31.

[11] L. Xu, S. Shahid, A.K. Holda, E.A.C. Emanuelsson, D.A. Patterson, Stimuli responsive conductive polyaniline membrane: In-filtration electrical tuneability of flux and MWCO, Journal of Membrane Science, 552 (2018) 153-166.

[12] M. Sairam, X.X. Loh, K. Li, A. Bismarck, J.H.G. Steinke, A.G. Livingston, Nanoporous asymmetric polyaniline films for filtration of organic solvents, Journal of Membrane Science, 330 (2009) 166-174.
[13] X.X. Loh, M. Sairam, A. Bismarck, J.H.G. Steinke, A.G. Livingston, K. Li, Crosslinked integrally skinned asymmetric polyaniline membranes for use in organic solvents, Journal of Membrane Science, 326 (2009) 635-642.
[14] H. Hu, J.L. Cadenas, J.M. Saniger, P.K. Nair, Electrically conducting polyaniline–poly(acrylic acid) blends, Polymer International, 45 (1998) 262-270.
[15] M. Neetika, J. Rajni, P.K. Singh, B. Bhattacharya, V. Singh, S.K. Tomar, Synthesis and properties of polyaniline, poly(o-anisidine), and poly[aniline-co-(o-anisidine)] using potassium iodate oxidizing agent, High Performance Polymers, 29 (2016) 266-271.
[16] J. Yue, A.J. Epstein, Synthesis of self-doped conducting polyaniline, Journal of the American Chemical Society, 112 (1990) 2800-2801.
[17] J. Yue, Z.H. Wang, K.R. Cromack, A.J. Epstein, A.G. MacDiarmid, Effect of sulfonic acid group on polyaniline backbone, Journal of the American Chemical Society, 113 (1991) 2665-2671.
[18] X. Zhao, C. He, Efficient Preparation of Super Antifouling PVDF Ultrafiltration Membrane with One Step Fabricated Zwitterionic Surface, ACS applied materials & interfaces, 7 (2015) 17947-17953.
[19] B.T. McVerry, J.A.T. Temple, X. Huang, K.L. Marsh, E.M.V. Hoek, R.B. Kaner, Fabrication of Low-Fouling Ultrafiltration Membranes Using a Hydrophilic, Self-Doping Polyaniline Additive, Chemistry of Materials, 25 (2013) 3597-3602.
[20] G. Rong, D. Zhou, J. Pang, Preparation of high-performance antifouling polyphenylsulfone ultrafiltration membrane by the addition of sulfonated polyaniline, Journal of Polymer Research, 25 (2018) 66.
[21] S. Kiani, S.M. Mousavi, E. Saljoughi, N. Shahtahmassebi, Preparation and characterization of modified polyphenylsulfone membranes with hydrophilic

property for filtration of aqueous media, Polymers for Advanced Technologies, (2018).
[22] H. Strathmann, Membrane separation processes, Journal of Membrane Science, 9 (1981) 121-189.
[23] B.S. Lalia, V. Kochkodan, R. Hashaikeh, N. Hilal, A review on membrane fabrication: Structure, properties and performance relationship, Desalination, 326 (2013) 77-95.
[24] P. Vandezande, L.E.M. Gevers, I.F.J. Vankelecom, Solvent resistant nanofiltration: separating on a molecular level, Chemical Society Reviews, 37 (2008) 365-405.
[25] A. Sarihan, S. Shahid, J. Shen, I. Amura, D.A. Patterson, E.A.C. Emanuelsson, Exploiting the electrical conductivity of poly-acid doped polyaniline membranes with enhanced durability for organic solvent nanofiltration, Journal of Membrane Science, 579 (2019) 11-21.
[26] D.A. Patterson, L. Yen Lau, C. Roengpithya, E.J. Gibbins, A.G. Livingston, Membrane selectivity in the organic solvent nanofiltration of trialkylamine bases, Desalination, 218 (2008) 248-256.
[27] P. Marchetti, M.F. Jimenez Solomon, G. Szekely, A.G. Livingston, Molecular Separation with Organic Solvent Nanofiltration: A Critical Review, Chemical Reviews, 114 (2014) 10735-10806.
[28] A.-S. Jönsson, G. Trägårdh, Ultrafiltration applications, Desalination, 77 (1990) 135-179.
[29] L. Cseri, M. Razali, P. Pogany, G. Szekely, Chapter 3.15 - Organic Solvents in Sustainable Synthesis and Engineering, in: B. Török, T. Dransfield (Eds.) Green Chemistry, Elsevier, 2018, pp. 513-553.
[30] K.P. Lee, T.C. Arnot, D. Mattia, A review of reverse osmosis membrane materials for desalination—Development to date and future potential, Journal of Membrane Science, 370 (2011) 1-22.
[31] L.P. Raman, Cheryna, M., and Rajagopalan, N., Consider nanofiltration for membrane separations, Chem. Eng. Prog., 90 (1994) 68-74.

[32] J.G. Wijmans, R.W. Baker, The solution-diffusion model: a review, Journal of Membrane Science, 107 (1995) 1-21.
[33] M.M. Nasef, E.-S.A. Hegazy, Preparation and applications of ion exchange membranes by radiation-induced graft copolymerization of polar monomers onto non-polar films, Progress in Polymer Science, 29 (2004) 499-561.
[34] S. Rezaei Hosseinabadi, K. Wyns, V. Meynen, R. Carleer, P. Adriaensens, A. Buekenhoudt, B. Van der Bruggen, Organic solvent nanofiltration with Grignard functionalised ceramic nanofiltration membranes, Journal of Membrane Science, 454 (2014) 496-504.
[35] N. Scharnagl, H. Buschatz, Polyacrylonitrile (PAN) membranes for ultra- and microfiltration, Desalination, 139 (2001) 191-198.
[36] J. Wang, Z. Yue, J.S. Ince, J. Economy, Preparation of nanofiltration membranes from polyacrylonitrile ultrafiltration membranes, Journal of Membrane Science, 286 (2006) 333-341.
[37] M.N. Sarbolouki, Properties of asymmetric polyimide ultrafiltration membranes. I. Pore size and morphology characterization, Journal of Applied Polymer Science, 29 (1984) 743-753.
[38] A. Iwama, Y. Kazuse, New polyimide ultrafiltration membranes for organic use, Journal of Membrane Science, 11 (1982) 297-309.
[39] K. Vanherck, P. Vandezande, S.O. Aldea, I.F.J. Vankelecom, Cross-linked polyimide membranes for solvent resistant nanofiltration in aprotic solvents, Journal of Membrane Science, 320 (2008) 468-476.
[40] I. Soroko, Y. Bhole, A.G. Livingston, Environmentally friendly route for the preparation of solvent resistant polyimide nanofiltration membranes, Green Chemistry, 13 (2011) 162-168.
[41] L.L. Xu, S. Shahid, D.A. Patterson, E.A.C. Emanuelsson, Flexible electro-responsive in-situ polymer acid doped polyaniline membranes for permeation enhancement and membrane fouling removal, Journal of Membrane Science, 578 (2019) 263-272.

[42] J. Shen, S. Shahid, A. Sarihan, D.A. Patterson, E.A.C. Emanuelsson, Effect of polyacid dopants on the performance of polyaniline membranes in organic solvent nanofiltration, Separation and Purification Technology, 204 (2018) 336-344.

[43] K.Y. Wang, T.-S. Chung, Fabrication of polybenzimidazole (PBI) nanofiltration hollow fiber membranes for removal of chromate, Journal of Membrane Science, 281 (2006) 307-315.

[44] L. Zhu, M.T. Swihart, H. Lin, Tightening polybenzimidazole (PBI) nanostructure via chemical cross-linking for membrane H2/CO2 separation, J. Mater. Chem. A, 5 (2017) 19914-19923.

[45] K. Hendrix, M. Vaneynde, G. Koeckelberghs, I.F.J. Vankelecom, Synthesis of modified poly(ether ether ketone) polymer for the preparation of ultrafiltration and nanofiltration membranes via phase inversion, Journal of Membrane Science, 447 (2013) 96-106.

[46] W.J. Lau, A.F. Ismail, N. Misdan, M.A. Kassim, A recent progress in thin film composite membrane: A review, Desalination, 287 (2012) 190-199.

[47] R. Zimmermann, Condensation Polymers: By Interfacial and Solution Methods. Von P. W. Morgan. John Wiley & Sons, New York London-Sydney 1965. 1. Aufl., XVIII, 561 S., zahlr. Abb., mehrere Tab., geb. £ 9.10.–, Angewandte Chemie, 78 (1966) 787-787.

[48] J. Ren, R. Wang, Preparation of Polymeric Membranes, in: L.K. Wang, J.P. Chen, Y.-T. Hung, N.K. Shammas (Eds.) Membrane and Desalination Technologies, Humana Press, Totowa, NJ, 2011, pp. 47-100.

[49] D. Wandera, S.R. Wickramasinghe, S.M. Husson, Stimuli-responsive membranes, Journal of Membrane Science, 357 (2010) 6-35.

[50] S.M. Husson, Synthesis Aspects in the Design of Responsive Membranes, in: Responsive Membranes and Materials, John Wiley & Sons, Ltd., 2012, pp. 73-96.

[51] D.-M. Wang, J.-Y. Lai, Recent advances in preparation and morphology control of polymeric membranes formed by nonsolvent induced phase separation, Current Opinion in Chemical Engineering, 2 (2013) 229-237.
[52] C. Jao-Ming, W. Da-Ming, L. Fung-Ching, L. Juin-Yih, Formation and gas flux of asymmetric PMMA membranes, Journal of Membrane Science, 109 (1996) 93-107.
[53] I. Pinnau, B.D. Freeman, Formation and Modification of Polymeric Membranes: Overview, in: Membrane Formation and Modification, American Chemical Society, 1999, pp. 1-22.
[54] A.K. Hołda, I.F.J. Vankelecom, Integrally skinned PSf-based SRNF-membranes prepared via phase inversion—Part A: Influence of high molecular weight additives, Journal of Membrane Science, 450 (2014) 512-521.
[55] P. Vandezande, L.E.M. Gevers, J.S. Paul, I.F.J. Vankelecom, P.A. Jacobs, High throughput screening for rapid development of membranes and membrane processes, Journal of Membrane Science, 250 (2005) 305-310.
[56] I. Soroko, M. Sairam, A.G. Livingston, The effect of membrane formation parameters on performance of polyimide membranes for organic solvent nanofiltration (OSN). Part C. Effect of polyimide characteristics, Journal of Membrane Science, 381 (2011) 172-182.
[57] M.B. Thürmer, P. Poletto, M. Marcolin, J. Duarte, M. Zeni, Effect of non-solvents used in the coagulation bath on morphology of PVDF membranes, Materials Research, 15 (2012) 884-890.
[58] M. Amirilargani, M. Sadrzadeh, E.J.R. Sudhölter, L.C.P.M. de Smet, Surface modification methods of organic solvent nanofiltration membranes, Chemical Engineering Journal, 289 (2016) 562-582.
[59] S. Minko, Grafting on Solid Surfaces: “Grafting to” and “Grafting from” Methods, in: M. Stamm (Ed.) Polymer Surfaces and Interfaces: Characterization, Modification and Applications, Springer Berlin Heidelberg, Berlin, Heidelberg, 2008, pp. 215-234.

[60] Y. Liu, Y. Su, X. Zhao, Y. Li, R. Zhang, Z. Jiang, Improved antifouling properties of polyethersulfone membrane by blending the amphiphilic surface modifier with crosslinked hydrophobic segments, Journal of Membrane Science, 486 (2015) 195-206.

[61] X. Fan, Y. Su, X. Zhao, Y. Li, R. Zhang, J. Zhao, Z. Jiang, J. Zhu, Y. Ma, Y. Liu, Fabrication of polyvinyl chloride ultrafiltration membranes with stable antifouling property by exploring the pore formation and surface modification capabilities of polyvinyl formal, Journal of Membrane Science, 464 (2014) 100-109.

[62] M.G. Buonomenna, J. Bae, Organic Solvent Nanofiltration in Pharmaceutical Industry, Separation & Purification Reviews, 44 (2015) 157-182.

[63] Z. Dong, Z. Ren, S.J. Thompson, Y. Xu, G. Dong, Transition-Metal-Catalyzed C–H Alkylation Using Alkenes, Chemical Reviews, 117 (2017) 9333-9403.

[64] I. Nakamura, Y. Yamamoto, Transition-Metal-Catalyzed Reactions in Heterocyclic Synthesis, Chemical Reviews, 104 (2004) 2127-2198.

[65] S. Aerts, A. Buekenhoudt, H. Weyten, L.E.M. Gevers, I.F.J. Vankelecom, P.A. Jacobs, The use of solvent resistant nanofiltration in the recycling of the Co-Jacobsen catalyst in the hydrolytic kinetic resolution (HKR) of epoxides, Journal of Membrane Science, 280 (2006) 245-252.

[66] D. Nair, J.T. Scarpello, L.S. White, L.M. Freitas dos Santos, I.F.J. Vankelecom, A.G. Livingston, Semi-continuous nanofiltration-coupled Heck reactions as a new approach to improve productivity of homogeneous catalysts, Tetrahedron Letters, 42 (2001) 8219-8222.

[67] M. Janssen, C. Müller, D. Vogt, ‘Click’ Dendritic Phosphines: Design, Synthesis, Application in Suzuki Coupling, and Recycling by Nanofiltration, Advanced Synthesis & Catalysis, 351 (2009) 313-318.

[68] A. Keraani, T. Renouard, C. Fischmeister, C. Bruneau, M. Rabiller-Baudry, Recovery of Enlarged Olefin Metathesis Catalysts by Nanofiltration in an Eco-Friendly Solvent, ChemSusChem, 1 (2008) 927-933.
[69] K. De Smet, S. Aerts, E. Ceulemans, I.F.J. Vankelecom, P.A. Jacobs, Nanofiltration-coupled catalysis to combine the advantages of homogeneous and heterogeneous catalysis, Chemical Communications, (2001) 597-598.
[70] H.-t. Wong, C.J. Pink, F.C. Ferreira, A.G. Livingston, Recovery and reuse of ionic liquids and palladium catalyst for Suzuki reactions using organic solvent nanofiltration, Green Chemistry, 8 (2006) 373-379.
[71] A.B. Sitanggang, A. Drews, M. Kraume, Influences of operating conditions on continuous lactulose synthesis in an enzymatic membrane reactor system: A basis prior to long-term operation, Journal of Biotechnology, 203 (2015) 89-96.
[72] M.S.M. Sueb, J. Luo, A.S. Meyer, H. Jørgensen, M. Pinelo, Impact of the fouling mechanism on enzymatic depolymerization of xylan in different configurations of membrane reactors, Separation and Purification Technology, 178 (2017) 154-162.
[73] T.A. Butterworth, D.I.C. Wang, A.J. Sinskey, Application of ultrafiltration for enzyme. Retention during continuous enzymatic reaction, Biotechnology and Bioengineering, 12 (1970) 615-631.
[74] S. Fukui, A. Tanaka, Enzymatic reactions in organic solvents, Endeavour, 9 (1985) 10-17.
[75] G.M. Rios, M.P. Belleville, D. Paolucci, J. Sanchez, Progress in enzymatic membrane reactors – a review, Journal of Membrane Science, 242 (2004) 189-196.
[76] D. Darnoko, M. Cheryan, W.E. Artz, Saccharification of cassava starch in an ultrafiltration reactor, Enzyme and Microbial Technology, 11 (1989) 154-159.
[77] M. Janssen, C. Muller, D. Vogt, Recent advances in the recycling of homogeneous catalysts using membrane separation, Green Chemistry, 13 (2011) 2247-2257.

[78] J.S. Vrouwenvelder, D. van der Kooij, Diagnosis of fouling problems of NF and RO membrane installations by a quick scan, Desalination, 153 (2003) 121-124.
[79] S. Lee, C.-H. Lee, Effect of operating conditions on CaSO4 scale formation mechanism in nanofiltration for water softening, Water Research, 34 (2000) 3854-3866.
[80] N. Nady, M.C.R. Franssen, H. Zuilhof, M.S.M. Eldin, R. Boom, K. Schroën, Modification methods for poly(arylsulfone) membranes: A mini-review focusing on surface modification, Desalination, 275 (2011) 1-9.
[81] C.-G. Gölander, E. Kiss, Protein adsorption on functionalized and ESCA-characterized polymer films studied by ellipsometry, Journal of Colloid and Interface Science, 121 (1988) 240-253.
[82] D.M. Davenport, J. Lee, M. Elimelech, Efficacy of antifouling modification of ultrafiltration membranes by grafting zwitterionic polymer brushes, Separation and Purification Technology, 189 (2017) 389-398.
[83] P.-F. Ren, Y. Fang, L.-S. Wan, X.-Y. Ye, Z.-K. Xu, Surface modification of polypropylene microfiltration membrane by grafting poly(sulfobetaine methacrylate) and poly(ethylene glycol): Oxidative stability and antifouling capability, Journal of Membrane Science, 492 (2015) 249-256.
[84] J. Ayyavoo, T.P.N. Nguyen, B.-M. Jun, I.-C. Kim, Y.-N. Kwon, Protection of polymeric membranes with antifouling surfacing via surface modifications, Colloids and Surfaces A: Physicochemical and Engineering Aspects, 506 (2016) 190-201.
[85] A. Akbari, Z. Derikvandi, S.M. Mojallali Rostami, Influence of chitosan coating on the separation performance, morphology and anti-fouling properties of the polyamide nanofiltration membranes, Journal of Industrial and Engineering Chemistry, 28 (2015) 268-276.
[86] S. Gahlot, H. Gupta, P.K. Jha, V. Kulshrestha, Enhanced Electrochemical Performance of Stable SPES/SPANI Composite Polymer Electrolyte Membranes by Enriched Ionic Nanochannels, ACS Omega, 2 (2017) 5831-5839.

[87] S. Dai, P. Ravi, K.C. Tam, pH-Responsive polymers: synthesis, properties and applications, Soft Matter, 4 (2008) 435-449.
[88] B. Yang, X. Yang, B. Liu, Z. Chen, C. Chen, S. Liang, L.-Y. Chu, J. Crittenden, PVDF blended PVDF-g-PMAA pH-responsive membrane: Effect of additives and solvents on membrane properties and performance, Journal of Membrane Science, (2017).
[89] R. Hoogenboom, 2 - Temperature-responsive polymers: properties, synthesis and applications, in: Smart Polymers and their Applications, Woodhead Publishing, 2014, pp. 15-44.
[90] R. Huang, L.K. Kostanski, C.D.M. Filipe, R. Ghosh, Environment-responsive hydrogel-based ultrafiltration membranes for protein bioseparation, Journal of Membrane Science, 336 (2009) 42-49.
[91] P. Kaner, X.R. Hu, S.W. Thomas, A. Asatekin, Self-Cleaning Membranes from Comb-Shaped Copolymers with Photoresponsive Side Groups, ACS Appl. Mater. Interfaces, 9 (2017) 13619-13631.
[92] P.H.H. Duong, P.Y. Hong, V. Musteata, K.V. Peinemann, S.P. Nunes, Thin Film Polyamide Membranes with Photoresponsive Antibacterial Activity, ChemistrySelect, 2 (2017) 6612-6616.
[93] I.-H. Loh, R.A. Moody, J.C. Huang, Electrically conductive membranes: Synthesis and applications, Journal of Membrane Science, 50 (1990) 31-49.
[94] F. Ahmed, B.S. Lalia, V. Kochkodan, N. Hilal, R. Hashaikeh, Electrically conductive polymeric membranes for fouling prevention and detection: A review, Desalination, 391 (2016) 1-15.
[95] H.Y. Wen, T. Gao, Z.Z. Fu, X. Liu, J.T. Xu, Y.S. He, N.X. Xu, P. Jiao, A. Fan, S.P. Huang, W.M. Xue, Enhancement of membrane stability on magnetic responsive hydrogel microcapsules for potential on-demand cell separation, Carbohydr. Polym., 157 (2017) 1451-1460.
[96] T. Miyata, T. Uragami, K. Nakamae, Biomolecule-sensitive hydrogels, Advanced Drug Delivery Reviews, 54 (2002) 79-98.

[97] I. Amura, S. Shahid, E.A.C. Emanuelsson, Stimuli-responsive Materials for Membrane Fabrication, in: S. Gary, T. Toshinori, Y. Cohen, W.-J. Lau (Eds.) Advanced Materials for Membrane Fabrication and Modification, Taylor and Francis, 2018, pp. 51-70.
[98] D.L. Pile, A.C. Hillier, Electrochemically modulated transport through a conducting polymer membrane, Journal of Membrane Science, 208 (2002) 119-131.
[99] D.A. Reece, S.F. Ralph, G.G. Wallace, Metal transport studies on inherently conducting polymer membranes containing cyclodextrin dopants, Journal of Membrane Science, 249 (2005) 9-20.
[100] X. Sun, J. Wu, Z. Chen, X. Su, B.J. Hinds, Fouling Characteristics and Electrochemical Recovery of Carbon Nanotube Membranes, Advanced Functional Materials, 23 (2013) 1500-1506.
[101] B.S. Lalia, F.E. Ahmed, T. Shah, N. Hilal, R. Hashaikeh, Electrically conductive membranes based on carbon nanostructures for self-cleaning of biofouling, Desalination, 360 (2015) 8-12.
[102] S. Haider, S.-Y. Park, S.-H. Lee, Preparation, swelling and electro-mechano-chemical behaviors of a gelatin-chitosan blend membrane, Soft Matter, 4 (2008) 485-492.
[103] H. Chen, G.R. Palmese, Y.A. Elabd, Electrosensitive Permeability of Membranes with Oriented Polyelectrolyte Nanodomains, Macromolecules, 40 (2007) 781-782.
[104] R. Balint, N.J. Cassidy, S.H. Cartmell, Conductive polymers: Towards a smart biomaterial for tissue engineering, Acta Biomaterialia, 10 (2014) 2341-2353.
[105] J.L. Bredas, G.B. Street, Polarons, bipolarons, and solitons in conducting polymers, Accounts of Chemical Research, 18 (1985) 309-315.
[106] G. Ćirić-Marjanović, Recent advances in polyaniline research: Polymerization mechanisms, structural aspects, properties and applications, Synthetic Metals, 177 (2013) 1-47.

[107] B.C. Sih, M.O. Wolf, Metal nanoparticle—conjugated polymer nanocomposites, Chemical Communications, (2005) 3375-3384.
[108] O. Breuer, U. Sundararaj, Big returns from small fibers: A review of polymer/carbon nanotube composites, Polymer Composites, 25 (2004) 630-645.
[109] N.-R. Chiou, A.J. Epstein, Polyaniline Nanofibers Prepared by Dilute Polymerization, Advanced materials, 17 (2005) 1679-1683.
[110] J. Molina, A.I. del Río, J. Bonastre, F. Cases, Influence of the scan rate on the morphology of polyaniline grown on conducting fabrics. Centipede-like morphology, Synthetic Metals, 160 (2010) 99-107.
[111] H. Wang, Q. Hao, X. Yang, L. Lu, X. Wang, Effect of Graphene Oxide on the Properties of Its Composite with Polyaniline, ACS applied materials & interfaces, 2 (2010) 821-828.
[112] X.S. Du, M. Xiao, Y.Z. Meng, Facile synthesis of highly conductive polyaniline/graphite nanocomposites, European Polymer Journal, 40 (2004) 1489-1493.
[113] L. Huang, J. Chen, T. Gao, M. Zhang, Y. Li, L. Dai, L. Qu, G. Shi, Reduced Graphene Oxide Membranes for Ultrafast Organic Solvent Nanofiltration, Advanced materials, 28 (2016) 8669-8674.
[114] M.R. Anderson, B.R. Mattes, H. Reiss, R.B. Kaner, Conjugated Polymer Films for Gas Separations, in: Science, **1991**, pp. 1412-1415.
[115] M.R. Anderson, B.R. Mattes, H. Reiss, R.B. Kaner, Conjugated polymer films for gas separations, Science, 252 (1991) 1412-1415.
[116] J. Pellegrino, The Use of Conducting Polymers in Membrane-Based Separations, Annals of the New York Academy of Sciences, 984 (2003) 289-305.
[117] R. Mukherjee, R. Sharma, P. Saini, S. De, Nanostructured polyaniline incorporated ultrafiltration membrane for desalination of brackish water, Environmental Science: Water Research & Technology, 1 (2015) 893-904.

[118] I.J. Ball, S.-C. Huang, K.J. Miller, R.A. Wolf, J.Y. Shimano, R.B. Kaner, The pervaporation of ethanol/water feeds with polyaniline membranes and blends, Synthetic Metals, 102 (1999) 1311-1312.
[119] Y.S. Negi, P.V. Adhyapak, DEVELOPMENT IN POLYANILINE CONDUCTING POLYMERS, Journal of Macromolecular Science, Part C, 42 (2002) 35-53.
[120] A.G. Macdiarmid, J.C. Chiang, A.F. Richter, A.J. Epstein, Polyaniline: a new concept in conducting polymers, Synthetic Metals, 18 (1987) 285-290.
[121] G.E. Asturias, A.G. MacDiarmid, R.P. McCall, A.J. Epstein, The oxidation state of "emeraldine" base, Synthetic Metals, 29 (1989) 157-162.
[122] K.G. Neoh, M.Y. Pun, E.T. Kang, K.L. Tan, Polyaniline treated with organic acids: doping characteristics and stability, Synthetic Metals, 73 (1995) 209-215.
[123] M. Jaymand, Recent progress in chemical modification of polyaniline, Progress in Polymer Science, 38 (2013) 1287-1306.
[124] Y. Cao, J. Qiu, P. Smith, Effect of solvents and co-solvents on the processibility of polyaniline: I. solubility and conductivity studies, Synthetic Metals, 69 (1995) 187-190.
[125] L. Chao, Y.-K. Han, B.-Z. Hiseh, Y.-J. Huang, T.-H. Hsieh, C.-M. Lin, S.-Z. Lin, P.-H. Tseng, K.-S. Ho, Conducting polymer blends prepared from polyaniline with n-dodecylbenzenesulfonic acid zinc salt as the secondary dopant, Journal of Applied Polymer Science, 108 (2008) 3516-3522.
[126] M.M. Ayad, E.A. Zaki, Doping of polyaniline films with organic sulfonic acids in aqueous media and the effect of water on these doped films, European Polymer Journal, 44 (2008) 3741-3747.
[127] J. Tarver, J.E. Yoo, T.J. Dennes, J. Schwartz, Y.-L. Loo, Polymer Acid Doped Polyaniline Is Electrochemically Stable Beyond pH 9, Chemistry of Materials, 21 (2009) 280-286.
[128] O.L. Gribkova, A.A. Nekrasov, M. Trchova, V.F. Ivanov, V.I. Sazikov, A.B. Razova, V.A. Tverskoy, A.V. Vannikov, Chemical synthesis of polyaniline

in the presence of poly(amidosulfonic acids) with different rigidity of the polymer chain, Polymer, 52 (2011) 2474-2484.
[129] L. Xu, Electrically Tuneable Membranes: Revolutionising Separation and Fouling Control for Membrane Reactors, in: Chemical Engineering, University of Bath, 2016.
[130] I. Mav, M. igon, A. Šebenik, Sulfonated polyaniline, Synthetic Metals, 101 (1999) 717-718.
[131] M.T. Nguyen, M. Leclerc, A.F. Diaz, Water-soluble conductive-electroactive polymers, Trends in Polymer Science, 3 (1995) 186-190.
[132] S. Bhadra, N.H. Kim, J.H. Lee, Synthesis of water soluble sulfonated polyaniline and determination of crystal structure, Journal of Applied Polymer Science, 117 (2010) 2025-2035.
[133] C.-H. Yang, Y.-K. Chih, H.-E. Cheng, C.-H. Chen, Nanofibers of self-doped polyaniline, Polymer, 46 (2005) 10688-10698.
[134] Y. Tao, J.X. Zhao, C.X. Wu, Polyacrylamide hydrogels with trapped sulfonated polyaniline, European Polymer Journal, 41 (2005) 1342-1349.
[135] L. Shi, F. Zeng, X. Cheng, K.H. Lam, W. Wang, A. Wang, Z. Jin, F. Wu, Y. Yang, Enhanced performance of lithium-sulfur batteries with high sulfur loading utilizing ion selective MWCNT/SPANI modified separator, Chemical Engineering Journal, 334 (2018) 305-312.
[136] E.T. Vilela, R.d.C.S. Carvalho, S. Yotsumoto Neto, R.d.C.S. Luz, F.S. Damos, Exploiting charge/ions compensating processes in PANI/SPANI/reduced graphene oxide composite for development of a high sensitive H2O2 sensor, Journal of Electroanalytical Chemistry, 752 (2015) 75-81.
[137] J. Yue, G. Gordon, A.J. Epstein, Comparison of different synthetic routes for sulphonation of polyaniline, Polymer, 33 (1992) 4410-4418.
[138] S. Ito, K. Murata, S. Teshima, R. Aizawa, Y. Asako, K. Takahashi, B.M. Hoffman, Simple synthesis of water-soluble conducting polyaniline, Synthetic Metals, 96 (1998) 161-163.

[139] X. Wei, A.J. Epstein, Synthesis of highly sulfonated polyaniline, Synthetic Metals, 74 (1995) 123-125.
[140] X.L. Wei, Y.Z. Wang, S.M. Long, C. Bobeczko, A.J. Epstein, Synthesis and Physical Properties of Highly Sulfonated Polyaniline, Journal of the American Chemical Society, 118 (1996) 2545-2555.
[141] Y. Yang, Y. Min, J.C. Wu, D.J. Hansford, S.E. Feinberg, A.J. Epstein, Synthesis and characterization of cytocompatible sulfonated polyanilines, Macromol Rapid Commun, 32 (2011) 887-892.
[142] J.Y. Lee, C.Q. Cui, Electrochemical copolymerization of aniline and metanilic acid, Journal of Electroanalytical Chemistry, 403 (1996) 109-116.
[143] I. Mav, M. Žigon, A. Šebenik, J. Vohlidal, Sulfonated polyanilines prepared by copolymerization of 3-aminobenzenesulfonic acid and aniline: The effect of reaction conditions on polymer properties, Journal of Polymer Science Part A: Polymer Chemistry, 38 (2000) 3390-3398.
[144] R. Rohani, M. Hyland, D. Patterson, A refined one-filtration method for aqueous based nanofiltration and ultrafiltration membrane molecular weight cut-off determination using polyethylene glycols, Journal of Membrane Science, 382 (2011) 278-290.
[145] L. Xu, S. Shahid, J. Shen, E.A.C. Emanuelsson, D.A. Patterson, A wide range and high resolution one-filtration molecular weight cut-off method for aqueous based nanofiltration and ultrafiltration membranes, Journal of Membrane Science, 525 (2017) 304-311.
[146] C.J. Davey, Z.-X. Low, R.H. Wirawan, D.A. Patterson, Molecular weight cut-off determination of organic solvent nanofiltration membranes using poly(propylene glycol), Journal of Membrane Science, 526 (2017) 221-228.
[147] Junhua, L. Zhao, N. Ran, Recent Advances in Developing Chemoenzymatic Processes for Active Pharmaceutical Ingredients, Organic Process Research & Development, 11 (2007) 259-267.

[148] D. Nair, S.S. Luthra, J.T. Scarpello, L.S. White, L.M. Freitas dos Santos, A.G. Livingston, Homogeneous catalyst separation and re-use through nanofiltration of organic solvents, Desalination, 147 (2002) 301-306.
[149] Metal-Catalyzed Cross-Coupling Reactions of Organoboron Compounds with Organic Halides, in: Metal-Catalyzed Cross-Coupling Reactions, pp. 41-123.
[150] N. Miyaura, A. Suzuki, Palladium-Catalyzed Cross-Coupling Reactions of Organoboron Compounds, Chemical Reviews, 95 (1995) 2457-2483.
[151] R. Martin, S.L. Buchwald, Palladium-Catalyzed Suzuki−Miyaura Cross-Coupling Reactions Employing Dialkylbiaryl Phosphine Ligands, Accounts of Chemical Research, 41 (2008) 1461-1473.
[152] U. Christmann, R. Vilar, Monoligated Palladium Species as Catalysts in Cross-Coupling Reactions, Angewandte Chemie International Edition, 44 (2005) 366-374.
[153] F. Barrios-Landeros, J.F. Hartwig, Distinct Mechanisms for the Oxidative Addition of Chloro-, Bromo-, and Iodoarenes to a Bisphosphine Palladium(0) Complex with Hindered Ligands, Journal of the American Chemical Society, 127 (2005) 6944-6945.
[154] P.W.N.M. van Leeuwen, Decomposition pathways of homogeneous catalysts, Applied Catalysis A: General, 212 (2001) 61-81.
[155] K. Nakamura, T. Matsuda, Enzymatic kinetic resolution, in: F. Toda (Ed.) Enantiomer Separation: Fundamentals and Practical Methods, Springer Netherlands, Dordrecht, 2004, pp. 231-266.
[156] P. Shivaprasad, M.D. Jones, D.A. Patterson, E.A.C. Emanuelsson, Kinetic resolution of 1-phenylethanol in the spinning mesh disc reactor: Investigating the reactor performance using immobilised lipase catalyst, Chemical Engineering and Processing - Process Intensification, 132 (2018) 56-64.
[157] K.-E. Jaeger, K. Liebeton, A. Zonta, K. Schimossek, M.T. Reetz, Biotechnological application of Pseudomonas aeruginosa lipase: efficient

kinetic resolution of amines and alcohols, Applied Microbiology and Biotechnology, 46 (1996) 99-105.
[158] M. Habulin, Ž. Knez, Optimization of (R,S)-1-phenylethanol kinetic resolution over Candida antarctica lipase B in ionic liquids, Journal of Molecular Catalysis B: Enzymatic, 58 (2009) 24-28.
[159] I. Hoffmann, V.D. Silva, M.d.G. Nascimento, Enantioselective resolution of (R,S)-1-phenylethanol catalyzed by lipases immobilized in starch films, Journal of the Brazilian Chemical Society, 22 (2011) 1559-1567.
[160] M. Primožič, M. Paljevac, Ž. Knez, Hydrolase-catalyzed reactions in membrane reactors at atmospheric and high pressure, Desalination, 241 (2009) 14-21.
[161] C. Amatore, A. Jutand, A. Thuilliez, Formation of Palladium(0) Complexes from Pd(OAc)2 and a Bidentate Phosphine Ligand (dppp) and Their Reactivity in Oxidative Addition, Organometallics, 20 (2001) 3241-3249.
[162] C. Amatore, A. Jutand, G. Le Duc, Mechanistic Origin of Antagonist Effects of Usual Anionic Bases (OH−, CO32−) as Modulated by their Countercations (Na+, Cs+, K+) in Palladium-Catalyzed Suzuki–Miyaura Reactions, Chemistry – A European Journal, 18 (2012) 6616-6625.
[163] R. Chan, V. Chen, Characterization of protein fouling on membranes: opportunities and challenges, Journal of Membrane Science, 242 (2004) 169-188.
[164] V. Athawale, N. Manjrekar, M. Athawale, Enzymatic synthesis of chiral menthyl methacrylate monomer by pseudomonas cepacia lipase catalysed resolution of (±)-menthol, Journal of Molecular Catalysis B: Enzymatic, 16 (2001) 169-173.
[165] Y. Kitamoto, Y. Kuruma, K. Suzuki, T. Hattori, Effect of Solvent Polarity on Enantioselectivity in Candida Antarctica Lipase B Catalyzed Kinetic Resolution of Primary and Secondary Alcohols, The Journal of Organic Chemistry, 80 (2015) 521-527.

[166] I.I. Yusoff, R. Rohani, A.W. Mohammad, Investigation of the formation characteristics of polyaniline and its application in forming free-standing pressure filtration membranes, Journal of Polymer Research, 23 (2016).
[167] L.L. Xu, S. Shahid, D.A. Patterson, E.A.C. Emanuelsson, Flexible electro-responsive in-situ polymer acid doped polyaniline membranes for permeation enhancement and membrane fouling removal, Journal of Membrane Science, (2018).
[168] D.F.A. Maria C. Miras, Natalia Monge, Evelina Frontera, Claudia R. Rivarola , Cesar A. Barbero Organic Chemistry of Polyanilines: Tailoring Properties to Technological Applications, The Open Macromolecules Journal (2008) 58-73.
[169] Q. Wu, Z. Qi, F. Wang, The six-member ring self-doping structure in sulfonated polyaniline, Synthetic Metals, 105 (1999) 191-194.
[170] N. Cheng, Q. Yan, S. Liu, D. Zhao, Probing the intermolecular interactions of aromatic amides containing N-heterocycles and triptycene, CrystEngComm, 16 (2014) 4265-4273.
[171] Y. Cao, S. Li, Z. Xue, D. Guo, Spectroscopic and electrical characterization of some aniline oligomers and polyaniline, Synthetic Metals, 16 (1986) 305-315.
[172] Y. Furukawa, F. Ueda, Y. Hyodo, I. Harada, T. Nakajima, T. Kawagoe, Vibrational spectra and structure of polyaniline, Macromolecules, 21 (1988) 1297-1305.
[173] Y. Ma, F. Shi, J. Ma, M. Wu, J. Zhang, C. Gao, Effect of PEG additive on the morphology and performance of polysulfone ultrafiltration membranes, Desalination, 272 (2011) 51-58.
[174] S. Bhadra, D. Khastgir, Determination of crystal structure of polyaniline and substituted polyanilines through powder X-ray diffraction analysis, Polymer Testing, 27 (2008) 851-857.

[175] Y. Wang, H.D. Tran, L. Liao, X. Duan, R.B. Kaner, Nanoscale Morphology, Dimensional Control, and Electrical Properties of Oligoanilines, Journal of the American Chemical Society, 132 (2010) 10365-10373.
[176] P. Srinivasa Rao, B. Smitha, S. Sridhar, A. Krishnaiah, Preparation and performance of poly(vinyl alcohol)/polyethyleneimine blend membranes for the dehydration of 1,4-dioxane by pervaporation: Comparison with glutaraldehyde cross-linked membranes, Separation and Purification Technology, 48 (2006) 244-254.
[177] T.-H. Young, L.-W. Chen, Pore formation mechanism of membranes from phase inversion process, Desalination, 103 (1995) 233-247.
[178] J. Aburabie, A.-H. Emwas, K.-V. Peinemann, Silane-Crosslinked Asymmetric Polythiosemicarbazide Membranes for Organic Solvent Nanofiltration, Macromolecular Materials and Engineering, 304 (2019) 1800551.
[179] K.M. Persson, V. Gekas, G. Trägårdh, Study of membrane compaction and its influence on ultrafiltration water permeability, Journal of Membrane Science, 100 (1995) 155-162.
[180] P. Kolář, J.-W. Shen, A. Tsuboi, T. Ishikawa, Solvent selection for pharmaceuticals, Fluid Phase Equilibria, 194-197 (2002) 771-782.
[181] L.L. Xu, Y. Xu, L. Liu, K.P. Wang, D.A. Patterson, J. Wang, Electrically responsive ultrafiltration polyaniline membrane to solve fouling under applied potential, Journal of Membrane Science, 572 (2019) 442-452.
[182] X. Wang, Y. Zhao, E. Tian, J. Li, Y. Ren, Graphene Oxide-Based Polymeric Membranes for Water Treatment, Advanced Materials Interfaces, 5 (2018).
[183] X. Wang, M. Feng, Y. Liu, H. Deng, J. Lu, Fabrication of graphene oxide blended polyethersulfone membranes via phase inversion assisted by electric field for improved separation and antifouling performance, Journal of Membrane Science, 577 (2019) 41-50.

[184] A. Abdel-Karim, S. Leaper, M. Alberto, A. Vijayaraghavan, X. Fan, S.M. Holmes, E.R. Souaya, M.I. Badawy, P. Gorgojo, High flux and fouling resistant flat sheet polyethersulfone membranes incorporated with graphene oxide for ultrafiltration applications, Chemical Engineering Journal, 334 (2018) 789-799.
[185] S. Bhadra, N.K. Singha, D. Khastgir, Effect of aromatic substitution in aniline on the properties of polyaniline, European Polymer Journal, 44 (2008) 1763-1770.
[186] J. Alam, A.K. Shukla, M. Alhoshan, L. Arockiasamy Dass, M.R. Muthumareeswaran, A. Khan, F.A. Ahmed Ali, Graphene oxide, an effective nanoadditive for a development of hollow fiber nanocomposite membrane with antifouling properties, Advances in Polymer Technology, 37 (2018) 2597-2608.
[187] S.P. Deshmukh, K. Li, Effect of ethanol composition in water coagulation bath on morphology of PVDF hollow fibre membranes, Journal of Membrane Science, 150 (1998) 75-85.
[188] R. Thomas, E. Guillen-Burrieza, H.A. Arafat, Pore structure control of PVDF membranes using a 2-stage coagulation bath phase inversion process for application in membrane distillation (MD), Journal of Membrane Science, 452 (2014) 470-480.
[189] C.W. Yao, R.P. Burford, A.G. Fane, C.J.D. Fell, Effect of coagulation conditions on structure and properties of membranes from aliphatic polyamides, Journal of Membrane Science, 38 (1988) 113-125.
[190] M.H. Razzaghi, M. Tavakolmoghadam, F. Rekabdar, F. Oveisi, Investigation of the effect of coagulation bath composition on PVDF/CA membrane by evaluating critical flux and antifouling properties in lab-scale submerged MBR, Water and Environment Journal, 32 (2018) 366-376.
[191] G.R. Guillen, Y. Pan, M. Li, E.M.V. Hoek, Preparation and Characterization of Membranes Formed by Nonsolvent Induced Phase Separation: A Review, Industrial & Engineering Chemistry Research, 50 (2011) 3798-3817.

[192] J.-M. Sansiñena, J. Gao, H.-L. Wang, High-Performance, Monolithic Polyaniline Electrochemical Actuators, Advanced Functional Materials, 13 (2003) 703-709.
[193] G.R. Guillen, G.Z. Ramon, H.P. Kavehpour, R.B. Kaner, E.M.V. Hoek, Direct microscopic observation of membrane formation by nonsolvent induced phase separation, Journal of Membrane Science, 431 (2013) 212-220.
[194] A.K. Hołda, I.F.J. Vankelecom, Understanding and guiding the phase inversion process for synthesis of solvent resistant nanofiltration membranes, 132 (2015).
[195] R.-C. Ruaan, T. Chang, D.-M. Wang, Selection criteria for solvent and coagulation medium in view of macrovoid formation in the wet phase inversion process, 37 (1999) 1495-1502.
[196] M. Bláha, A. Suchánková, E. Watzlová, J. Prokeš, O. Pop-Georgievski, Partially sulfonated polyaniline: conductivity and spectroscopic study, Chemical Papers, 71 (2016) 329-338.
[199] P. Izák, Š. Hovorka, T. Bartovský, L. Bartovská, J.G. Crespo, Swelling of polymeric membranes in room temperature ionic liquids, Journal of Membrane Science, 296 (2007) 131-138.
[198] C. Hansen, Hansen Solubility Parameters: A User's Handbook, Second Edition, 2012.
[199] Y.H. See Toh, X.X. Loh, K. Li, A. Bismarck, A.G. Livingston, In search of a standard method for the characterisation of organic solvent nanofiltration membranes, Journal of Membrane Science, 291 (2007) 120-125.
[200] L.S. Sandell, D.A.I. Goring, Solvent-Induced Conformational Expansion of Oligomeric Propylene Glycols, Macromolecules, 3 (1970) 54-57.
[201] A.R. Dolan, T.D. Wood, Analysis of polyaniline oligomers by laser desorption ionization and solventless MALDI, Journal of the American Society for Mass Spectrometry, 15 (2004) 893-899.

[202] M. Sairam, S.K. Nataraj, T.M. Aminabhavi, S. Roy, C.D. Madhusoodana, Polyaniline Membranes for Separation and Purification of Gases, Liquids, and Electrolyte Solutions, Separation & Purification Reviews, 35 (2006) 249-283.
[203] J.M. Ginder, A.J. Epstein, A.G. MacDiarmid, Electronic phenomena in polyaniline, Synthetic Metals, 29 (1989) 395-400.
[204] A.G. MacDiarmid, A.J. Epstein, Polyanilines: a novel class of conducting polymers, Faraday Discussions of the Chemical Society, 88 (1989) 317-332.
[205] A. Pron, P. Rannou, Processible conjugated polymers: from organic semiconductors to organic metals and superconductors, Progress in Polymer Science, 27 (2002) 135-190.
[206] H. Hu, J.L. Cadenas, J.M. Saniger, P.K. Nair, Electrically conducting polyaniline-poly(acrylic acid) blends, Polymer International, 45 (1998) 262-270.

Appendix A

Analysis of the reaction components and membrane characterisation

A.1. Nuclear magnetic resonance

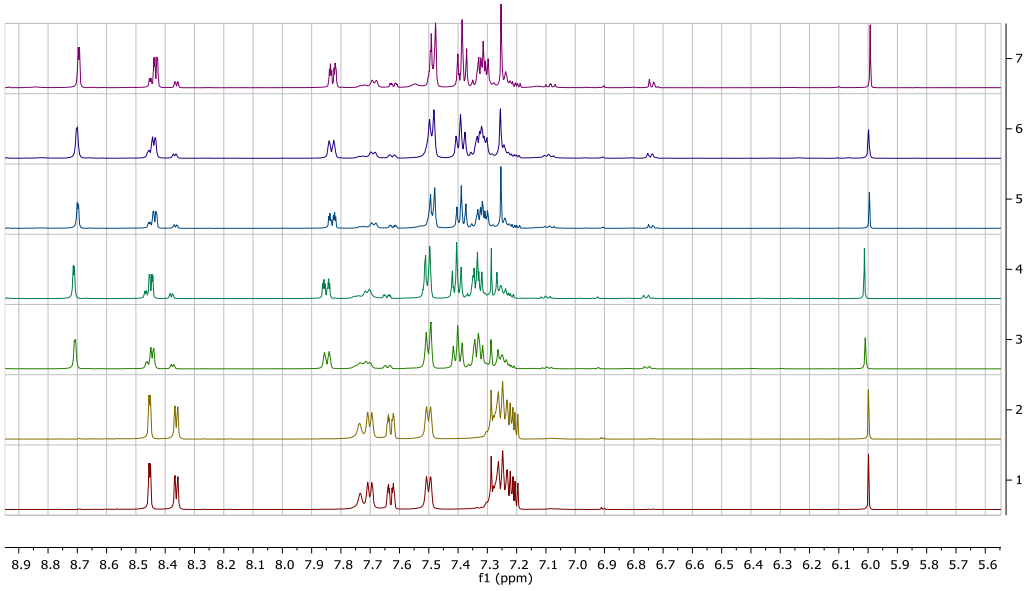

Figure 61: 1H NMR spectra showing the evolution of the Suzuki coupling reaction when the conversion of 3-chloropyridine is not complete. Offline acquisition. Reaction IASC57, conditions: 1 eq. 3-choloropyridine, 1 eq. phenylboronic acid, 2% mol of $Pd(OAc)_2$.

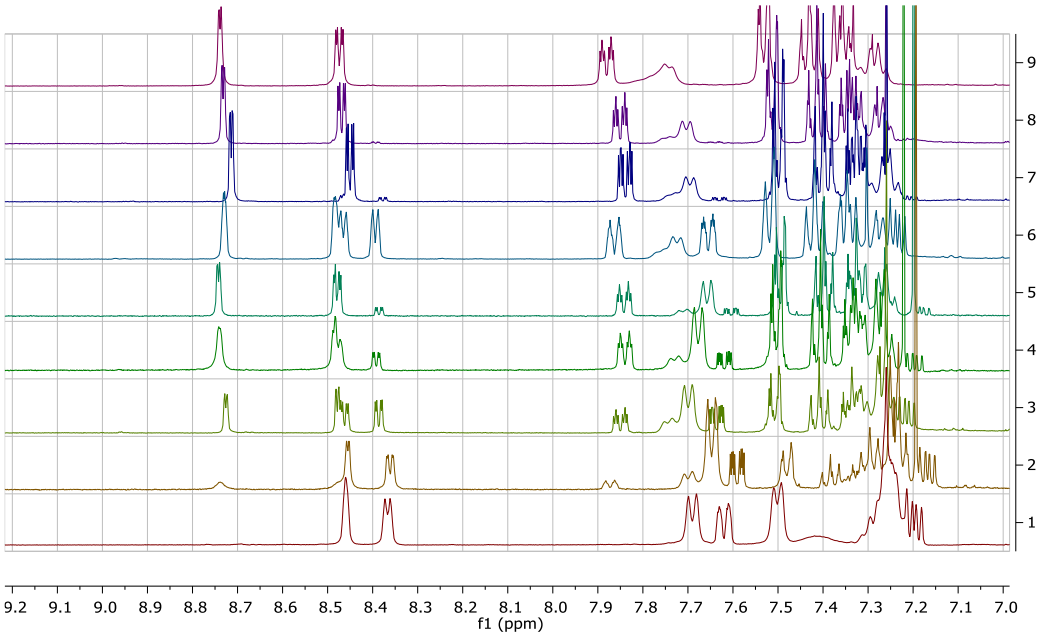

Figure 62: ^{1}H NMR spectra showing the evolution of the conversion of 3-chloropyridine over time for reaction IASC65. Standard Reaction conditions: 1 eq. 3-choloropyridine, 1 eq. phenylboronic acid, 2% mol of $Pd(OAc)_2$.

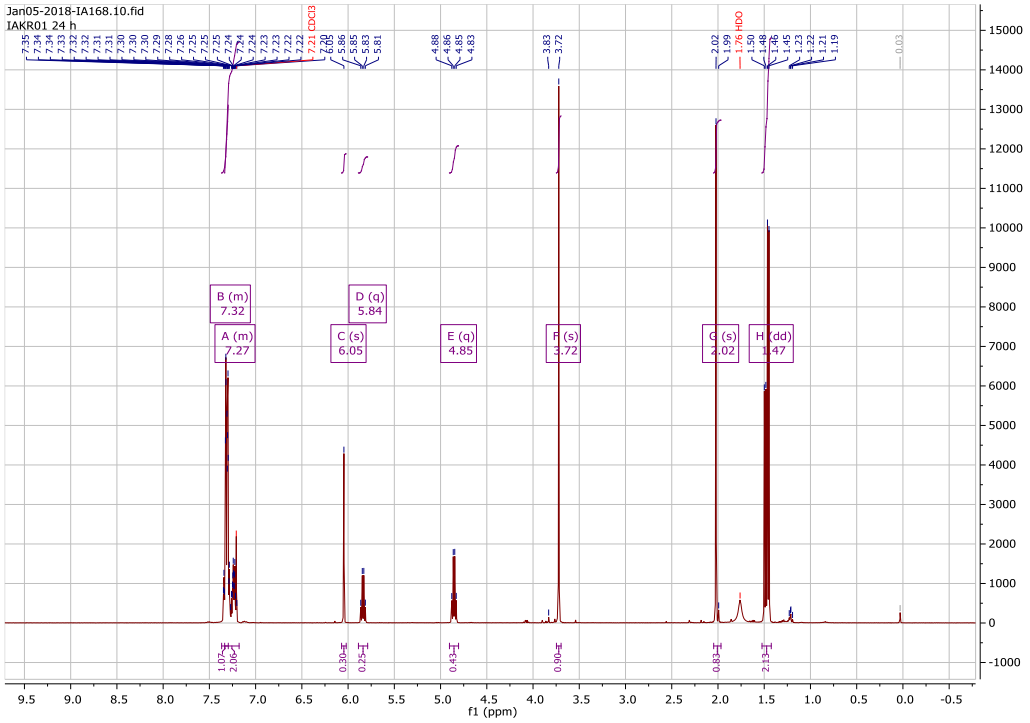

Figure 63:1H NMR spectrum of the reaction IAKR01in toluene - kinetic resolution of 1-phenylethanol mediated by lipase. Reaction conditions: Pseudomonas lipase (1g), 1-phenylethanol (5 mmol), vinyl acetate (25 mmol) and 1,3,5-TMB (1 mmol) as internal NMR standard.

A.2. Chemical characterisation of Pd-XPhos complex

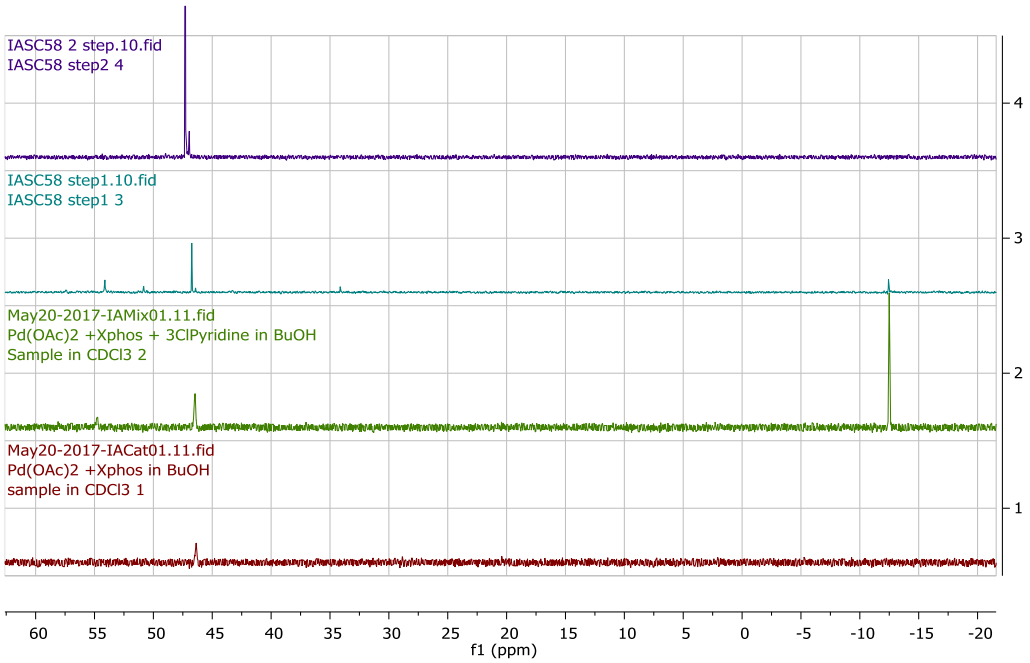

Figure 64: ^{31}P NMR spectra showing the shift of the peak of the XPhos ligand in different stage of the catalytic cycle. The samples were prepared by dissolving XPhos (0.16 mmol) and $Pd(OAc)_2$ (0.08 mmol) in 5 ml of butanol. 0.5 ml of the solution was then collected in an NMR tube and analysed by ^{31}P NMR on 500 MHz Bruker instrument using the solvent suppression technique.

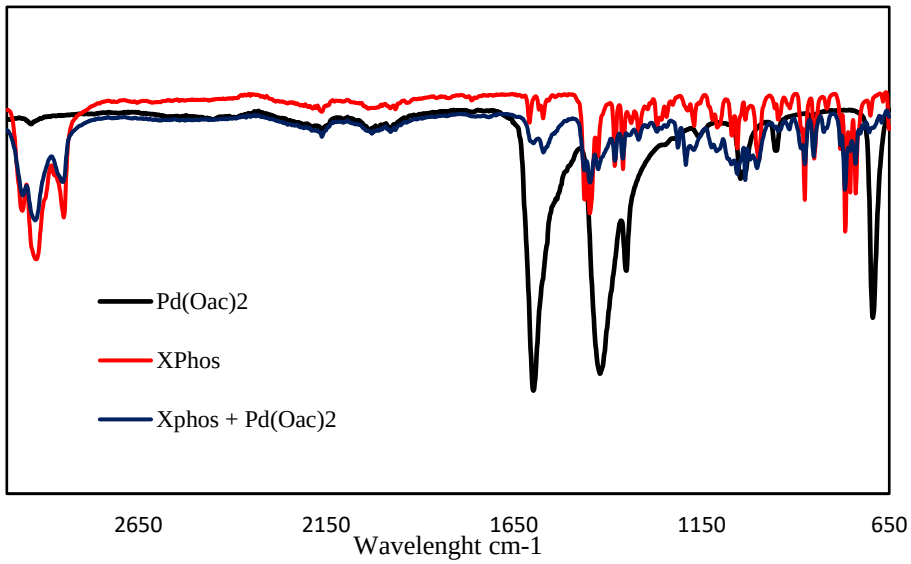

Figure 65:FTIR spectra showing XPhos (red), $Pd(OAc)_2$ (black) and the $Pd(OAc)_2$ -XPhos mixture (blue).

A.3. Polymers and membranes properties

A.3.1. Matrix-assisted laser desorption/ionization MALDI

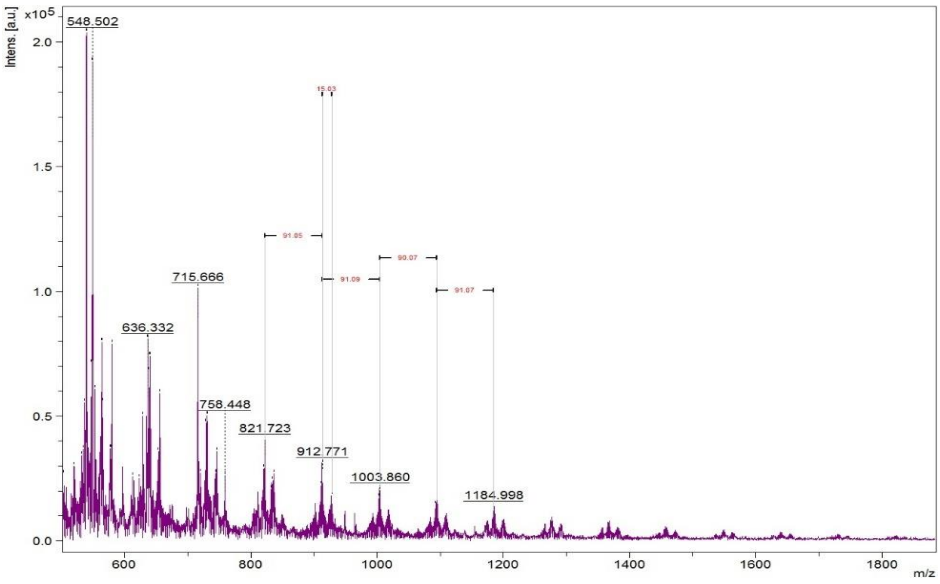

Figure 66: Example of MALDI spectrum of the S-PANI powder showing its chemical composition based on the elemental analysis. The data were obtained using a Bruker AutoFlex

MALDI coupled with Time of Flight (TOF) mass spectrometer. The sample was prepared via solventless technique [201]. S-PANI and a matrix (DHB) were used in molar ratio 1:30 and mixed and ground for 15 minutes. The prepared ground sample was then spread out on the plate and then any excess was removed in order to obtain a thin film ready to be analysed. Spectra were generated with an acceleration voltage of 19 kV and were the average of 200 laser shots.

A.3.2. Additional SEM images of the S-PANI polymer and membranes

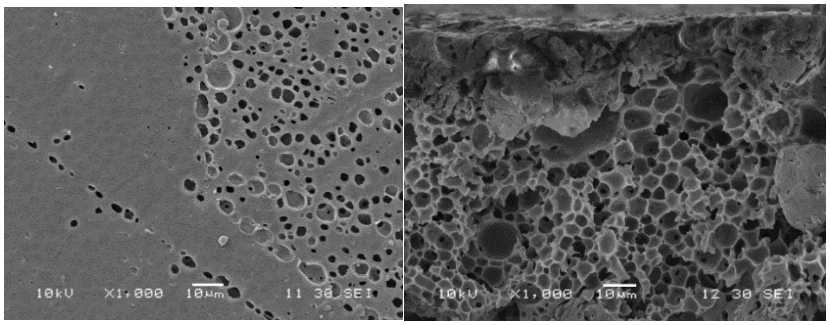

Figure 67:SEM surface and cross-section of SPHX membrane prepared via phase inversion in hexane. Fabrication conditions: S-PANI 21% wt 4.5 g NMP, 1.0 g 4-MP and 300 µm thickness.

:

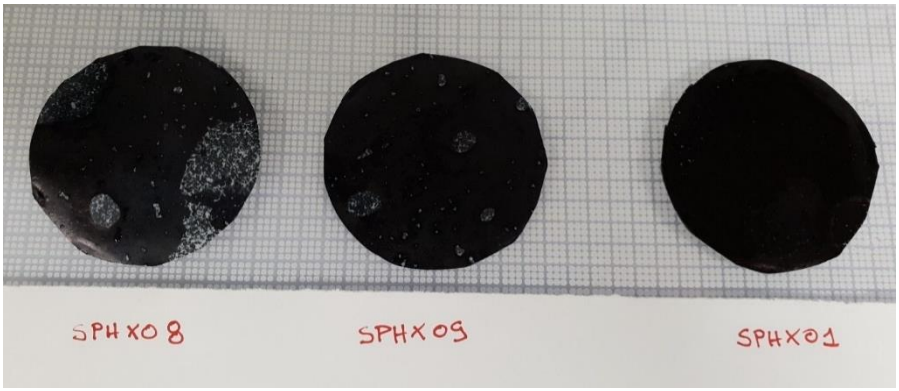

Figure 68:Picture displaying the bottom surface of SPHX membranes prepared via phase inversion in hexane using different concentration of 4-MP and NMP in the dope solution and different thickness. Fabrication conditions are reported in Table 8: Optimization of membrane fabrication conditions

A.3.3. FTIR of thermally cross-linked S-PANI membranes

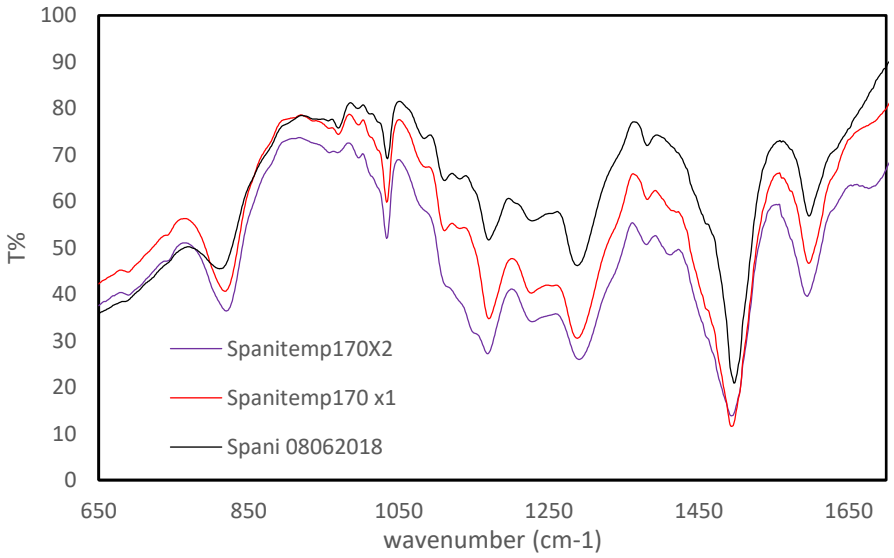

Figure 69: FTIR spectra of thermally cross-linked S-PANI membranes.

A.3.4. Mechanical properties of chemically cross-linked membranes

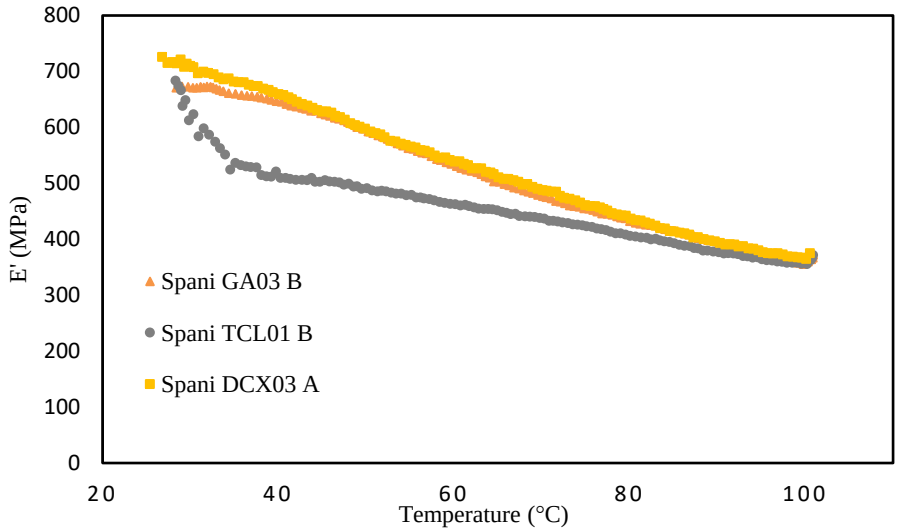

Figure 70: Change in Young Modulus E' with temperature for chemically cross-linked S-PANI membranes

A.4. Membrane performance

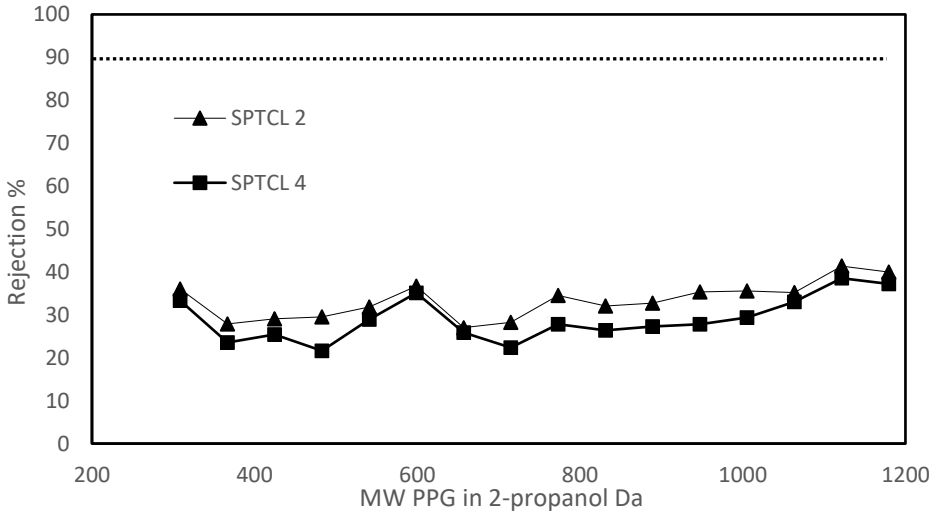

Figure 71: Additional PPG rejection curves for S-PANI TCL membrane in 2-propanol. Filtration condition: 5 bar. Permeance is 1.3 L m^{-2} h^{-1} bar^{-1}

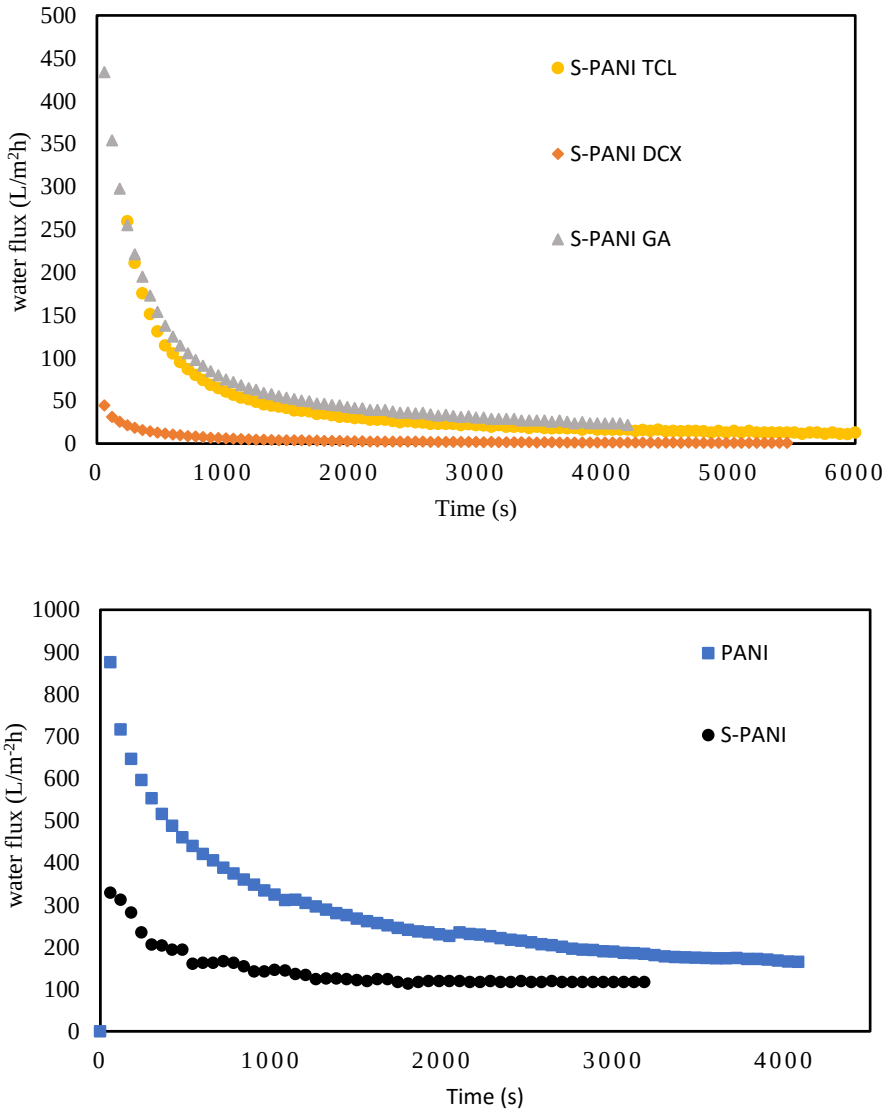

Figure 72: Typical flux profile of initial period for filtration in dead-end cell of S-PANI, PANI and chemically cross-linked S-PANI membranes. Operation conditions: 1 bar and 25 °C.

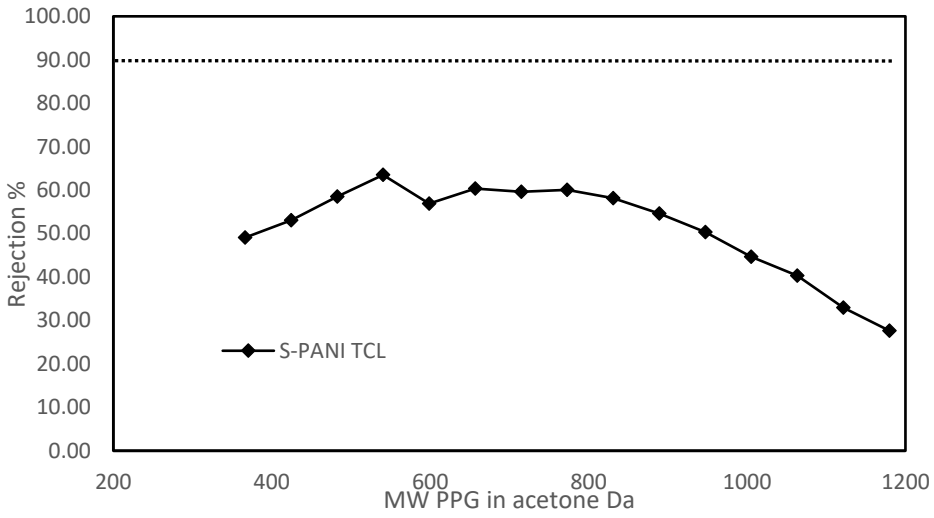

Figure 73: Additional PPG rejection curves for S-PANI TCL membrane in acetone. Filtration conditions: 6 bar. Permeance is 3.7 L m^{-2} h^{-1} bar^{-1}.

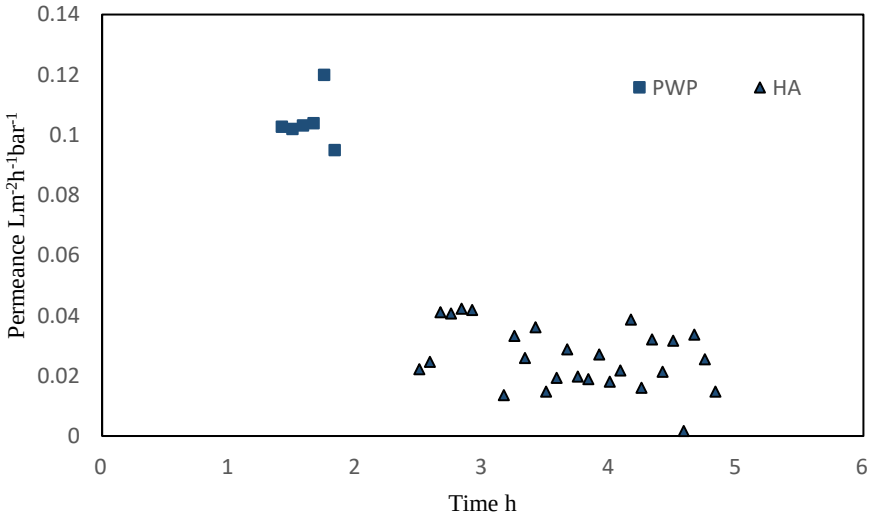

Figure 74: Fouling experiment using HA and SPHX membrane. Filtration conditions: 30 bar.

Appendix B **Calibration curves**

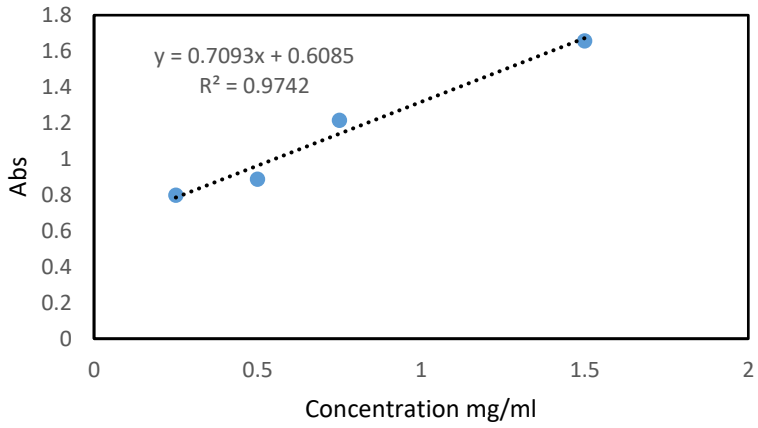

Figure 75: Calibration curve of the UV-Vis Bradford Essay of the lipase in the permeate samples from the semi-continuous kinetic resolution of 1-phenylethanol in solvents.

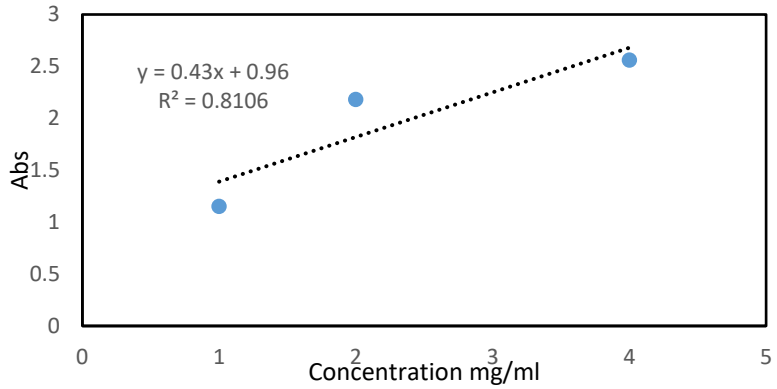

Figure 76: Calibration curve of the UV-Vis analysis of $Pd(OAc)_2$ in the permeate samples from the semi-continuous Suzuki coupling nanofiltration in dead-end cell.

Appendix C **Preparation of solvent stable PANI-PAMPSA membrane: Characterisation, Chemical cross-linking and phase inversion in hexane**

C.1. Introduction

Polyaniline is one of the most studied conducting polymers because of its complex oxidation chemistry and mechanism of polymerisation that is investigated for various applications including membrane technology [202]. PANI is prepared from polymerisation of the aniline in acidic conditions and can exist in three forms that correspond to three different oxidation states: i) leucomeraldine -fully reduced-, ii) pernigraniline -fully oxidised- and iii) emeraldine base -semi oxidised-. Both leucomeraldine and pernigraniline are environmentally unstable, whereas the emeraldine base exists in the solid physical form of a dark blue powder and can be stored for long time without any loss in chemical properties[203, 204]. Through doping it is possible to convert PANI in a conducting polymer. Different dopant ion can be used to obtain PANI with different properties. Protonic acid dopants generally used for PANI doping are inorganic acids such as HCl, H2SO4, HBF4, and organic acids like camphorsulfonic acid (CSA), 5-sulphosalicylic acid, dodecylbenzene sulfonic acid (BDSA) with large anions [205]. Recent studies on the fabrication of PANI membranes, report that small acid dopants, like HCl, leaches out during filtration leading to a change in membrane performance, brittleness of the membrane and loss of electrical conductivity [41, 181, 206]. A recent work reported the preparation of an electrically conductive, organic solvent nanofiltration (OSN) membrane made from Polyaniline (PANI) in-situ doped by poly(2-acrylamido-2-methyl-1-propanesulfonic acid) (PAMPSA) [25]. The membrane was heat treated at 120 °C to shrink the pore size, and it was stable during filtration in a wide range of solvents as the bulky polymer acid does not leave the doping site and was tested in a wide range of solvents.

Because of the stability of the PANI-PAMPSA system, it was explored the possibility to i) chemically cross-linked the PANI PAMPSA membrane and ii) investigate the effect of hexane in the coagulation bath during phase inversion. To date only thermal cross-linking [42] and low thermal treatment [25] has been investigated as a mean to tight the pore size and improve the solvent stability of PANI-PAMPSA but the produces membranes were not stable in harsh polar aprotic solvents. To overcome this limited solvent applicability, we investigate cross-linking of PANI PAMPSA with DCX, and compare the membrane properties with a pristine PANI PAMPSA membrane. Furthermore, the method reported in Chapter 6 to prepare membranes via phase inversion in hexane will be applied to the synthesis of PANI PAMPSA membrane.

C.2. Materials and methods

C.2.1. Materials

Aniline, ammonium persulfate (APS), hydrochloric acid (HCl), HPLC grade acetone, DMF, DMAc, Toluene, N-methyl-2-pyrrolidone (NMP) and 4-methyl piperidine (4-MP) and poly (2-acrylamido-2-methyl-1-propanesulfonic acid) (PAMPSA)were purchased from Sigma-Aldrich (UK) along with the chemical crosslinker α,α′-Dichloro-p-xylene (DCX). Commercial grade polyethylene glycols (PEGs of molecular weight 1000, 1500, 4000 and 6000), ethanol, methanol and isopropanol were obtained from Fisher (UK). Tripropylene glycol and poly(propylene) glycols (PPGs, MW=400, 725 and 1000 g mol−1), were purchased from Alfa Aesar. PET/PBT backing layer- Novatexx 2484 (120 μm) was supplied by Freudenberg Filter technologies (Germany). All solutions were prepared with deionised (DI) water produced from an ELGA deioniser (PURELAB Option).

C.2.2. Synthesis of PANI-PAMPSA

PANI-PAMPSA powder was synthesized by oxidative polymerisation of aniline in PAMPSA using a method reported elsewhere [25]. The obtained PANI-

PAMPSA was filtered and washed with DI water and with acetone until the pH of the filtrate became neutral. The filtered cake was dried in a vacuum oven at 65 °C for 24 h. Finally, the powder was ground in a mortar and a dark green product was obtained.

C.2.3. Membrane preparation

The Novatexx 2484 membrane backing layer was secured using scotch tape on a flat glass plate and all membranes were cast on a bench top laboratory caster. An adjustable casting knife was used to cast 200 µm thick films using an adjustable film applicator (Elcometer 4340 automatic film applicator, Elcometer, UK). Evaporation time of 30 s was used before immersing the casted membrane solution into a DI water coagulation bath for 24 h. The membrane was then rinsed with DI water and chemical cross-linking took place at 20° C. A cross-linking solution of 0.2 M DCX in acetone/hexane (35/65 v/v%) mixture was used, and the membranes were cross-linked following a procedure previously reported [23]. The membranes were kept in the cross-linker solution for 3 days and after crosslinking membranes were washed 2 times with acetone and store in water for future use. The membrane cross-linked with this method was labelled PPDCX01, PPDCX02 etc.

The same dope solution was used to cast a membrane and prepare it via phase inversion using 2.5 L of hexane in the coagulation bath as reported in 3.4.2.2. The membrane prepared following this method was labelled PPHX01, PPHX02 etc.

C.2.4. Physical and chemical characterisation

The FTIR spectra of dry PANI PAMPSA membranes were obtained by using a Spectrum 100™ – FTIR Spectrometer (PerkinElmer, USA) fitted with an attenuated total reflectance (ATR) detector. A background scan was run prior to sample testing and spectra were recorded from 4000 to 650 cm^{-1} in transmission mode with a spectral resolution of 4 cm^{-1} and 32 scans.

Membrane morphology was studied using FSEM (JSM-6301F, JEOL, Germany). All samples were prepared by freeze fracturing them in liquid nitrogen and drying them in vacuum overnight. Before the analysis was performed the samples were coated in chromium using a sputter coater (Q150T S, Quorum) under argon for 5 min.

Membrane hydrophilicity was studied by dynamic contact angle analysis. (Contact Angle System OCA 15Pro, Dataphysics, Germany). The analysis was performed using sessile drop technique (4 μL) and data were recorded for 800 s and repeated 2 times.

C.2.5. Evaluation of membrane performance in dead-end cell

Solvent permeance and solute rejections of the pure PANI PAMPSA, PANI PAMPSA-DCX and PPHX membranes were studied using a dead-end cell. Filtration experiments were performed using the methodology reported in 3.7.1.

C.3. Results and discussion

C.3.1. Membrane fabrication and characterization

FTIR was used to characterise the chemical structure of the PANI PAMPSA, PANI PAMPSA-DCX and PPHX membrane. As reported in Figure 77, the PANI PAMPSA spectrum has two main absorption peaks at 1497 cm^{-1} and 1590 cm^{-1} that have been assigned to the benzenoid and quinoid form of PANI. The FT-IR spectrum has also additional bands at ~1026-1113 cm^{-1} (S=O stretching). The sulfonic group of the acidic dopant is also identified by a band at 1653 cm^{-1} representing the C=O stretching of the dopant. The spectra of PPDCX and PPHX membrane have the same main absorption peaks of the pure PANI PAMPSA but differ in the intensity of those peaks which could be attributed in an increased cross-linking effect.

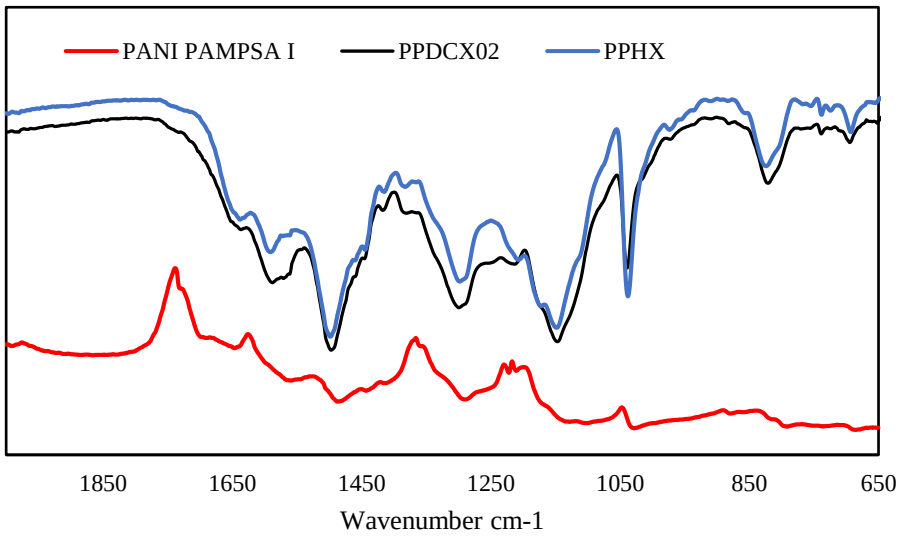

Figure 77: FTIR spectra of PANI PAMPSA membrane, PPDCX membrane and PPHX membrane

Solvent stability in DMF was studied for pure PANI PAMPSA membrane prepared via phase inversion in water and for the DCX-cross-linked membrane. As reported in Figure 78, the stability in DMF after 24 h of immersion is enhanced after the cross-linking of the membrane with DCX. In particular, the weight loss for the PPDCX membrane prepared with THF in the dope solution (right) was only 0.07% after 24 h immersion whereas the PPDCX membrane prepared from a dope solution in NMP/4-MP showed a 4.7% total weight loss. The non-cross-linked PANI PAMPSA readily dissolved in DMF giving a blue solution.

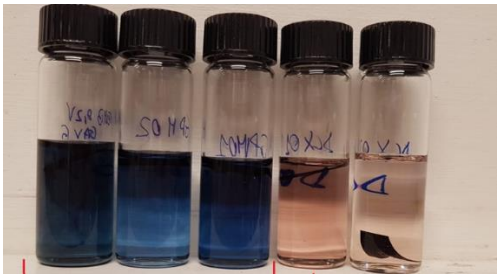

Figure 78: DMF stability - 24h immersion test. From left to right: PANI PAMPSA membrane (20% wt NMP/4-MP, PANI PAMPSA membrane (20%wt NMP/4-MP/THF), PANI PAMPSA membrane (20% wt NMP), PPDCX01 (20%wt NMP/4-MP), PPDCX02 (20% wt NMP/4-MP/THF).

SEM was used to investigate membrane morphology of surface and cross-section. Figure 79 reports the morphologies of the prepared PANI PAMPA membrane at different magnification. The surface of pure PANI PAMPSA appears smooth with no defects but only small impurities due to membrane storage conditions. The most important information about membrane morphology are gained from the cross-sectional images. They show a highly porous loose structures and no formation of macrovoids as it was observed for PANI in 5.3.2.1. It has been suggested that the inclusion of large dopants can expand the intermolecular spacing between PANI polymer chains and clusters forming bigger pores[167]. Further magnification confirms the high porosity of the cross section. Figure 79 B and B-1 and B-2 show that the chemical cross-linking only partially made the large pores smaller, most likely because of the bulky sulfonic groups of the PAMPSA acid which sits between the polymer chains forming a double strand and hindered the further shrinkage of the membrane structure. Figure 79 C to C-4 show the surface of the PPHX membrane. The membrane was casted at 300 µm thickness and immersed for 24 hours in hexane. The surfaces show a very rough top layer with bulges distributed along it.

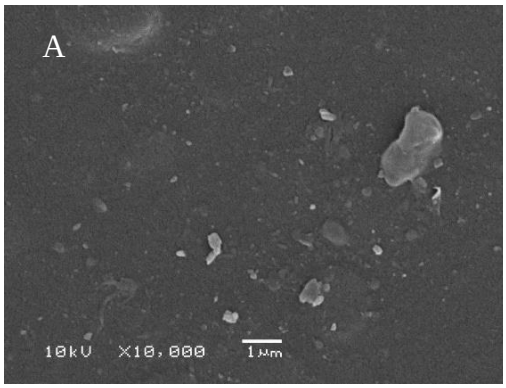
A
10kV X10,000 1μm

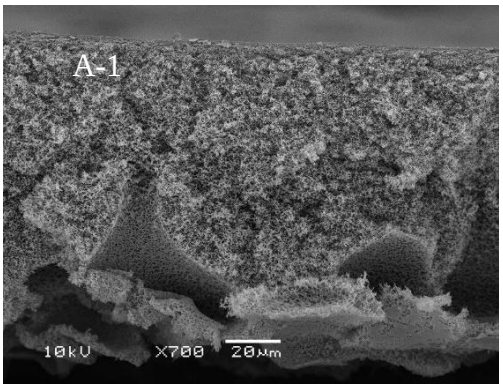
A-1
10kV X700 20μm

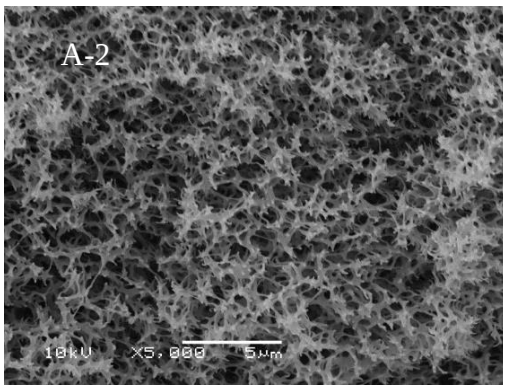
A-2
10kV X5,000 5μm

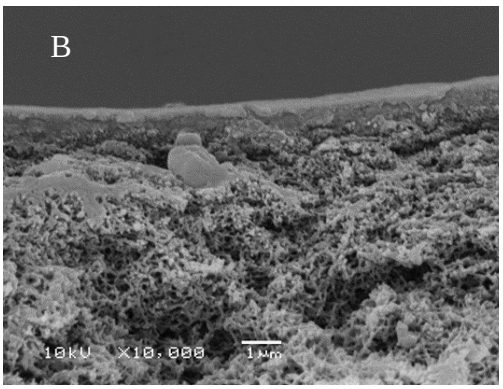
B
10kV X10,000 1μm

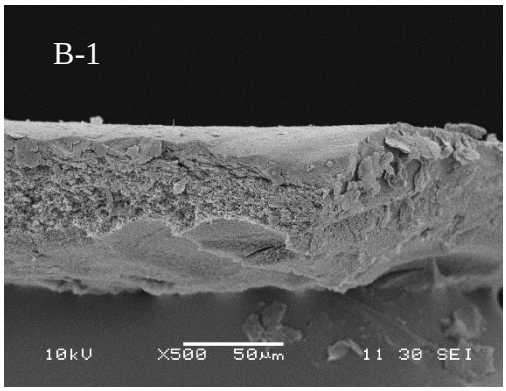
B-1
10kV X500 50μm 11 30 SEI

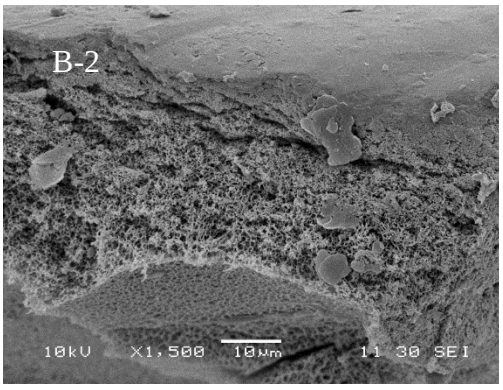
B-2
10kV X1,500 10μm 11 30 SEI

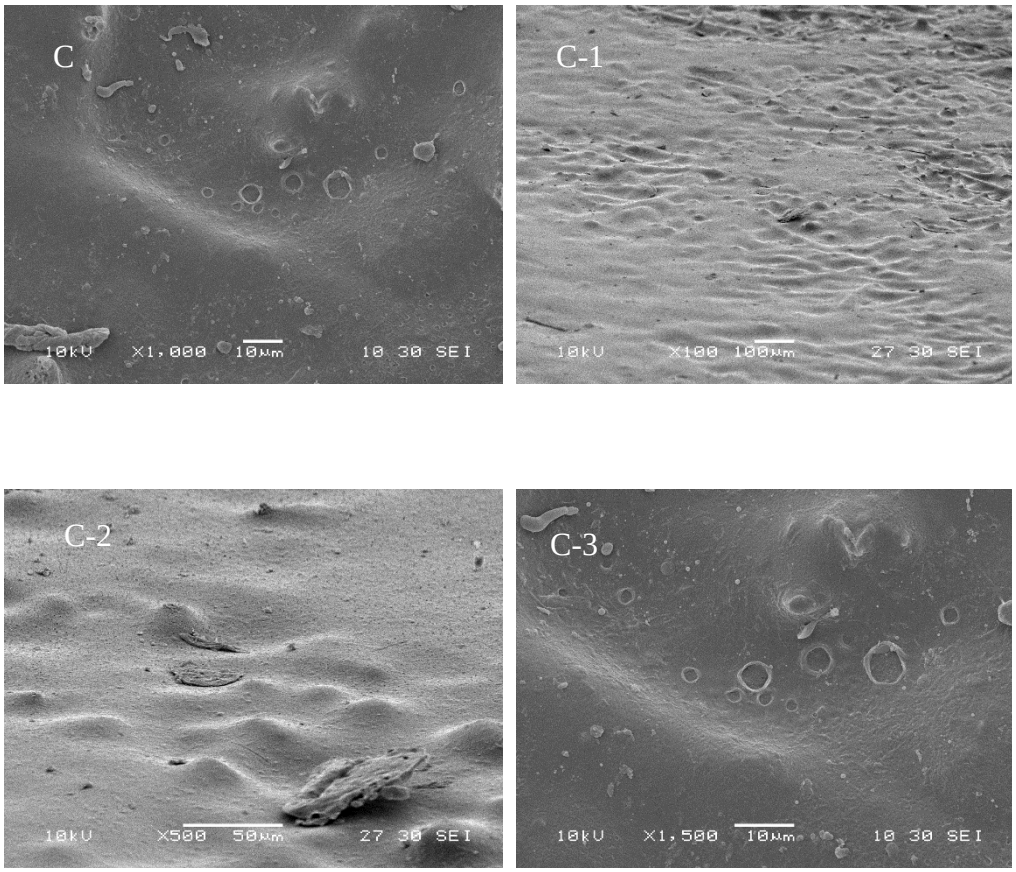

Figure 79: SEM surface and cross-section of (A) PANI PAMPSA membrane prepared from a solution of 20 %wt PANI PAMPSA in NMP, 4-MP and THF, (B) PPDCX prepared from a 20% wt solution of PANI PAMPSA in NMP, 4-MP and THF and later cross-linked for 3 days in 0.2M DCX, (C) PPHX prepared from a 20% wt solution of PANI PAMPSA in NMP, 4-MP and THF.

Hydrophilicity of the prepared membranes was studied via dynamic contact angle and results are shown in Figure 80. PANI PAMPSA had the lowest initial contact angle of 40° that quickly dropped to 15 ° after 80 seconds. PPHX and PPDDCX, in contrast, had both a higher initial contact angle of 85° and 83° with PPDCX having the highest decreasing rate. The higher initial contact angle could be related to the denser structure obtained through chemical cross-linking of the PANI PAMPSA and thorough immersion in hexane during phase inversion. The

rougher surface of PPHX membrane could also contribute to slowing down the water permeation rate.

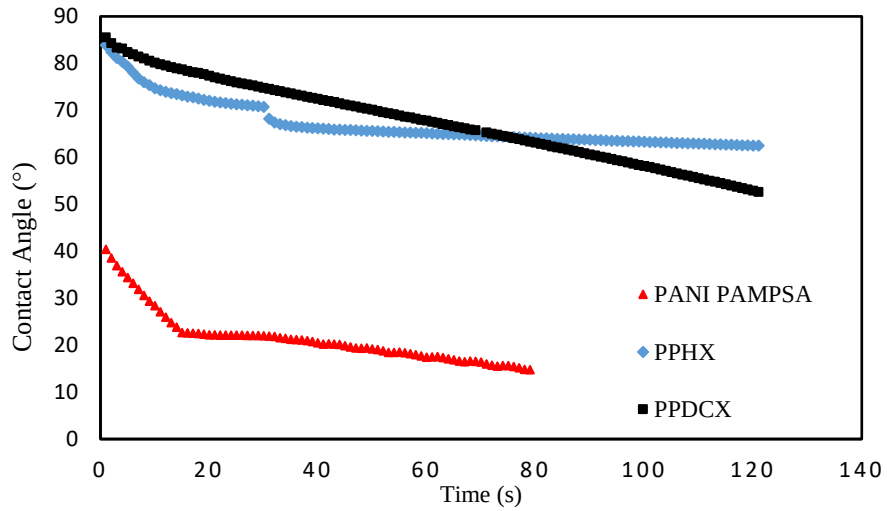

Figure 80: Evolution of contact angle with time of PANI PAMPSA, PPHX, and PPDCX membrane.

C.4. Membrane performance

Figure 81 reports the PPG rejection for the PPHX and the PPDCX membranes in acetone. The pure PANI PAMPSA membrane showed a lower stability in acetone and from previous works [25, 41] it is known that the MWCO is in the UF range, hence, the two novel membrane systems were the object of the filtration tests in solvents. PPHX membrane showed a pure acetone permeance of 0.59 $Lm^{-2}h^{-1}bar^{-1}$ at 20 bar and a PPG permeance of 0.36 $Lm^{-2}h^{-1}bar^{-1}$ with a good rejection of 58 % for the highest MW PPG. The pure acetone permeance of the PPDCX membrane was 6 ±3 36 $Lm^{-2}h^{-1}bar^{-1}$ and 3±2 36 $Lm^{-2}h^{-1}bar^{-1}$ for the PPG permeance in acetone, but the membrane was not able to reject the PPGS. However, in 2-propanol the PPDCX membrane showed good rejection of

the PPG, a permeance of 0.014 $Lm^{-2}h^{-1}bar^{-1}$ and a pure solvent permeance of 0.16±0.02 $Lm^{-2}h^{-1}bar^{-1}$ as shown in Figure 82.

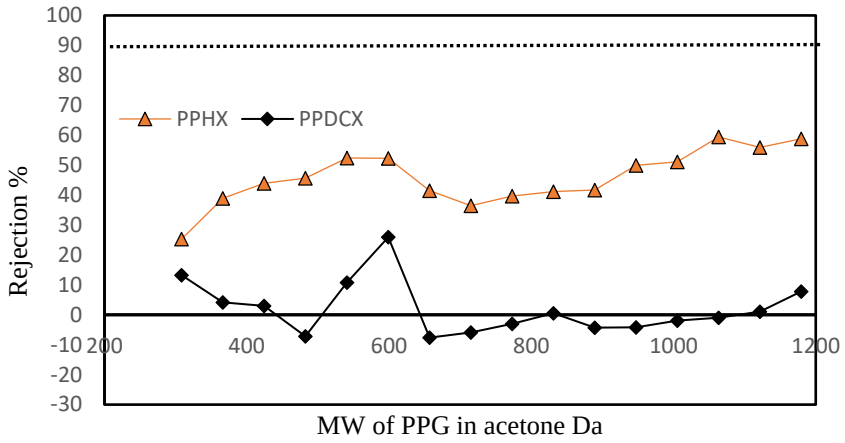

Figure 81: PPG rejection of the PPHX and PPDCX in acetone. Filtration condition is 20 bar, 20 °C in dead-end cell.

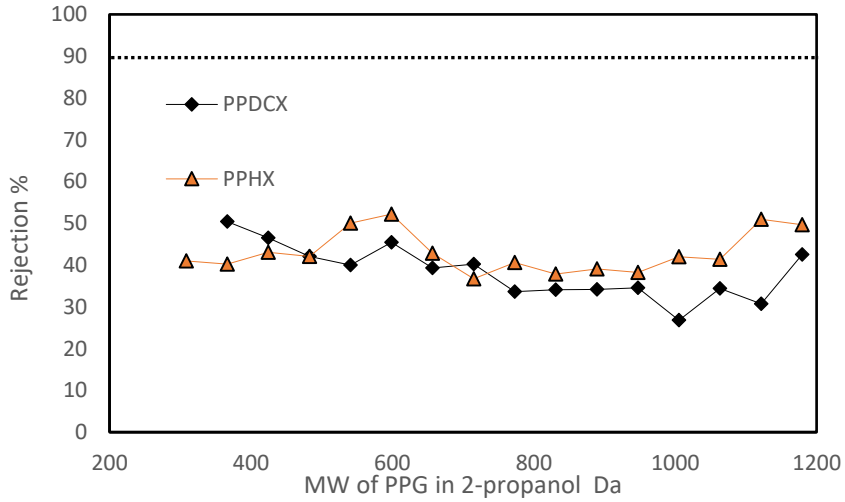

Figure 82: PPG rejection of the PPHX and PPDCX in 2-propanol. Filtration condition is 35 bar, 20 °C in dead-end cell for PPHX membrane and 20 bar, 20 °C in dead-end cell for PPDCX membrane.

C.5. Conclusion

In summary, this work has reported the chemical cross-linking of PANI PAMPSA membrane to obtain a solvent stable membrane with good hydrophilicity and 50% rejection of PPG in 2-propanol. Furthermore, the phase inversion in hexane densify the structure of the PANI PAMPSA membrane that show a rougher surface, a higher water permeance resistance and 50% rejection of PPG in acetone and 2-propanol.